



**Politecnico
di Torino**

Master's Degree Thesis.
Corso di Laurea Magistrale in
Ingegneria Civile

Modelling long-term deterioration of lining in tunnels

Juliana LÓPEZ OCHOA

Supervisor(s):
Prof. Marco Barla
Eng. Francesco Campana
Prof. Alessandra Insana

Politecnico di Torino
October, 2024

Abstract

Tunnel linings constructed using traditional methods typically consist of two layers. The outer layer, known as the primary or first-stage lining, is installed immediately after excavation and is designed to provide the necessary ground stability, allowing for partial stress release within the rock mass. The inner layer, or secondary lining, is usually applied at a later stage and is intended to bear the long-term ground load and, potentially, water pressure.

Current design practices for simulating the load transfer between the two linings are based on semi-empirical approaches, assuming that the full load presented at the primary lining is eventually transferred directly to the secondary lining at the end of the primary lining's service life. However, several studies have shown that in many cases, even after 30-40 years, the primary lining remains effective, with only limited ground load transferred to the secondary lining.

This master thesis aims to explore the effect of the load transfer generated due to degradation of the first-stage lining, considering the different degrees of deterioration in the sprayed concrete layer and steel ribs. A series of finite element analyses is used to study this process parametrically, with the goal of identifying less conservative yet reliable design choices.

The design parameters varied in this analysis include the rock mass properties (deformability and strength parameters) as well as their quality (GSI), the tunnel cross section and the final lining characteristics. This study is conducted to assess the sensitivity of each factor to the degradation of the primary lining and its impact on the final lining structural integrity in the long term.

Dedication

Este logro no es solo fruto de mi esfuerzo, sino también del apoyo de quienes siempre creyeron en mí. A mis padres y a mi hermana María, mi pilar y mi mayor inspiración, gracias por darme la fuerza cuando más la necesitaba. A mis tíos, por sus sonrisas y palabras de aliento, y a Pablo, mi luz en los momentos más difíciles, este logro también es tuyo. Finalmente, a mis amigos, los que están cerca y los que no y que siempre han estado a mi lado, gracias por ser parte de este camino y por creer en mí.

Contents

1. Introduction.....	1
2. Long-term degradation phenomena in tunnels: state of the art	3
2.1 Degradation of the rock mass	5
2.1.1. Kong et al. (2022)	5
2.1.2. Sandrone & Labiouse (2010).....	6
2.1.3. Showkati et al. (2021).....	7
2.2. Degradation of the primary lining	9
2.2.1. Ziller & Cont (2018)	9
2.2.2. Usman & Galler (2013)	11
2.2.3. Sandrone & Labiouse (2010) and Kong et al. (2022).....	12
2.2.4. Showkati et al. (2021).....	13
2.3. Summary of modelling cases.....	16
2.4. Methodology discussion.....	17
2.5. Modelling process	20
2.5.1. General Setup.....	20
2.5.2. Tunnel construction	21
2.5.3. Lining deterioration	24
3. Numerical model set up	25
3.1. Geometry	25
3.2. Geotechnical parameters and lining properties	27
3.3. Model combinations	30
3.4. Computational stages.....	32

4. Analysis of the results.....	37
4.1. Influence of the excavation geometry	37
4.2. Degradation of primary lining and influence of the rock mass degradation.....	42
4.3. Influence of the rock mass quality.....	44
4.4. Influence of the presence of steel reinforcement.....	46
4.5. Results overview	49
5. Conclusions.....	54
6. References.....	57
7. Appendix A. Summary modeling cases.....	61
8. Appendix B.1. Axial forces	62
9. Appendix B.2. Bending moments.....	70
10. Appendix B.3. Stresses	78
11. Appendix B.3. Stresses	86
12. Appendix B.4. Displacements	90
13. Appendix B.5. Verifications	98

Chapter 1

Introduction

Over the years, regions separated by complex topography have overcome connectivity challenges through different mobility infrastructures. Tunnels have emerged as a common solution throughout recent history, with a diverse range of technologies developed for their construction. Nowadays, many of these aging infrastructures require maintenance to extend its service life, leading to a growing demand of the evaluation of the current condition of these structures and its behavior over time.

Currently, very small attention is paid to the study of long-term interaction between rock mass and linings, nevertheless, this phenomenon represents a crucial factor in terms of tunnel stability and safety during its service life (Liu et al., 2023), since a progressive transfer of loadings from the primary support to the final lining take place and can jeopardize the performance of the tunnel. This evolution of stress can be divided into phases according to different authors (Kong et al., 2022; Sandrone & Labiouse, 2010; Showkati et al., 2021). The main stages are: just after the excavation takes place the primary support is the one receiving the main pressure from the rock mass; then, when the secondary lining is placed, both contribute to the stability; nevertheless, the support pressure from the primary lining progressively decreases over time and transfers more load to the secondary lining due to the deterioration of material properties, up to the point where only the final (or secondary) lining is the one sustaining the loads formed from the excavation and degradation of the rock mass.

Consequently, following what is previously outlined, to estimate closely the behavior of tunnel reinforcement and rock mass in the long term, the necessity of modelling strategies has been more pressing. Hence, this Master Thesis, is aimed to focus on the long-term deterioration of primary lining and rock mass from the geotechnical point of view and define modelling approaches of this phenomena using commercial tools like softwares that implement the Finite Element Method (FEM) such as RS2 from Rocscience suite ®.

Therefore, in the following chapters, the development of this study is exposed. Chapter 2 presents the state of art of the long-term degradation of primary lining and rock mass, indicating the different methodologies and findings present in the literature that can be applied to this research. Additionally in Chapter 3, the problem definition is explained,

pointing out the initial conditions and input parameters of the different modelling cases. Moreover, Chapter 4 exposes the results obtained during the analysis of the developed models and Chapter 5 the conclusions derived from this study.

Chapter 2

Long-term degradation phenomena in tunnels: state of the art

To perform an appropriate evaluation of the long-term degradation of primary lining in tunnels, it is important to highlight what different researchers have developed through the years. Therefore, a bibliographic review aimed to describe the main findings is exposed in this chapter.

Temporary support systems also known as primary linings are crucial to support the stability of the excavation while final lining is placed. These systems can be categorized into four main types according to their structural functions: (1) Application of confining pressure, which includes shotcrete and shotcrete with lattice girders; (2) Application of both confining pressure and reinforcement, including for instance rock bolts; (3) Strength support such as steel ribs, lattice girders, steel lining, umbrella arches and ground consolidation to improve geotechnical and hydrological properties, including grouting, compressed air and freezing (AITES, 2024). This study specifically focuses on shotcrete and steel ribs as principal components of the primary lining.

In the traditional approach, to perform static evaluation of a supported tunnel, there is the assumption of complete degradation of the primary lining, however some research of tunnels previously constructed indicate that the degradation of the primary lining is lower than expected (Trunda & Hilar, 2020). Furthermore, it has been proved that the function of a primary support system composed of a concrete inner shell might be unaffected even after 30 years and probably can continue its service life for even more (Galler & Lorenz, 2018). Therefore, to have a more precise idea of the actual state of this type of infrastructure, the quantification of the lining's contribution and performance is crucial.

The causes of degradation of concrete in the primary lining can be classified into three types according to several authors:

- Time-dependent changes of concrete's internal structure, which is commonly modelled by decreasing the stiffness of the material (Granata et al., 2013; Wang & Gong, 2019).

- Weathering effects in the concrete that interacts with the rock mass and groundwater, that can be represented as a reduction of deformability and mechanical properties (e.g. stiffness and strength) (Showkati et al., 2021; Usman & Galler, 2013a)
- Increase of loading caused by the deterioration of the rock mass, generating a disturbance in the equilibrium conditions of the tunnel lining (Kamel et al., 2015).

Regarding the modification of concrete's internal structure and its weathering, a key factor is the presence of water, which can spread through the cracks formed in the lining, carrying chemicals that promote the degradation such as sulphates, chlorides and alkali. This effect causes the dissolution of minerals in the cement bonded element, reducing the composition of the concrete up to the aggregates (Ziller & Cont, 2018a).

Additionally, this deterioration effect can be translated in the reduction of the primary lining thickness, for instance cementitious materials degrade when are in contact with underground water or bentonite, releasing alkali components. Different evaluations were performed on structures from 34 to 104 years old, observing a deterioration of 100 mm over 100 years (Yokozeki et al., 2004).

With respect to rock bolts installed in the primary lining, different tests performed in this type of reinforcements for existing tunnels of 40 years old show that corrosive effects can be present in the surface of the elements, however no significant damage takes place regarding the strength properties of the bolt (Galler & Lorenz, 2018). Moreover, experimental studies carried out to simulate the corrosion for rock bolts under low pH groundwater, showed that the ultimate tensile strength of the bolts loaded to 20 t was reduced 21% and for unloaded bolts decrease up to 39%. Additionally, the borehole diameter was reduced about 11.7% on a period of 3.5 years of corrosion testing (Aziz et al., 2014).

On the other hand, analyzing the deterioration of the rock mass, the deformations and the behavior of tunnels under time-dependent phenomena such as creep, squeezing and swelling are widely studied, while weathering of rocks around underground excavations has not received enough attention to the matter, even if weathering is a great factor of influence of the decrease of the mechanical properties of the rock. Therefore, normally the deterioration of the rock can be taken into account by placing additional loads on the tunnel lining in the long term, causing anticipated lining failure and tunnel collapse (Showkati et al., 2021).

For the case of weathering of the rock mass caused by external factors, these results in a change in the chemical composition and decrease of particle size and cohesion strength (Kong et al., 2022). In addition, the evolution of mechanical parameters of the rock mass in time can be associated to the propagation of existing and excavation induced cracks. These cracks cause the brittle behavior and delayed failure; however, this delay depends on the amount of applied stress and the presence of fluid and temperature

changes (Tran-Manh et al., 2016). Those effects related to degradation can be translated in a decrease of deformability and strength properties of the rock mass (Ladanyi, 1974).

Concerning the implementation of case studies, the convergence in short and long term of Saint-Martin-la-Porte tunnel was analyzed and it was established that the long-term deformations can be obtained from the short ones only reducing the cohesion of the rock mass. However, this approach does not consider the evolution of this deterioration, meaning a gap between short-term and long-term rock mass response (Vu et al., 2013).

Nevertheless, previous numerical modelling cases are analyzed in order to implement them as a reference in this study. In this context, considering that the rock and concrete have different behavior and properties under normal and deteriorated conditions, the methodologies applied to simulate the explained phenomena are divided for both materials. Hence, in the following a detailed evaluation of each methodology is presented.

2.1 Degradation of the rock mass

2.1.1. Kong et al. (2022)

In this research Kong et al.(2022) evaluated the long-term behavior of tunnels in weak rock mass, simulating the degradation of both lining and rock mass by performing a 3D Finite Element (FE) model.

These authors applied a constitutive model that describes the time dependent behavior of the rock found by Yoshida et al. (1990) who proposed a nonlinear failure criterion for materials characterized by time-dependent softening. It relates strength parameters A, B and S with Mohr-Coulomb (M-C) strength parameters, as shown in Equation 1, Equation 2 and Equation 3, assuming B=1 in order to apply them within this failure criteria.

$$\sigma_1 = \sigma_3 + A\sigma_3 \left(\frac{\sigma_3}{\sigma_1} - S \right)^{1/B}$$

Equation 1: Constitutive model proposed by Yoshida et al. (1990)

$$A = \frac{2\sin\phi}{1 - \sin\phi}$$

Equation 2: Relation between A parameter and friction angle proposed by Yoshida et al.(1990)

$$S = - \frac{c\sqrt{4 + 2A}}{A\sigma_c}$$

Equation 3: Definition of S parameter proposed by Yoshida et al. (1990)

In the numerical modelling the rock mass is considered an element supported by the Mohr-Coulomb failure criteria and its generic mechanical properties are derived from empirical equations that relate the RMR and Q systems with M-C properties.

To simulate the degradation, three scenarios were considered: rock mass deteriorates in short time (mechanical parameters of rock A_0 and S_0 decrease up to a quarter of its original value in 10 years); rock mass deteriorates slowly over a long-time (mechanical parameters of rock A_0 and S_0 decrease up to a quarter of its original value in 100 years); and rock mass rarely deteriorates, meaning a null decrease in its properties over time. It is important to remark that primary lining deterioration was modelled simultaneously in the three cases with the approach explained in the following subchapter 2.2.3. *Sandrone & Labiouse (2010) and* . Additionally, to model the excavation, at first a geostatic stage is inserted and then the removal area is divided in two parts to simulate traditional procedures: the upper part which is removed in a new step before the primary lining is inserted and then, the bottom part is extracted before the secondary lining is placed.

In this study the modeling focused only on extreme degradation hypotheses representing opposite conditions, from one extreme to the other. However the scope of the conclusions of the research is limited since no field or laboratory tests can support the results of this investigation.

2.1.2. Sandrone & Labiouse (2010)

An analysis regarding the degradation rate of both rock mass and lining was performed by Sandrone & Labiouse (2010). Both aspects were related between each other through the convergence-confinement method, therefore, the tunnel equilibrium was evaluated at the intersection between the Ground Reaction Curve (GRC) and the Support Reaction Line (SRL), and the deterioration of the materials was represented as an evolution in time of this intersection.

Additionally, in this paper they identified three main causes of rock mass degradation. First, rock mass ageing is considered by the application of rheological constitutive models such as Maxwell, Kelvin-Voigt, Bringham, among others. These ageing pathologies can be translated into squeezing and swelling behavior. The second cause is related to weathering of the rock which can be translated in a decrease of strength and stiffness properties of the material. Finally, pore water pressure behavior in time and its contact with the tunnel lining represent a cause of deterioration and can be modelled as a permeable or impermeable interface.

The effects of rock mass and support degradation are evaluated in an independent approach and combining both effects. For the first case, the rock mass degradation is modelled in terms of ageing from which the equation proposed by Boidy (2002) is applied (Equation):

$$\varepsilon_{vp} = a \cdot (q - \sigma_s)^\beta \cdot t^\alpha$$

Equation : Constitutive model to consider ageing of rock mass proposed by Boidy (2002) and applied by Sandrone & Labiouse (2010)

where q is the deviatoric stress, σ_s is limit stress where in this case is considered as zero for the sake of simplicity, t is the time in seconds, α and β are creep constants and a is the viscosity parameter.

On the other hand, the weathering effect in the strength properties of the rock mass was analyzed considering a decrease of its values at 30% in the long term based on uniaxial compression tests carried out by Ladanyi (1974). In this way, the influence of ground properties is analyzed in Equation 4 applying the hyperbolic law which is commonly used to analyze degradation states (Ladanyi, 1974; Sulem, 1994), where T is a constant related to rock mass weathering process, V_{ST} is the short-term value of the parameter (e.g. friction angle and cohesion) and V_{LT} is the value in the long term.

$$V(t) = V_{ST} - \left[(V_{ST} - V_{LT}) \cdot \left(1 - \frac{1}{1 + \frac{1}{T}} \right) \right]$$

Equation 4: Evolution of rock mass properties due to weathering.

For this analysis T is considered equal to 1 year with no theoretical or bibliographic support and, considering the findings related to the long-term values of the strength parameters, V_{LT} is equal to 70% of the initial value in the short term V_{ST} .

It was found that this decrease implies a reduction of 55% in the safety factor that relates the maximum pressure that the structure can sustain with respect to the one at equilibrium and degraded conditions, evidencing the importance of the evaluation of degradation in the long term. In addition, it is important to remark that in this reaserch only c and φ are the properties reduced while Young's Modulus is kept constant, different than what was suggested by Ladanyi (1974) who state that this deformability parameter should be reduced in the same proportions.

2.1.3. Showkati et al. (2021)

Analyzing a real study case Showkati et al. (2021) performed a degradation model for both rock mass and primary lining to evaluate the Torshon tunnel located in Iran by

implementing the Finite Difference Method. In the case of the rock mass the authors obtained an expression based on the findings of Huisman et al. (2006), Shimamoto et al. (2009); Tating et al. (2013) and Colman (1981). For instance, the empirical relationship shown in Equation 5 is implemented to correlate the weathering rate (R_{WE}) with the weathering quantitative reduction value ($WE(t)$) and the WE value at the time of excavation ($WE_{initial}$). It is important to remark that this expression is then adapted by these authors to describe the change of rock properties such as the intact rock strength as a function of time and further used by Showkati et al. (2021) for strength and deformability properties of the rock mass.

$$R_{WE} = \frac{WE_{initial} - WE(t)}{\log(1 + t)}$$

Equation 5. Degradation rate according to Tating et al. (2013)

This was implemented in order to analyze the time-related degradation effects of rocks with slope stability conditions by comparing results obtained from fieldwork by the International Institute for Geo-Information Science and Earth.

In addition, Shimamoto et al. (2009) proposed different models that related the strength property of cohesion with time: a straight line type, exponential and logarithmic. The three of them simulate the strength reduction curve of the rock mass properties where the interpolation coefficients were found by implementing convergence measurements of 30 years in two different existing tunnels located in China. It was found that the first two models facilitate the simulation of the tunnel in which the convergence speed increases over time, while the logarithmic relationship was useful for the excavation where the convergence remained constant, behaviour wanted for a tunnel with stability conditions in time.

Moreover, Tating et al. (2013) research which took place in Sabah (Malaysia) was aimed to establish the relationship between the weathering effect for rock slopes in time and the intact rock strength, where by interpolating the results of Uniaxial Compressive Strength (UCS) and Point Load Strength (PLS) tests, it was found that the best fitted equation is a logarithmic one considering the initial property value and the apparent reduction rate.

In this way, based on the previous outcomes, these authors implemented the relationship exposed in Equation 6 contending that the degradation of mineralogical heterogenous rocks can be expressed in logarithmic time functions, meaning that anyparameter of the geological material that varies in time ($P(t)$), depends on its initial value (P_0) and the apparent degradation rate (R_d) evaluated in an elapsed time (t) in terms of years.

$$R_d = \frac{P_0 - P(t)}{\log(t + 1)}$$

Equation 6: Apparent degradation of rock mass according to Showkati et al. (2021)

Nevertheless, these authors, based on previous experimental research (Ladanyi, 1974) suggest to reduce strength and deformability parameters by up to 30% and 40% respectively at the end of the tunnel design life (i.e. 100 years) as mentioned by the authors previously introduced in this chapter. Therefore, $P(t=100 \text{ years})=0.6P_0$ for deformability properties and $P(t=100 \text{ years})=0.7P_0$ in terms of strength parameters. Based on this, the degradation rates are derived: $R_{d(\text{strength})}=0.15P_0$ and $R_{d(\text{Young's modulus})}=0.2P_0$ from which Equation 7 and Equation 8 can be obtained.

$$(c, \varphi)(t) = (c, \varphi)_o [1 - 0.15 \log(t + 1)], 0 \leq t \leq 100$$

Equation 7: Strength parameters degradation in time according to Showkati et al. (2021)

$$E(t) = E_o [1 - 0.2 \log(t + 1)], 0 \leq t \leq 100$$

Equation 8: Deformability parameters degradation in time according to Showkati et al. (2021)

Different values of t (e.g. 0, 1, 10, 20, 50, 100 years) are imposed and the respective Ground Reaction Curves (GRC) and Support characteristic curve (SCC) are analyzed. For the GRC it was observed an increase in the displacements as the service life of the tunnel increases, increasing the ground pressure on the final lining.

2.2. Degradation of the primary lining

2.2.1. Ziller & Cont (2018)

Ziller & Cont (2018) suggest the Degradation of Primary Lining method (DPL) which simulates the deterioration of shotcrete in the long term and allows a more reliable and economical design of tunnel lining system. In this case two different constitutive models are applied, i) the Elastic perfectly plastic Mohr Coulomb failure criterion and ii) the Plaxis Shotcrete Model which is an Elastoplastic strain hardening-softening plasticity model where the yielding surface depends on the minor and major principal plastic strains.

For this research, the shotcrete degradation model is based on the decrease of stiffness and strength. For the case of stiffness, the Young's Modulus of composite material can be expressed in terms of the elasticity modulus of particle phase (E_p) and matrix phase

(E_m) and the fractional volume of the particles (g) (Neville & Brooks, 1987). Generally, g for shotcrete can take the value of 0.67, E_m 16000 MPa implementing a mean capillary porosity and E_p can be considered equal to 65000 MPa for limestone and 40000 MPa for granite. Assuming that the cement paste degradation is directly related to the increase of the porosity cement paste, the progressive decrease takes place by reducing every 10% the deformability modulus of the matrix.

$$E_c = \left[\frac{1-g}{E_m} + \frac{g}{E_p} \right]^{-1}$$

Equation 9: Definition of Young's modulus considering a composite material according to Ziller & Cont (2018).

For the strength, it is considered that the concrete mechanical characteristics are directly related to the porosity coefficient. In this case the progressive degradation is modeled through the increase of ω_{cap} (capacity of capillary pores) causing a reduction in the compressive strength of the mix, which at the same time is related to the cohesion derived from Mohr circles, while a constant friction angle is assumed.

The definition of this phenomena is expressed in Equation 10, where ω_{gel} , ω_{cap} and ω_a are the capacity of molecular, capillary and air pores respectively, additionally, the porosity coefficient (χ) is directly related to compressive strength of concrete (R_{ck}) through a linear relation according to laboratory tests (Ślusarek, 2010).

$$\chi = \frac{\omega_{gel}}{\omega_{gel} + \omega_{cap} + \omega_a}$$

Equation 10: Definition of porosity coefficient with respect of capacity of pores in different states according to Ziller & Cont (2018).

According to these authors, the traditional procedure of modelling primary lining and its contribution in the long term is to apply long-term rock loads, by transferring the 100% of these stresses from the primary to the secondary lining. However, they proposed a progressive decalcification which is represented as a loss of strength and stiffness of the shotcrete layer, which at the same time for the Mohr Coulomb constitutive model is translated as a gradual reduction in the cohesion and elastic modulus, while for the Plaxis Shotcrete Model the phenomena is evaluated reducing the parameters E_{28} , $f_{c,28}$ and $f_{t,28}$.

Furthermore, it was observed that, by only degrading the shotcrete's Young's Modulus, it not only caused a transfer of loads into the inner liner but the rock mass in the surroundings had to carry the redistribution of stresses, showing more influence on the stress transition than in the cohesion degradation case. In addition, decreasing both Young's Modulus and cohesion of shotcrete there was a significant increase in the effect of deterioration, causing sufficient damage of the material at the point where the

secondary lining had to carry the stresses. For the case where the three properties are reduced simultaneously, the shotcrete functionality stop at the point where it hardly supports any quantity of stress. Additionally, it was found that the axial force increased from 415 kN/m for a 30% of deterioration up to 1580 kN/m at 90% degradation. For the negative bending moment at the sidewall, it increased up to 7635 Nm/m and up to 7757 Nm/m at the invert for 90% of degradation.

2.2.2. Usman & Galler (2013)

A similar approach is used by Usman & Galler (2013) who performed a 3D numerical analysis analyzing the stresses of the shotcrete lining in a deep tunnel and its respective deterioration by decreasing the strength parameters individually or in different combinations.

To model the deterioration of the shotcrete, the material properties such as cohesion, friction angle and Young's Modulus are reduced by 10% at each calculation step. However, those parameters are reduced separately and in different combinations: the three parameters simultaneously and only Young's Modulus and cohesion. It is important to remark that, according to authors, the mechanical properties are based on a series of uniaxial compression tests and triaxial tests for 30-year-old concrete and shotcrete samples performed in the laboratory of the chair of Subsurface Engineering Montan University.

It is observed that, by only degrading the shotcrete's Young's Modulus, it not only caused a transfer of loads into the inner liner but the rock mass in the surroundings had to carry the redistribution of stresses, showing more influence on the stress transition than in the cohesion degradation case. On the other hand, decreasing both Young's Modulus and cohesion of shotcrete there was a significant increase in the effect of deterioration, causing sufficient damage of the material at the point where the secondary lining had to carry the stresses.

Finally, for the case where the three properties are reduced simultaneously, the shotcrete functionality stop at the point where it hardly supports any quantity of stress. Additionally, it was found that the axial force increased from 415 kN/m for a 30% of deterioration up to 1580 kN/m at 90% degradation. For the negative bending moment at the sidewall, it increased up to 7635 Nm/m and up to 7757 Nm/m at the invert for 90% of degradation.

At the same time, Showkati et al. (2021) model the deterioration of bolts as a reduction on its cross section, and is in terms of its corrosion rate, which at the same time depends on the concentration of chloride ions in the ground water. In contrast, the deterioration rate of shotcrete depends on different chemical parameters, this rate dictated

how the Young's Modulus and compression strength decrease with respect to its initial value.

2.2.3. Sandrone & Labiouse (2010) and Kong et al. (2022)

In this study the concrete lining degradation is divided into two main causes: the Calcium leaching of the material and the de-icing salt corrosion. Both scenarios can be modelled based on the findings from laboratory tests performed by Nguyen (2005), in which is stated that the decrease of mechanical properties such as Young's Modulus and compressive strength is proportional to the ratio between the degraded area (A_d) and the original section (A_0). Thus, this ratio can be obtained through Equation 11 hence, the decrease of parameters such as Young's modulus and compressive strength can be defined as in Equation 12 and Equation 13, where k_m and k_r are 0.66 and 0.76 respectively for a medium quality concrete.

$$\delta A_d = \frac{A_d}{A_0}$$

Equation 11: Decrease of original cross section according to Nguyen (2005)

$$\frac{\delta E}{E_0} = \frac{E_0 - E}{E_0} = k_m \cdot \delta A_d$$

Equation 12: Change in Young's modulus according to Nguyen (2005)

$$\frac{\delta f_c}{f_{c_0}} = \frac{f_{c_0} - f_c}{f_{c_0}} = k_r \cdot \delta A_d$$

Equation 13: Change in compressive strength according to Nguyen (2005)

The quantification of the degraded area is implemented by Sandrone & Labiouse (2010) and Kong et al. (2022), and proposed by Nguyen (2005), where the deterioration thickness, X_d given in meters is equal to the product of factor α and the square root of time t in days as shown in Equation 14.

$$X_d = \alpha \sqrt{t}$$

Equation 14: Thickness of degraded zone according to Nguyen (2005)

Since the shotcrete's properties are not improved due to the difficult access this factor α can vary according to the cause of concrete's deterioration. For the case of Calcium leaching, α is equal to $5E-4 \text{ m}/\sqrt{\text{days}}$.

On the other hand, the de-icing salt corrosion, which can be analyzed by exposure zones in which the degraded area can vary depending on the regularity of maintenance

and effects influenced by humidity, temperature and salt concentration. Therefore, using the Equation 14, two cases are considered for the value of α :

- For the lower part of the sidewalls $\alpha=5E-4 \text{ m}/\sqrt{\text{days}}$, reaching a reduction of 50 mm over 30 years.
- For the higher part of the sidewalls and crown $\alpha=2.5E-4 \text{ m}/\sqrt{\text{days}}$ corresponding a thickness decrease of around 25 mm in 30 years of operation.

In this research it was found that, considering the degradation of final lining and rock mass in separate ways, it shows that the influence of reduction of lining properties is lower for the long-term stability with respect to the rock mass degradation. However, a good estimation of rock mass degradation must be done so the tunnel safety factor is more appropriate.

2.2.4. Showkati et al. (2021)

In this study the degradation of primary lining was divided into the decrease in properties of rock bolts, steel sets and shotcrete. For the case of bolts, the deterioration was measured in terms of time, which at the same time is represented as the total between the corrosion free lifetime of grouted rock bolt (t_i) and ultimate service life of corroded rock bolts (t_{ULS}). It is important to remark that non-grouted rock bolts have no protection components, therefore $t_i=0$. In this way, t_i is computed from Fick's second law of diffusion and experimental data obtained by Bae et al. (2006) and can be obtained using Figure 1 which represent this time measurement in terms of the concentration of chlorides in the ground water (C_{CL}) expressed in ppm and the grout thickness (d_g) in mm.

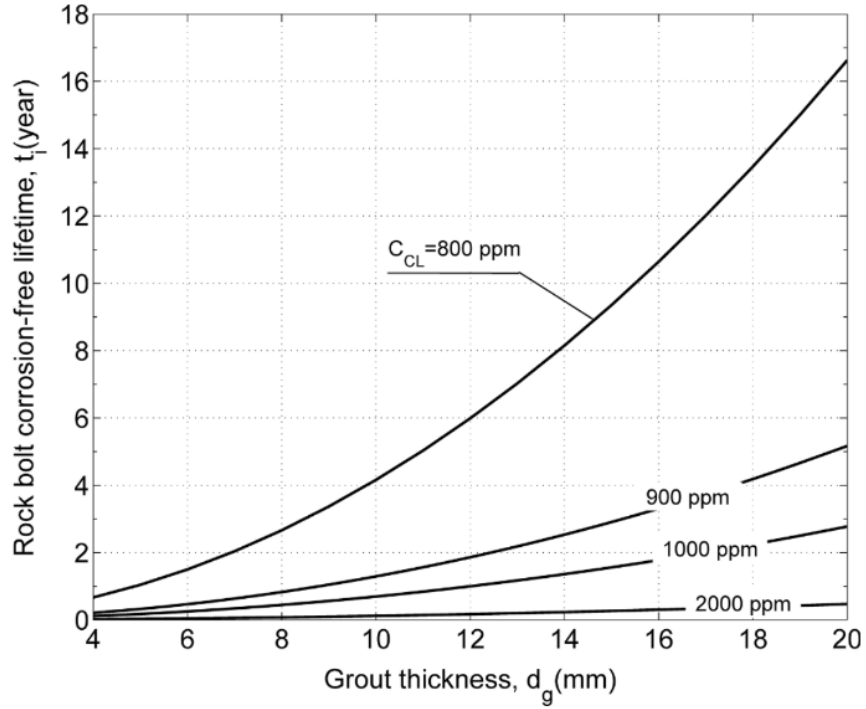


Figure 1: Estimation of rock bolt corrosion-free lifetime t_i according to Showkati et al. (2021)

Furthermore, t_{ULS} is found knowing the rock bolt diameter (d_b) in mm, tensile factor of safety ($S.F_b$) and corrosion rate (R_c) in mm/year as shown in Equation 15. In this way, the deterioration of this primary support is modelled as a decrease of the rock bolt cross section, grout bond strength and grout stiffness.

$$t_{ULS} = \left(1 - \frac{1}{\sqrt{S.F_b}}\right) \cdot \frac{d_b}{2R_c}$$

Equation 15: Computation of ultimate service life of corroded rock bolts [year] implemented by Showkati et al. (2021)

At the same time, deterioration of steel sets is modelled for a I-beam section steel by reducing its cross-sectional area and consequently its moment of inertia as shown in Equation 16.

$$I_{r(xx)} = \frac{1}{12} [(B - 2R_c t)(H - 2R_c t)^3 - (h + 2R_c t)^3 (B - w)]$$

Equation 16: Degraded moment of inertia of an I-beam steel section used in Showkati et al. (2021) study

On the contrary, the shotcrete property's decrease is evaluated in terms of its deterioration rate (R_s) obtained by implementing a mechanistic model proposed by

Atkinson & Hearne (1989) where the depth of sulphate penetration is computed. This model is simplified by Kosmatka et al. (2002) for a general condition of Portland cement obtaining the expression shown in Equation 17.

$$R_s = 1.04 \times 10^{-3} \cdot \frac{E c_{sulf} D_i W_{cem} \phi_{AO}}{(1 - \nu)}$$

Equation 17: Deterioration rate of shotcrete R_s [mm/year] implemented by Showkati et al. (2021)

Where E represents the elastic modulus of concrete [Pa], c_{sulf} the concentration of sulphate in groundwater [mol/m³], D_i the intrinsic diffusion coefficient of sulphate ions in concrete [m²/s], W_{cem} the cement content in concrete [kg/m³] and ϕ_{AO} the amount of aluminium oxide of cement [%].

This rate is applied as in Equation 18 to reduce property's initial value of the lining with a certain thickness d_s [mm] at a specific time t [year], the mechanical characteristics that are decrease are the compressive strength $f_{c(t)}$ and the Young's Modulus E_t . It was found that both properties reduced with a linear behavior up to 20% its original value at 100 years of operation as shown in

$$\frac{f_{c(t)}}{f_{c0}} = \frac{E_t}{E_0} = \left(1 - \frac{R_s t}{d_s}\right)$$

Equation 18: Decrease of initial properties proposed by Showkati et al. (2021)

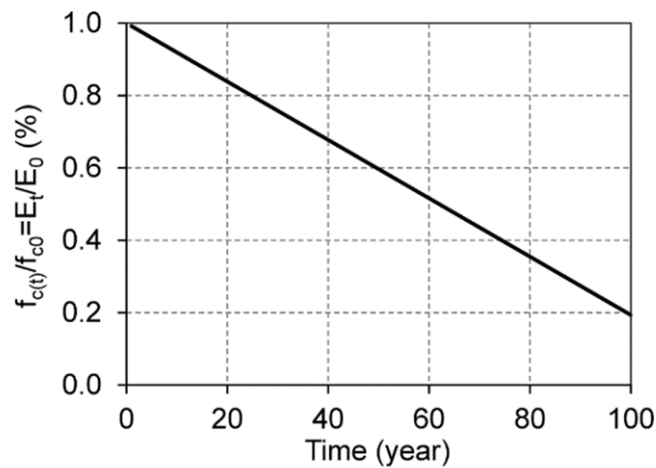


Figure 2: Decrease of shotcrete properties according to study case of Showkati et al. (2021)

It was observed that at early stages the only force simulated for the final lining is its self-weight, however since the tunnel primary support system starts to deteriorate, tunnel loads are gradually transferred to the final lining, causing an increase in thrust and

bending moments. Specially for the bending moments there is an important increase in the long-term at the tunnel sidewalls.

2.3. Summary of modelling cases

The summary of support properties and degradation modelling approaches exposed in this chapter is shown in Table 1. For a more detailed review see Appendix A.

Table 1: Summary modelling cases

Reference	Rock mass constitutive model	Support properties	Support constitutive model	Rock mass degradation model	Support degradation model
Numerical Simulation of Long-Term Deterioration of Rock Mass Supported by Shotcrete Lining (Kong et al., 2022).	Proposed by Yoshida et al., 1990 implementing A, S and B parameters which depend on the cohesion and friction angle of the rock.	SHOTCRETE: $\gamma=21$ kN/m ³ , $E=15000$ MPa, $\nu=0.2$, $\phi=45^\circ$, $c=3$ MPa, $\sigma_t=1$ MPa, $t=200$ mm LINER (CONCRETE): $\gamma=25$ kN/m ³ , $E=30000$ MPa, $\nu=0.2$, $t=350$ mm.	Mohr Coulomb failure criteria	3 cases: 1. A_0 and S_0 decreased to a quarter of its original value in 10 years. 2. A_0 and S_0 decreased to a quarter of its original value in 100 years. 3. Parameters are equal to the original ones.	Deteriorated thickness (X_d) depends on time and factor α .
Predicting long-term stability of tunnels considering rock mass weathering and deterioration of primary support (Showkati, Salari-rad, & Hazrati, 2021).	Isotropic Elasto-plastic	PRIMARY LINING: Shotcrete of 150 mm thick, fully grouted bolts of 6 m length with 2x2 spacing. SECONDARY LINING= Concrete lining of 400 mm thickness reinforced with 8 ϕ 25 rebars.	Elastic Perfectly plastic	An expression in terms of time and an apparent degradation rate (Rd) is used for cohesion and Young's Modulus degradation. Imposing different values of time (e.g. 0, 10, 20, 50, 100 years).	BOLTS: Reduction of bolts cross section arease in terms of corrosion rate. SHOTCRETE: Degradation of Young's Modulus and compressive strength, whose gradual decrease depends on chemical characteristics
Analysis of the evolution of road tunnels equilibrium conditions with a convergence–confinement approach (Sandrone & Labiouse, 2010)	Mohr Coulomb failure criteria (to implement GCC).	SHOTCRETE: 0.25 m thick, $E=23$ GPa, $\nu=0.2$, $f_c=14$ MPa SECONDARY LINING: 0.3 m thick, $E=35$ GPa, $\nu=0.2$, $f_c=40$ MPa	Elastic Perfectly plastic	1. Agening: Lemaitre's law (evolution of primary creep in terms of viscoplastic strain). 2. Weathering: Reduction of c and ϕ	Reduction of Young's Modulus and compressive strength, based on the affirmation that reduce of mechanical properties is elated to the ratio between the degraded area and the original section.
Long-term deterioration of lining in tunnels (Usman & Galler, 2013).	Mohr Coulomb failure criteria.	SHOTCRETE: $\gamma=23.64$ kN/m ³ , $E=10000$ MPa, $\nu=0.2$, $\phi=36^\circ$, $c=9$ MPa LINER (CONCRETE): $\gamma=25.02$ kN/m ³ , $E=30500$ MPa, $\nu=0.2$, $t=300$ mm.	Mohr Coulomb for shotcrete and Elastic for liner	(-)	By reducing 10% at each calculation step the properties: *Only Young's Modulus *Only cohesion *Young's Modulus and cohesion *Young's Modulus, cohesion and friction angle
Evaluation of long-term ground load on conventional tunnel linings (Ziller & Cont, 2018).	Elasto-plastic behavior with Hoek and Brown failure criteria.	PRIMARY LINING: 200 mm thick layer of shotcrete (C25/30), $E=5000$ MPa. SECONDARY LINING: 350 mm thick layer of shotcrete (30/37).	Plaxis shotcrete model and Mohr Coulomb failure criteria	(-)	For the Mohr-Coulomb case it was represented as a decrease of cohesion (in terms of UCS) and elastic modulus. For the Plaxis Shotcrete Model was evaluated with the decrease of E_{28} , $f_{c,28}$ and $f_{t,28}$.
Numerical Methods for Tunneling using ABAQUS and Investigations of Long-Time-Effects of the Shotcrete Shell and its Impact on the Combined Support System (Modlhammer, 2011)	Mohr Coulomb failure criteria.	SHOTCRETE SHELL: 20 cm thick, $E=10000$ MPa (Young)-15000 MPa (Hardened), $\nu=0.2$. INNER LINER: 30 cm thick, $E=30500$ MPa.	Linear elastic perfectly plastic	(-)	Deterioration of Young's Modulus and compressive strength reducing steps by 10% each. Both parameters are reduced independently and then simultaneously.

2.4. Methodology discussion

In order to select an appropriate approach for both modelling degradation of rock mass and primary lining, three main factors are considered. The first one is related to the practical and theoretical support that the methodology has, in other words, the amount of in situ and laboratory tests, experimental studies, real cases and analytical models that validate the assumptions considered for each case. Moreover, the second characteristic to consider is the scope of the research regarding how easily the models can be applied to both generic studies and practical solutions. Finally, the third factor is the possibility to implement FEM softwares that ease the analysis.

Analyzing the models exposed in paragraph 2.1 *Degradation of the rock mass*, as previously explained, the one suggested by Kong et al. (2022) is based on a constitutive model proposed by Yoshida et al. (1990) which, despite its alignment with experimental data sourced from literature and analysis in terms of strength properties easily obtained, this formulation is specially carried out for geologic materials representing time-dependent softening. Hence, as this phenomenon represents a particular case of rheological behavior it cannot be adapted to a generic case, moreover as previously said, while the time-dependent models are widely study, the scope of the present analysis is more focused on the rock weathering.

Additionally, the research performed by Kong et al. (2022) it does not have field or laboratory tests that verify the numerical simulation. For the modelling cases involving rock mass degradation over time, there is no theoretical or practical support to suggest that these scenarios are specifically applicable in real-life situations.

Regarding the study performed by Sandrone & Labiouse (2010) it is possible to state that, for the aging analysis, different parameters (e.g. the creep and viscosity coefficients) are highly dependent on the rock and in situ rheological conditions. In addition, for the weathering analysis, even though some of the assumptions are based on uniaxial compression tests and studies carried out by Ladanyi (1974), other conjectures (e.g. parameter T equal to 1 year) are not well explained and support by theoretical or applied research.

On the other hand, analyzing the methodology suggested by Showkati et al. (2021), the degradation model exposed in Equation 6 has different theoretical and practical support from different authors such as Huisman et al. (2006), Shimamoto et al. (2009), Tating et al. (2013) and can be derived for different mechanical properties of the rock which can be defined for practical and generic scenarios and conveniently inserted in FEM softwares. Furthermore, the assumptions carried out to simplify the main equation for strenght and deformability paameters are backed from experimental test performed by Ladanyi (1974).

In contrast, analyzing the models exposed in subchapter 2.2 such as the one proposed by Ziller & Cont (2018), it could be suggested that, since the degradation model is expressed in terms of common strength and stiffness properties, its easily applicable for generic and practical cases and in numerical modelling tools specially analyzing the M-C model. Additionally, for the case of stiffness reduction the expression shown in Equation 9 is based on a wide analysis of concrete properties from Neville & Brooks (1987) and focuses on a real phenomenon since the decrease of properties is due to the loss of cement material (i.e. increase of matrix phase porosity). On the other hand, the reduce of strength properties considers cohesion and f_c based on laboratory tests performed by Ślusarek (2010), which determined that the relationship between the porosity and cubic strength of concrete is linear, and presumes a constant friction angle without adequate theoretical or practical justification. In this way, the model is carried out by assuming a linear decrease of the deformability modulus of the matrix (which must be translated into the Young's Modulus of the composite material), c and f_c .

A similar approach is addressed by Usman & Galler (2013), where the reduce of friction angle and cohesion is performed in a linear way, however, different than the previous model, the deformability modulus is deteriorated directly for the composite material. These assumptions are based on the results of different laboratory test for samples with 30 years old and the analysis is performed in a way that is applicable to modelling tools with practical mechanical characteristics.

Moreover, with a similar methodology, two different authors Kong et al. (2022) and Sandrone & Labiouse (2010) applied the experimental findings of Ladanyi (1974) into the degradation model suggested by Nguyen (2005), meaning a theoretical and practical back up in terms of its assumptions. Nonetheless, the degradation is represented as a reduction in the primary lining thickness using Finite Difference model. This process must guarantee the transfer of stresses to the final lining while modifying this geometric attribute. The mentioned investigation does not clearly explain how this transfer can be achieved and or what material the lining converts into after degradation, which is evidently not the rock mass.

Finally, for the methodology suggested by Showkati et al. (2021), it is accurate to state that, although it has a very wide theoretical and practical endorsement in its equations and assumptions for different applications of primary support, it requires a set of chemical parameters to define the degradation rates such as c_{sulf} , D_i and ϕ_{AO} which vary depending on the case and can be challenging to acquire from a practical point of view. However, as its research is well detailed and supported, its results can be applied to other practical scenarios.

In this way a comparison between the different approaches is performed considering if each of them follows the three criteria exposed at the beginning of this chapter. This

assessment is shown in Table 2, where each of the degradation models can satisfy the criteria (+), partially satisfied (+/-) and not satisfied it at all (-).

Table 2: Methodology comparison

Research	Practical and theoretical support	Scope	Application in FEM softwares
Rock mass degradation models			
Kong et al. (2022)	+	-	+
Sandrone & Labiouse (2010)	+/-	+/-	+/-
Showkati et al. (2021)	+	+	+
Primary support degradation models			
Ziller & Cont (2018)	+/-	+	+
Usman & Galler (2013)	+/-	+	+
Kong et al. (2022); Sandrone & Labiouse (2010)	+	+	-
Showkati et al. (2021)	+	-	-

Following what is presented in this chapter, the methodology selected to simulate the rock mass degradation, is the one implemented by Showkati et al. (2021) since it is supported by theoretical and experimental research and can be easily applied in a FEM software.

On the other hand, the approaches suggested by Kong et al. (2022); Sandrone & Labiouse (2010) and by Ziller & Cont (2018) were chosen for the primary lining degradation. Nevertheless, for the first methodology, where the degradation takes place as primary lining thickness reduction, it was determined, as the models were conceived that this approach is not applicable to the present study due to the significant computational effort required by FEM software to reduce the thickness by 10 mm at each stage while maintaining an appropriate mesh. Additionally, this methodology cannot serve as a reference because it does not clarify how stress is transferred between the material with degraded and unknown properties and the primary and final linings.

In this way, only the methodology proposed by Ziller & Cont (2018) and Usman & Galler (2013) is considered for the deterioration of primary lining properties. It is important to remark that both approaches are very similar by applying a linear decrease of parameters. For this study, the Ziller & Cont (2018) model is primarily implemented since it considers the shotcrete as a composite material, especially for the case of deformability modulus and analyze its behavior in more detail. However, the friction angle is also reduced in this study since Usman & Galler (2013) consider it an important factor for the degradation phenomena

2.5. Modelling process

According to different authors including Modlhammer (2011) a numerical model such as the one implemented in this study consists in three distinct phases: the general setup, tunnel construction and lining deterioration.

2.5.1. General Setup

The initial phase involves the conception of the model, which includes determining its size, mesh, boundary conditions, material properties and behavior. Careful attention is paid to ensuring that the model's size and mesh are defined in a way that minimizes boundary effects. Additionally, the stress field acting on the ground is incorporated as a boundary condition (Ziller & Cont, 2018). Support elements such as rollers and hinges are placed along the model's perimeter to constrain movement at the external boundaries. Between both first and second phase of the model, its division of phases takes place in order to excavate, place the linings and deteriorate the material (Usman & Galler, 2013).

For material properties, those obtained from laboratory tests are generally used for the rock mass, while properties defined by the designer are applied to the tunnel linings. In FEM modeling, the lining can be represented either by beam elements or by continuous finite elements. When analyzing a composite section made of two different materials (e.g., shotcrete with steel sets or reinforced concrete), an equivalent material that incorporates the properties of both materials must be implemented in the model.

To define the properties of this composite material, a method proposed by Carlos Carranza-Torres (2004) can be applied. This method involves analyzing 1- meter length of composite section formed by regularly spaced elements 1 and 2 which have different Young's modulus (E), cross sectional area (A) and moment of inertia (I) as illustrated in Figure 3.

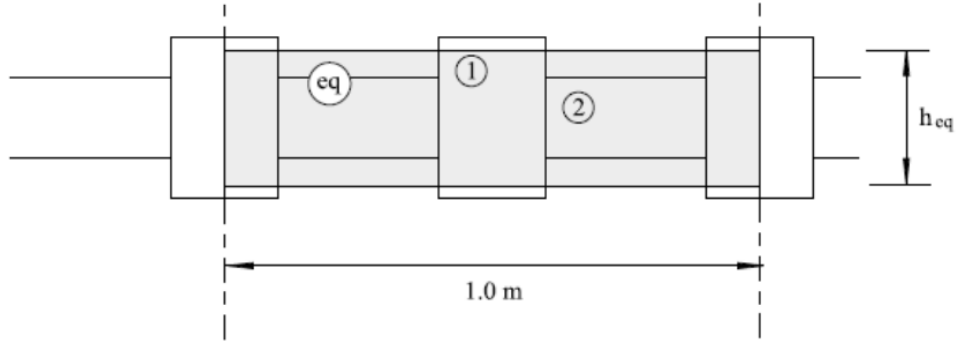


Figure 3: Problem statement of equivalent medium (Carranza-Torres, 2004)

For n elements of types 1 and 2 within a meter of section, characterized by parameters E_1, A_1, I_1 and E_2, A_2, I_2 , the equivalent height of the section (h_{eq}) and Young's Modulus (E_{eq}) are computed using Equation 19 and Equation 20 respectively.

$$h_{eq} = 2 \frac{\sqrt{3C_A C_1}}{C_A}$$

Equation 19: Height of the equivalent section (Carranza-Torres, 2004)

$$E_{eq} = \frac{\sqrt{3}}{6} \frac{C_A^2}{\sqrt{C_A C_1}}$$

Equation 20: Young's Modulus of the equivalent section (Carranza-Torres, 2004)

Where C_A and C_1 are obtained from Equation 21 and Equation 22.

$$C_A = n(A_1 E_1 + A_2 E_2)$$

Equation 21: C_A parameter (Carranza-Torres, 2004)

$$C_1 = n(I_1 E_1 + I_2 E_2)$$

Equation 22: C_1 parameter (Carranza-Torres, 2004)

2.5.2. Tunnel construction

In the tunnel construction phase of a numerical model, the focus is on analyzing the evolution of displacements as excavation progresses. These displacements activate the resistance of the surrounding ground, which at the same time reduces the load applied to the subsequently installed supports. To perform this analysis the Load Reduction Method (Panet, 1978) is implemented where at an initial state the internal pressure (p_0) is assumed to be equal to the external earth pressure at the excavation contour and then it is progressively reduced by a factor between 0 and 1 (Modlhammer, 2011).

To determine the appropriate stage at which the primary lining should be installed (i.e. specifically, the reduction factor of internal pressure) the Longitudinal Displacement Profile (LDP) is calculated (Figure 4). This involves establishing the maximum radial displacement at the tunnel boundary at a specific longitudinal point of the excavation. By correlating the theoretical displacement at a given distance from the excavation face with the results of the numerical model, the optimal internal pressure for installing the primary lining can be determined.

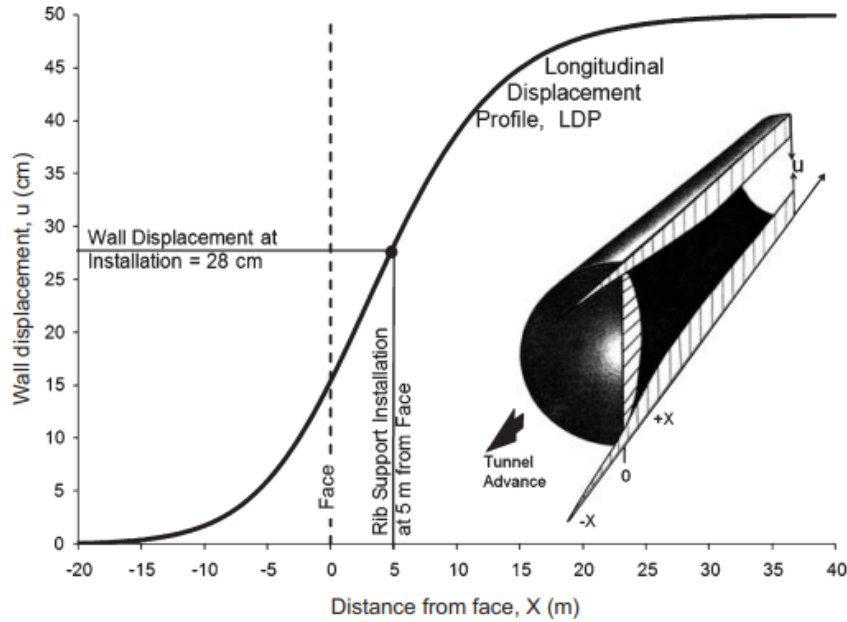


Figure 4: Example of a LDP to relate the support installation location to nominal wall displacement for a 10 m diameter deep tunnel according to (Vlachopoulos & Diederichs, 2009)

To build the LDP curve, different mathematical expressions from the literature can be considered. For instance, in the study performed by Carranza-Torres & Fairhurst (2000), the expression outlined in Equation 23 was implemented in which Hoek (1999) suggested it for a circular tunnel with radius (R) as the best-fit empirical relationship between radial displacement of tunnel and distance to the face (x).

$$\frac{u_r}{u_{r,max}} = \left[1 + e^{(-x/R/1.10)^{-1.7}} \right]$$

Equation 23: Displacement at an X distance implemented by Carranza-Torres & Fairhurst (2000)

Moreover, Vlachopoulos & Diederichs (2009) developed two different equations based on the normalized distance X^* to provide the best fit for LDP. These equations

were derived by analyzing the results of various models with differing rock mass properties.

The normalized distance X^* is defined as the ratio of the position of the measured radial displacement from the tunnel face (X) to the tunnel radius (R_T). A positive X^* indicates that the position is inside the tunnel measured away from the face (Equation 24), while a negative X^* denotes the position in the rock ahead of the face (Equation 25).

$$\frac{u}{u_{max}} = u_0^* \cdot e^{X^*} \quad \text{for } X^* \leq 0 \text{ (in the rock mass)}$$

Equation 24: Displacement at an X distance in the rock mass (Vlachopoulos & Diederichs, 2009)

$$\frac{u}{u_{max}} = 1 - (1 - u_0^*) \cdot e^{-\frac{3X^*}{2R^*}} \quad \text{for } X^* \geq 0 \text{ (in the tunnel)}$$

Equation 25: Displacement at an X distance in the tunnel (Vlachopoulos & Diederichs, 2009)

The variable u_0^* represents the normalized radial displacement at the face of the tunnel. It is defined as the ratio of the displacement at the tunnel face (u_0) and the maximum radial displacement (u_{max}). Meanwhile, R^* denotes the normalized plastic zone radius, calculated as the ratio of the plastic radius (R_p) to the tunnel radius (R_T). It is important to note that both u_{max} and R_p are derived from the numerical analysis in which the internal pressure is progressively reduced.

Panet (1995) performed a finite element analysis under elastic conditions obtaining an expression that is only applicable to the rear of the tunnel face as expressed in Equation 26. In contrast, Panet & Guenot (1982) proposed other expression in terms of tunnel distance to compute the radial displacement as outlined in Equation 27.

$$\frac{u}{u_{max}} = 0.25 + 0.75 \left[1 - \left(\frac{0.75}{0.75 + x/R_T} \right)^2 \right]$$

Equation 26: Displacement at an X distance in the tunnel (Panet, 1995).

$$\frac{u}{u_{max}} = 0.28 + 0.72 \left[1 - \left(\frac{0.84}{0.84 + x/R_T} \right)^2 \right]$$

Equation 27: Displacement at an X distance in the tunnel (Panet & Guenot, 1982).

By applying the four expressions and setting a fixed distance from the tunnel face where the primary lining is installed, it is possible to correlate these theoretical radial displacements with those that occur during the progressive reduction of pressure. This allows for the determination of the pressure at which these theoretical displacements occur. To ensure a conservative approach and allow for maximum convergence, the final

percentage of pressure release used during the installation of the primary lining is the maximum one (Vlachopoulos & Diederichs, 2009). In this way, the primary lining is placed at the previously mentioned stage, while the final lining is inserted once the total internal pressure release has occurred.

2.5.3. Lining deterioration

The primary lining degradation takes place at different model stages, in which the properties of the material are reduced at a certain proportion according to the approach selected on the previous chapters from Ziller & Cont (2018) and Usman & Galler (2013).

Chapter 3

Numerical model set up

To enhance the study of the long-term behavior of the primary lining on a tunnel's stability, it is essential to define a practical case. Therefore, the present chapter aims to establish several cases that consider different scenarios applicable in the practical point of view to analyze the effects of degradation depending on the geometry, rock mass state and final lining composition.

The 2D FEM modelling software RS2 from the Rocscience suite ® is adopted as a modelling tool in this study. This software is designed for analyzing geotechnical structures in both rock and soil, with specific application in tunnel and support design, underground excavations, surface excavation, slope stability, embankments, dynamic analysis, foundations, consolidation, and ground water seepage. In tunneling applications, RS2 enables the design and analysis of the tunnel excavation and its support system through multi-stage modeling. This approach allows the simulation of stress and strain development as the tunnel pressure is gradually released.

3.1. Geometry

Analyzing the most common cross sections for traditional excavating methods (Yoon et al., 2014), the horseshoe shape with (Figure 5) and without invert arch (Figure 6) are considered for the analysis. Since the study cases are intended to be generic, the predetermined cross sections suggested by RS2 software are considered with excavation areas and dimensions as similar as possible.

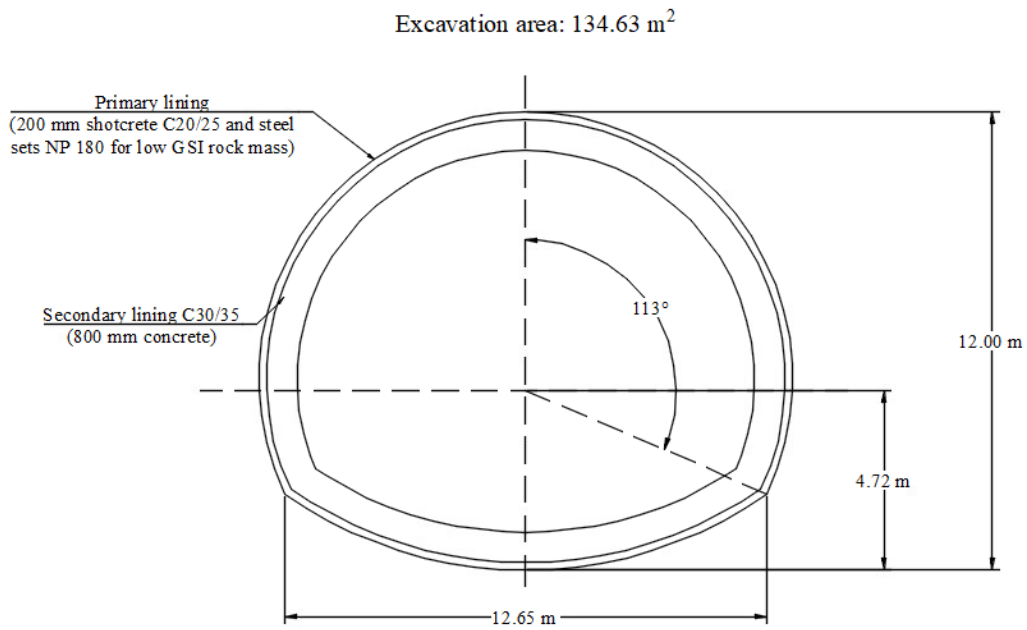


Figure 5: Proposed horseshoe cross section with invert arch

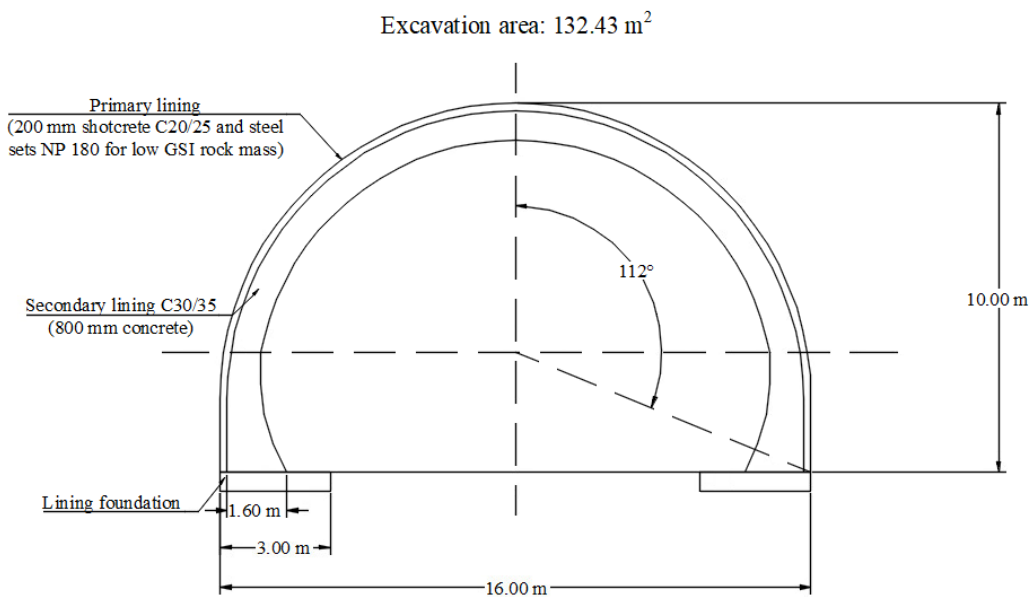


Figure 6: Proposed horseshoe cross section without invert arch

The insertion of these geometries in the model requires the discretization of a graded mesh formed by 3-noded elements. Nevertheless, a refinement of the mesh is performed near the tunnel excavation boundary and at sections that represent the primary and final lining of the tunnel, allowing a more accurate numerical solution of the stress strain phenomena. In addition, the external boundaries of the model are placed at a sufficient distance in order to avoid its influence in the final solution at the area of interest (i.e. External boundaries placed at 10 times the diameter of the tunnel from the excavation contour). The analysis is carried out for deep tunnel conditions (100 m), assuming a

constant geostatic stress state (i.e. $K_0=1$) and constraining horizontal and vertical displacements by introducing rollers placed in the borders and hinges in the vertices of the external boundary, as shown in Figure 7 and Figure 8.

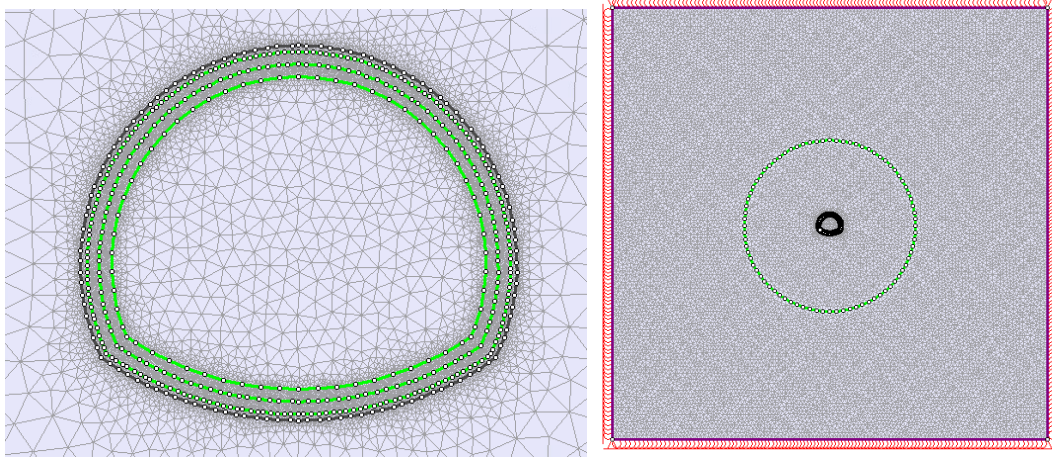


Figure 7: Discretization and boundary conditions of model with a horseshoe-shaped tunnel with an invert arch

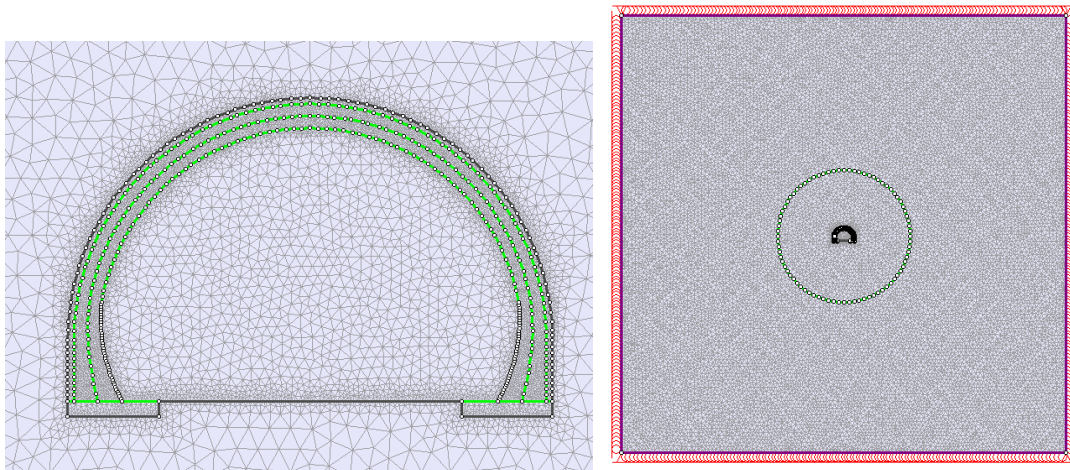


Figure 8: Discretization and boundary conditions of model with a horseshoe-shaped tunnel without an invert arch

3.2. Geotechnical parameters and lining properties

The numerical models described in this chapter adopts two geological materials with the aim to represent the case of a weaker and of a stronger rock mass, for instance, with values of GSI equal to 30 and 50. The deformability and strength parameters for both materials are highlighted in Table 3.

Table 3: Rock mass mechanical and deformability parameters

Parameter	High GSI	Low GSI
GSI	50	30
γ_r [kN/m ³]	29	29
K_0 [-]	1	1
σ_t [MPa]	0.19	0.02
σ_c [MPa]	3.64	0.64
φ [°]	28	22.5
c [MPa]	2.70	1
E [MPa]	7600	1600
ν [-]	0.30	0.30

Both the rock mass and the lining material are assigned an ideal elastoplastic constitutive model with Mohr Coulomb failure criteria, using residual parameters equivalent to peak values. It is important to remark that the lining foundation placed at the base for the horseshoe section without invert arch is modeled with elastic behavior.

A 200 mm thick shotcrete (C20/25) is chosen as primary lining, based on the modelling cases studied in the previous chapter, the constitutive model selected is Elastic-Perfectly Plastic translated into a Mohr-Coulomb failure criterion (Kong et al., 2022; Usman & Galler, 2013). Its respective properties based on the previous research and also on EN 1992-1-1 are exposed in Table 4.

Nevertheless, in order to assign an appropriate reinforcement for each rock mass type, steel sets NP 180 are added to the primary lining for the poor-quality rock mass cases. In this way, it is required to insert the parameters of an equivalent medium that considers both the shotcrete, and the steel sets placed every 0.5 meters as shown in

Table 5. The computation of the equivalent medium properties is performed basing on the method proposed by Carlos Carranza-Torres (2004) exposed in the previous chapters.

Table 4: Primary lining properties

Parameter	Shotcrete	Equivalent medium (Shotcrete + Steel sets)
γ [kN/m ³]	24	24
E [MPa]	14000 (matrix) 65000 (particles)	33648
g [-]	0.67	-
ν [-]	0.20	0.20
f_{ck} [MPa]	20	33.23
f_{cd} [MPa]	11.33	18.83
f_{ctd} [MPa]	1.47	2.07
φ [°]	37	37
c [MPa]	2.83	4.69

Table 5: Initial properties for equivalent medium

Parameter	Shotcrete (1)	Steel sets (2)
E [MPa]	29516	200000
A [m ²]	33.23	0.00279
I [m ⁴]	0.000333	0.0000144

In contrast, literature research indicates that the secondary lining can be constructed using either reinforced or plain concrete. For both options, the designated concrete class is C30/35. However, in the case of reinforced concrete, steel reinforcement is specified with one $\phi 14$ bar placed both at the intrados and extrados with intervals of 0.33 m. Both structural types have a thickness of 0.8 m with linear elastic behavior. The equivalent properties used in the model are detailed in Table 6.

Table 6: Final lining parameters

Parameter	Plain concrete	Reinforced concrete
γ [kN/m ³]	24	25
E [MPa]	32837	33184
ν [-]	0.2	0.2
f_{ck} [MPa]	30	31.35
f_{cd} [MPa]	17	19
f_{ctd} [MPa]	2.88	2.98
ϕ [°]	37	37
c [MPa]	4.24	4.43

3.3. Model combinations

According to what is stated in previous chapter, one methodology is implemented for the rock mass deterioration and one model for the primary lining degradation. Nevertheless, since the focus is on the behavior of the primary support, two different types of analysis in this matter are considered: one performing the deterioration of only the primary lining and the other assuming that both rock and shotcrete are degraded.

Hence, considering also the rock mass types and different final lining compositions, different models are implemented with all these combinations and summarized in Table 7 in which X represents the case considered for that respective combination.

Table 7: Modelling combinations

Model	Degradation models		Rock mass types		Cross section cases		Composition of secondary lining	
	R.M.	P.L.	G.	P.	H.S.I.	H.S.N.I.	P.C.	R.C.
1	X	X	X		X		X	
2	X	X	X			X	X	
3	X	X		X	X		X	
4	X	X		X		X	X	
5		X	X		X		X	
6		X	X			X	X	
7		X		X	X		X	
8		X		X		X	X	
9	X	X	X		X			X
10	X	X	X			X		X
11	X	X		X	X			X
12	X	X		X		X		X
13		X	X		X			X
14		X	X			X		X
15		X		X	X			X
16		X		X		X		X

R.M.: Rock mass degradation model proposed by Showkati et al. (2021)
P.L.: Primary lining degradation model implemented by Ziller & Cont (2018)
G: Good quality rock mass material (high GSI from Table 3)
P: Poor quality rock mass material (low GSI from Table 3)
H.S.I.: Horseshoe with invert arch cross section exposed in Figure 5
H.S.N.I.: Horseshoe without invert arch cross section exposed in Figure 6
P.C.: Secondary lining composed of plain concrete
R.C.: Secondary lining composed of reinforced concrete

3.4. Computational stages

Following the process outlined in Chapter 2.5, 16 models are under varying conditions to investigate the effects of primary lining deterioration. The procedure implemented in this analysis is illustrated in Figure 9.

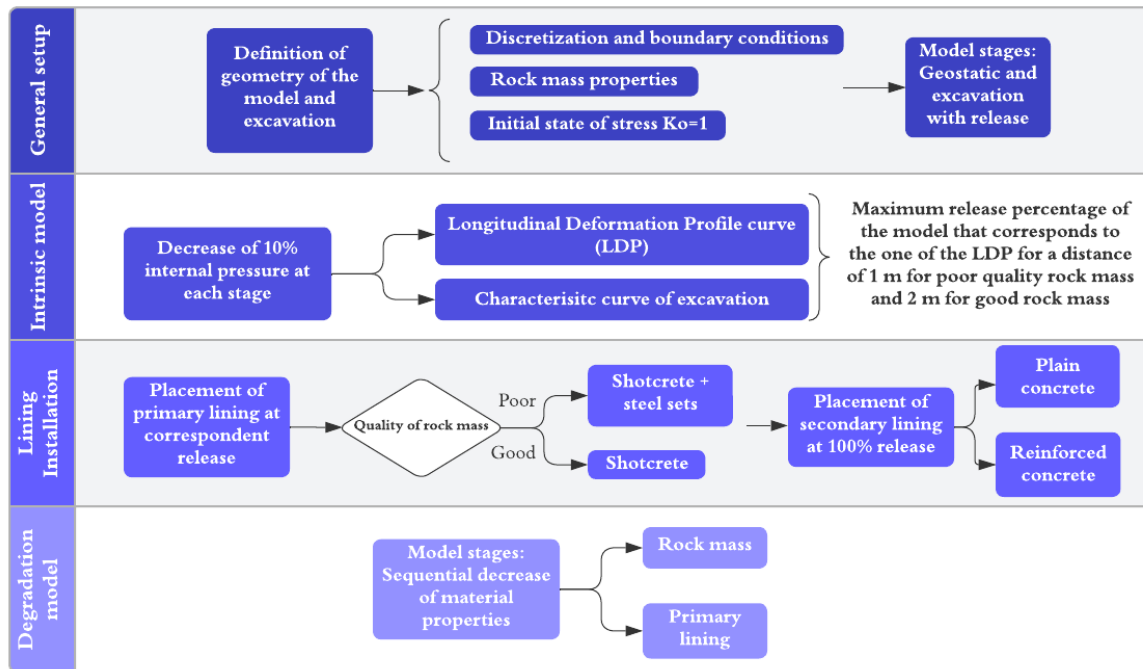


Figure 9: Modelling process

After defining the geometries and assigning the rock mass and lining properties to each model, 12 stages are incorporated to simulate the geostatic state, excavation, and internal pressure release in 10% increments. The pressure release is implemented by applying an induced stress load governed by stage factors that represent the gradual release.

Using two distinct geometries applied under different rock mass conditions, four models are developed initially to analyze the intrinsic conditions by measuring the radial displacements (u_{rx}) and internal pressure (p_i) at each stage at the tunnel crown and sidewalls. Figure 10 presents the characteristic curves for the intrinsic model, which serves as the baseline for models 1, 5, 9 and 13 considering a horseshoe-shaped tunnel with an invert arch geometry and good rock mass quality material. The same procedure is applied to the same geometry with poor-quality rock mass, as well as to a horseshoe-shaped tunnel with no invert arch with a rock mass characterized by both high and low GSI values.

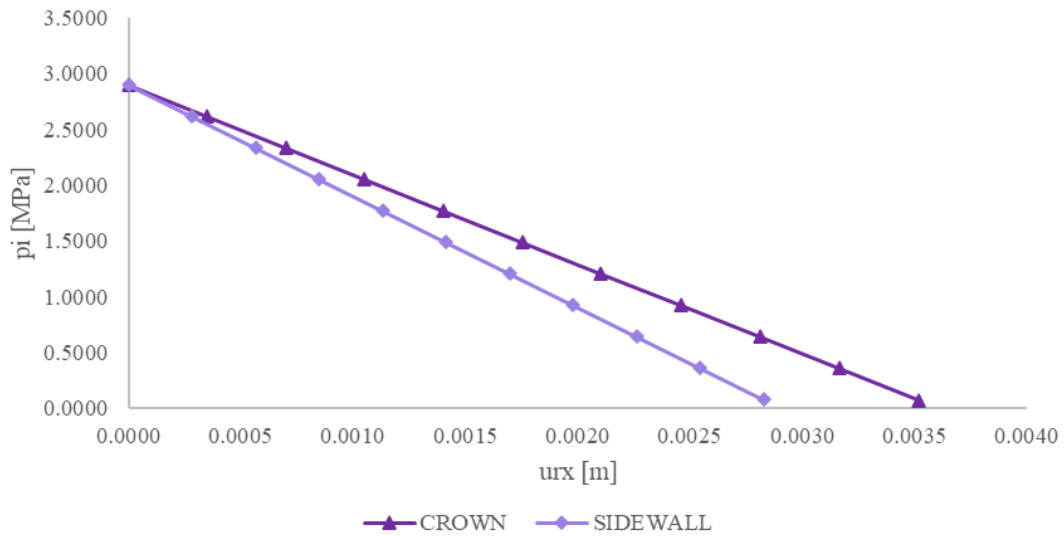


Figure 10: Characteristic curve of the intrinsic simulation for models 1, 5, 9, 13

Additionally, the plastic radius and radial displacement at total pressure released (i.e. p_i/p_0 equal to 100%) are taken for the realization of the LDP curves in order to implement the four approaches introduced in Paragraph 2.5.2

Figure 11 and Figure 12 illustrate the LDP curves at the tunnel crown and sidewalls respectively based on the intrinsic model used as starting point for models 1, 5, 9 and 13. These curves enable the determination of radial displacement at a certain distance from the tunnel face, which is then implemented to interpolate the internal pressure (p_i) from the characteristic curve. For this analysis, the distances considered are 1 m for the cases of poor-quality rock mass and 2 m for the cases of good quality of the rock mass.

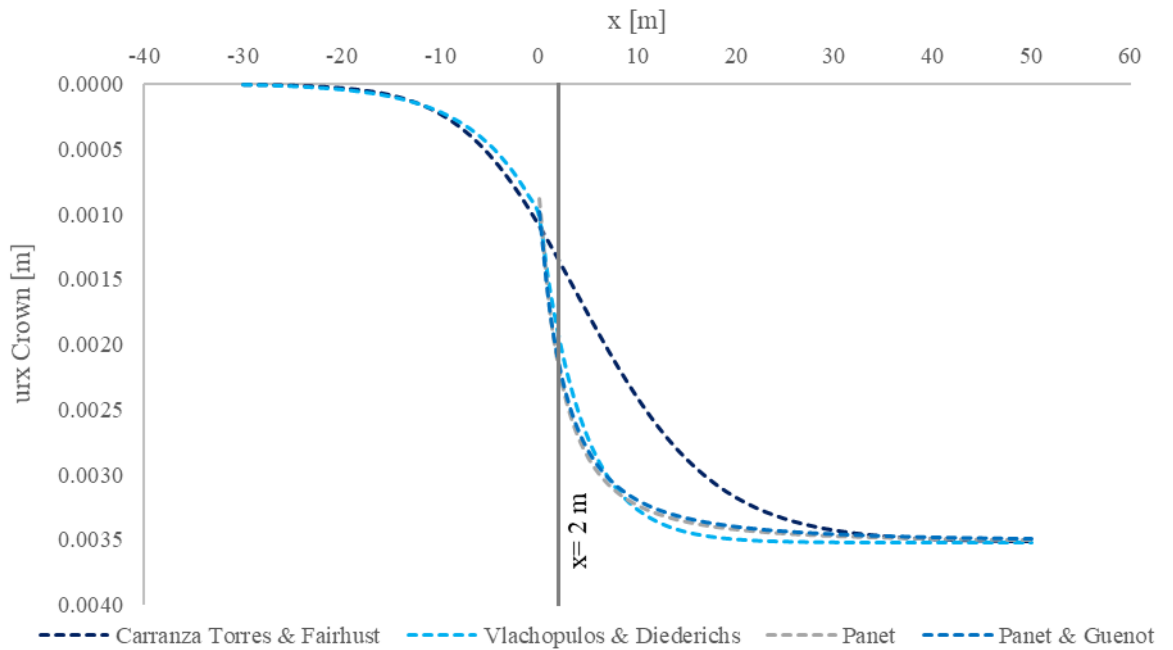


Figure 11: LDP curves of the intrinsic simulation for models 1, 5, 9, 13 at the tunnel crown

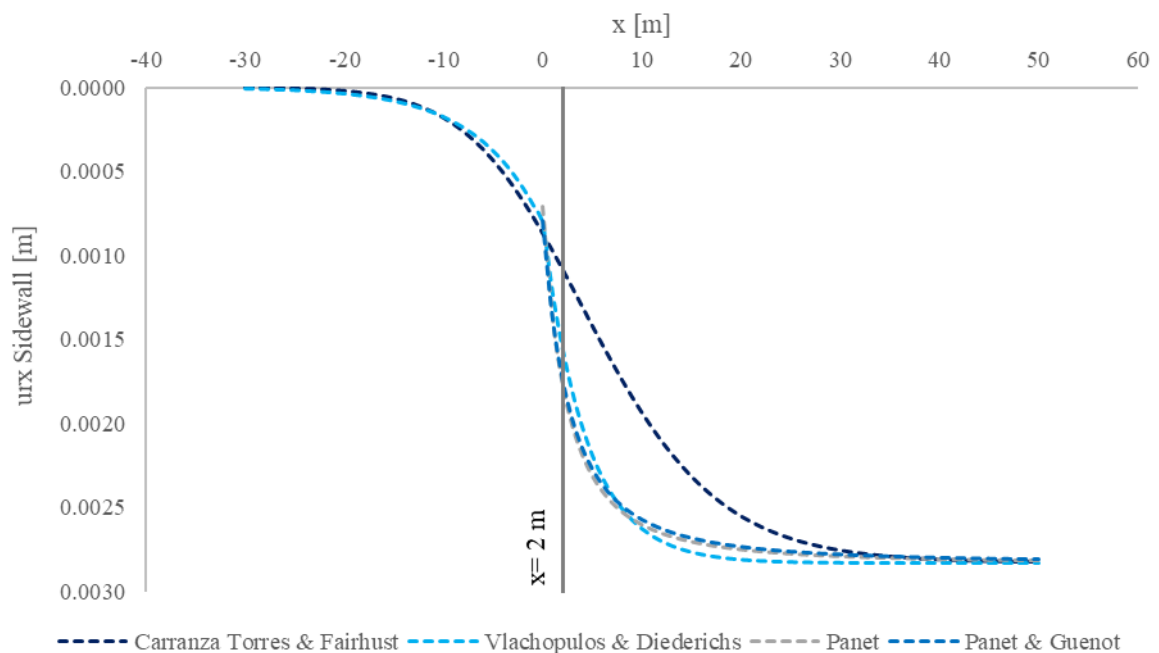


Figure 12: LDP curves of the intrinsic simulation for models 1, 5, 9, 13 at the tunnel sidewall

For the intrinsic model which serves as the baseline for models 1, 5, 9 and 13, the maximum internal pressure reaches up to 60% for both tunnel crown and sidewalls considering the Panet (1995) approach as shown in Table 8. Despite variations in

geometry and rock mass material across the four intrinsic simulations, in all of them, the maximum internal pressure release consistently reaches 60%. Consequently, in all models, the primary lining is installed at the stage when 40% of the induced stress load is applied, corresponding to a 60% release of internal pressure.

Table 8: Computation of release percentage of the intrinsic simulation for models 1, 5, 9, 13

		u_{rx} [m]	p_i [MPa]	λ [-]	% Pressure release
CROWN					
Carranza Torres & Fairhust	at 2 m	0.001350	1.81	0.38	37.50
Vlachopoulos & Diederichs	at 2 m	0.001933	1.34	0.54	53.69
Panet	at 2 m	0.002187	1.14	0.61	60.71
Panet & Guenot	at 2 m	0.002157	1.16	0.60	59.89
SIDEWALL					
Carranza Torres & Fairhust	at 2 m	0.001085	1.81	0.37	37.41
Vlachopoulos & Diederichs	at 2 m	0.001554	1.35	0.54	53.58
Panet	at 2 m	0.001758	1.14	0.61	60.63
Panet & Guenot	at 2 m	0.001734	1.17	0.60	59.80

In this way the primary and final linings are placed at the 60% and 100% of release respectively and then the degradation starts to take place in new inserted computational stages.

For this research the degradation at 0, 25, 50, 75 and 100 years is analyzed. Following the selected methodologies of degradation from Ziller & Cont (2018) and Usman & Galler (2013) for the primary lining and from Showkati et al. (2021) for the rock mass. In Table 9 and Table 10 are exposed the stage factors and decrease of parameters for each case.

Table 9: Degradation of primary lining properties at the new stages

t [years]	Ec [MPa]	Stage factor Ec	ϕ' [°]	Stage Factor ϕ'	c' [MPa]	Stage factor c'
SHOTCRETE						
0	29516.70	1	37.00	1.00	2.83	1.00
25	25143.33	0.85	31.04	0.84	2.26	0.80
50	20163.97	0.68	24.29	0.66	1.70	0.60
75	14443.30	0.49	16.75	0.45	1.13	0.40
100	7802.45	0.26	8.56	0.23	0.57	0.20
SHOTCRETE AND STEEL RIBS						
0	33648.00	1	37.00	1.00	4.69	1.00
25	28662.51	0.85	31.04	0.84	3.75	0.80
50	22986.21	0.68	24.29	0.66	2.81	0.60
75	16464.85	0.49	16.75	0.45	1.87	0.40
100	8894.52	0.26	8.56	0.23	0.94	0.20

Table 10: Degradation of rock mass properties at the new stages

t [year]	E [MPa]	Stage Factor E	ϕ' [°]	Stage Factor ϕ'	c' [MPa]	Stage Factor c'
GOOD QUALITY ROCK MASS						
0	7600.00	1.00	28.00	1.00	2.70	1.00
25	5449.24	0.72	22.73	0.81	2.13	0.79
50	5004.49	0.66	21.58	0.77	2.01	0.74
75	4741.16	0.62	20.89	0.75	1.94	0.72
100	4553.43	0.60	20.40	0.73	1.89	0.70
POOR QUALITY ROCK MASS						
0	1600	1.00	22.50	1.00	0.020	1.00
25	1147.21	0.72	18.07	0.80	0.02	0.79
50	1053.58	0.66	17.13	0.76	0.01	0.74
75	998.14	0.62	16.56	0.74	0.01	0.72
100	958.62	0.60	16.16	0.72	0.01	0.70

Chapter 4

Analysis of the results

In this chapter, a comprehensive analysis is presented, comparing the results obtained from all the 16 models carried out in terms of tangential stresses and displacements, axial forces and bending moments over a time span of 0, 25, 50, 75 and 100 years. The main purpose is to establish the influence of different conditions that led to the differentiation of these models, including variations in cross sectional geometry, the quality and degradation of the rock mass and the composition of the final lining.

By evaluating these factors, this analysis aims to define a clear understanding of how each parameter impacts the structural behavior of the tunnel lining over time. The set of models allows a detailed representation of the interaction between the rock mass and the lining, offering insights into the long-term performance and stability of the tunnel under different geological and construction contexts.

A key observation across all models is the general trend of increasing stresses, displacements, axial forces and bending moments as the primary lining degrades over time. These findings align with the initial hypothesis in which there is a progressive load transfer between the primary and final lining as the first one degrades, causing an increase of stresses in the final lining.

This chapter provides a detailed overview of the specific impacts of different factors on the long-term structural integrity of the tunnel lining. The results presented here are crucial for understanding the correlation between design parameters and the aging process in tunnel engineering, serving as a foundation for future tunnel designs.

4.1. Influence of the excavation geometry

Figure 13 illustrates the evolution of displacements and yielded elements around the horse-shoe-shaped excavation with an invert arch over time for Model 1 (PC_RM_PL_G_HSI), which assumes good rock mass quality, and accounts for the degradation of both primary lining and rock mass. The color scale on the right indicates the magnitude of total displacement, ranging from blue (minimal displacement) to red (maximum displacement).

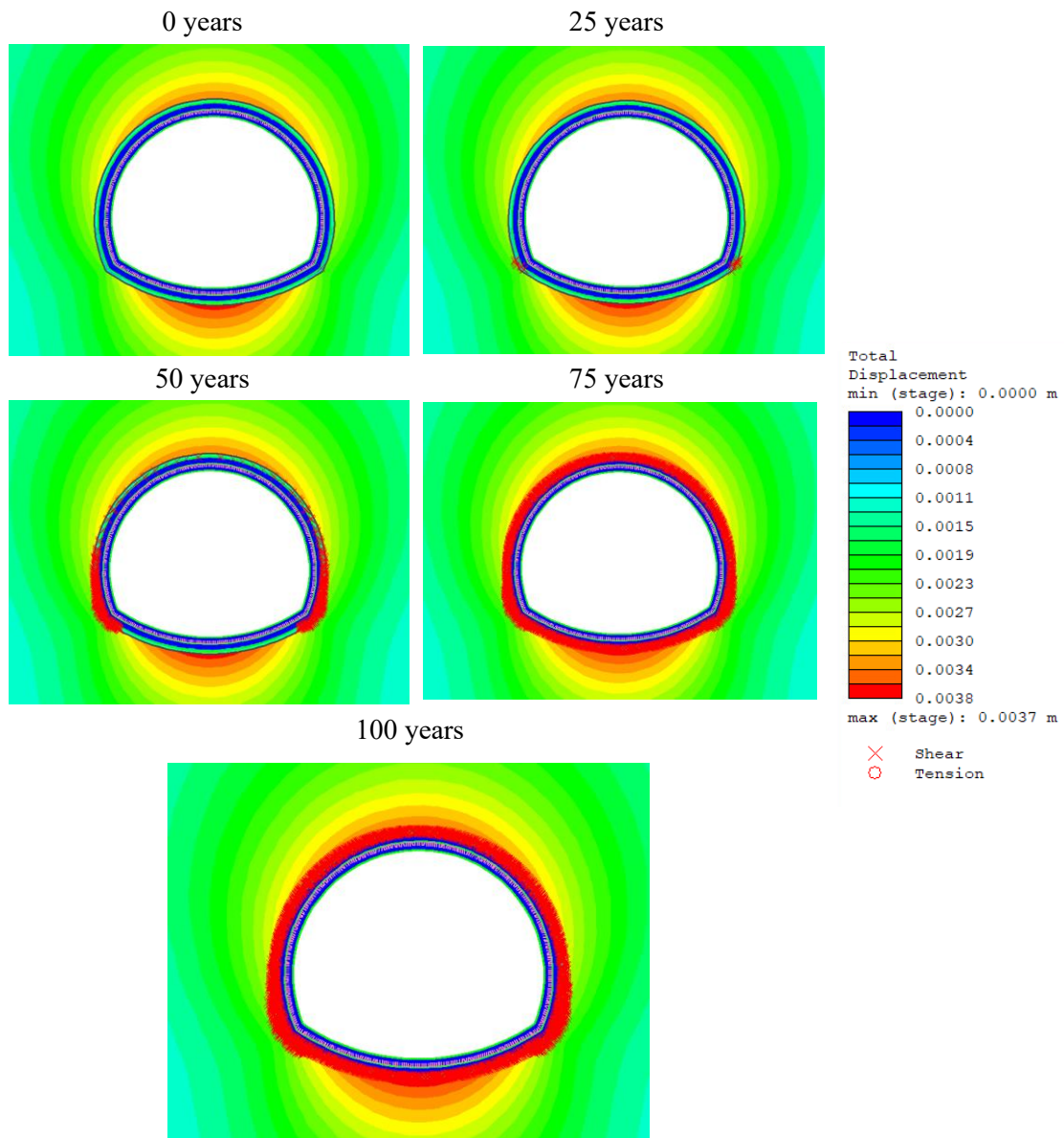


Figure 13: Evolution of displacements and yielded elements for Model 1

At initial conditions (i.e. 0 years), the contour plot indicates that displacement is predominantly concentrated at the top (crown) and bottom (invert) of the tunnel lining, with minimal yielded elements observed around the excavation. At this early stage, the structural integrity of the tunnel lining appears intact, showing no significant signs of stress or deformation. The surrounding rock mass remains unaffected as well, indicating that the primary lining is effectively bearing the load.

As time progresses, the contour plots for 25, 50 and 75 years illustrate a gradual deterioration of the tunnel primary lining. During this intermediate period, the displacements begin to increase particularly around the critical areas of the crown and invert. However, the highest sign of degradation is observed in the formation of the yielded elements in the rock mass surrounding the primary lining, more specifically at the

sidewalls, suggesting that the primary lining begins to lose its ability to effectively distribute the loads, leading to localized failures.

In the long term, particularly between 50 and 75 years, the displacement values reach their peak, with the plots showing that the entire excavation is surrounded by a zone that already reaches yielding, evidencing the lack of structural functionality of the primary lining at these stages.

In contrast, for a horse-shoe-shaped excavation without an invert arch, as represented in Model 2 (PC_RM_PL_G_HSNI), the development of displacements is indicated in Figure 14; **Error! No se encuentra el origen de la referencia..** In this case, the critical zone is primarily located at the invert, where displacements can reach up to 5.4 mm during degradation at the long-term.

By comparing this geometry to the previous model exposed with an invert arch, it becomes evident that this geometry configuration experiences a more abrupt change related to the presence of yielded elements. At 50 years the primary lining still presents full structural integrity while at 75 years the entire contour has already yielded. This suggests a less gradual failure process compared to the excavations that include an invert arch.

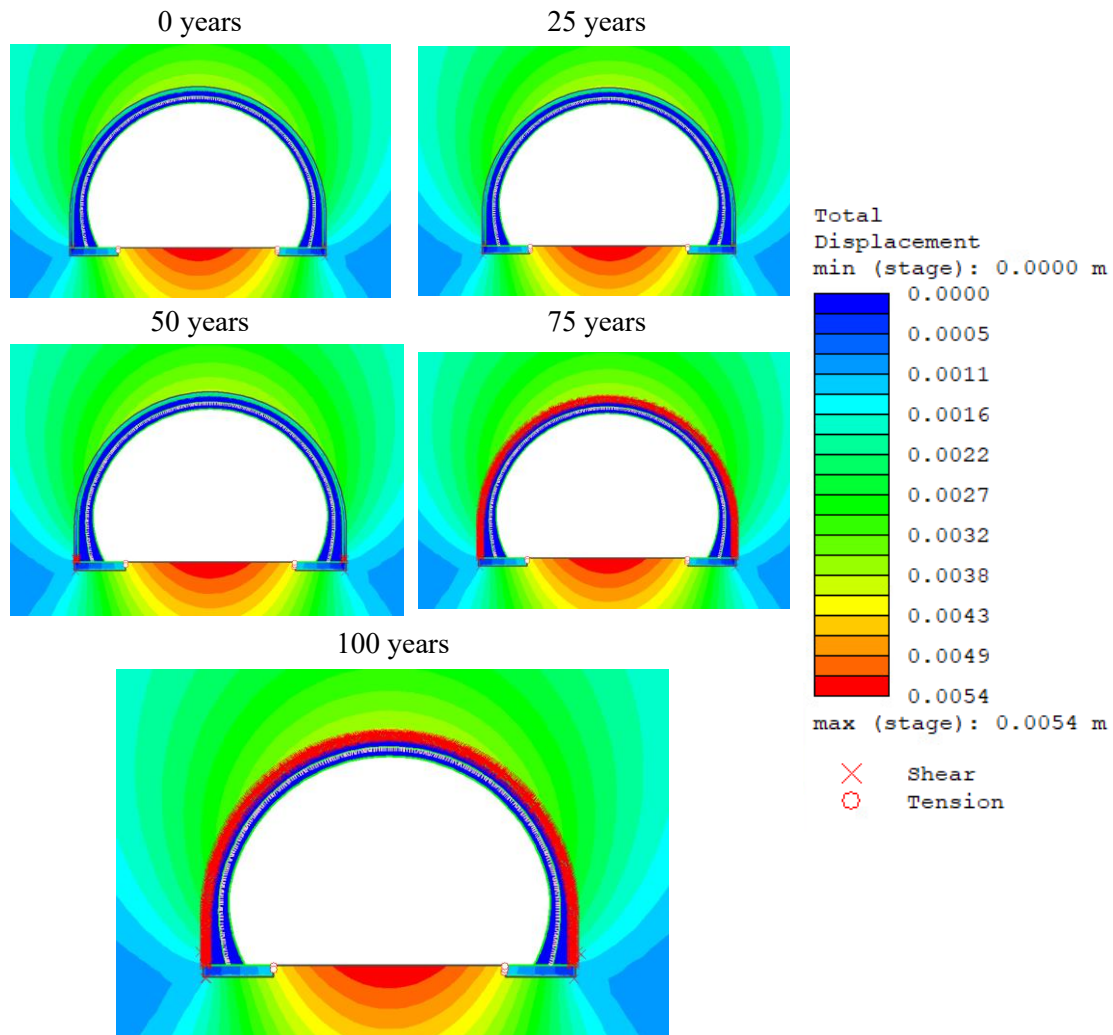


Figure 14: Evolution of displacements and yielded elements for Model 2

This pattern of progressive degradation and displacement for both geometries is consistent across all the models evaluated in this study. It highlights the significant time-dependent nature of tunnel lining degradation for any scenario. Nevertheless, it is important to note that in cases involving poor-quality rock mass, the load transfer is more gradual around all the stages, whereas for a good-quality rock mass, the significant effect is observed at the long-term stages. A more detailed analysis of these findings will be provided in the following paragraphs.

Additionally, when a change in excavation geometry is considered, Model 5 (Figure 15) and Model 6 (Figure 16) can be compared to analyze its overall influence. The change in the cross section as previously illustrated consists mainly of the presence of an arch in the invert of the tunnel.

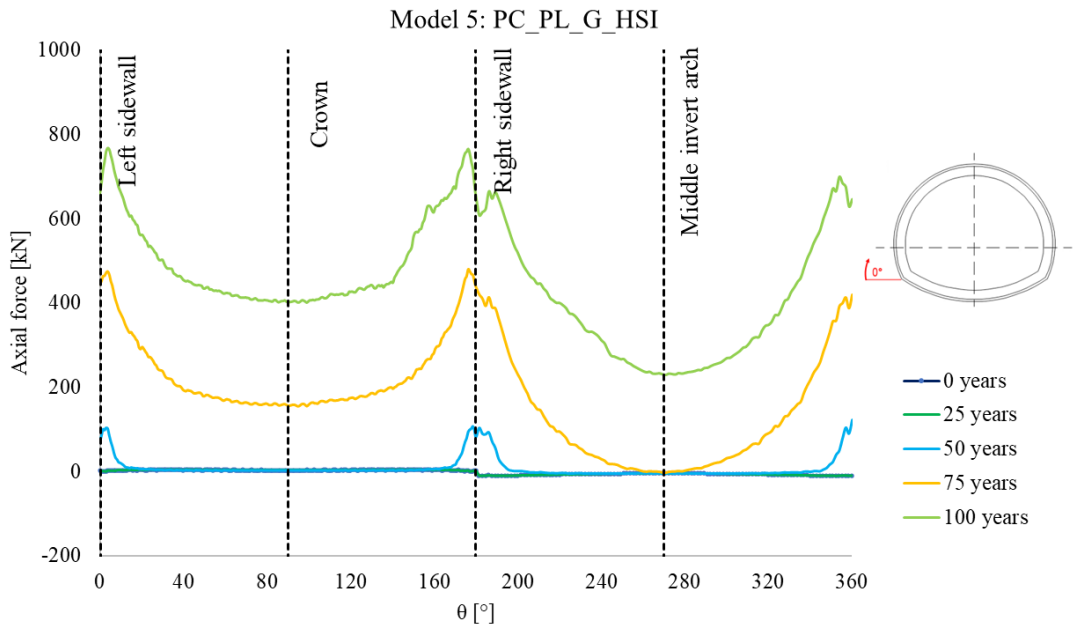


Figure 15: Axial force in the final lining of Model 5

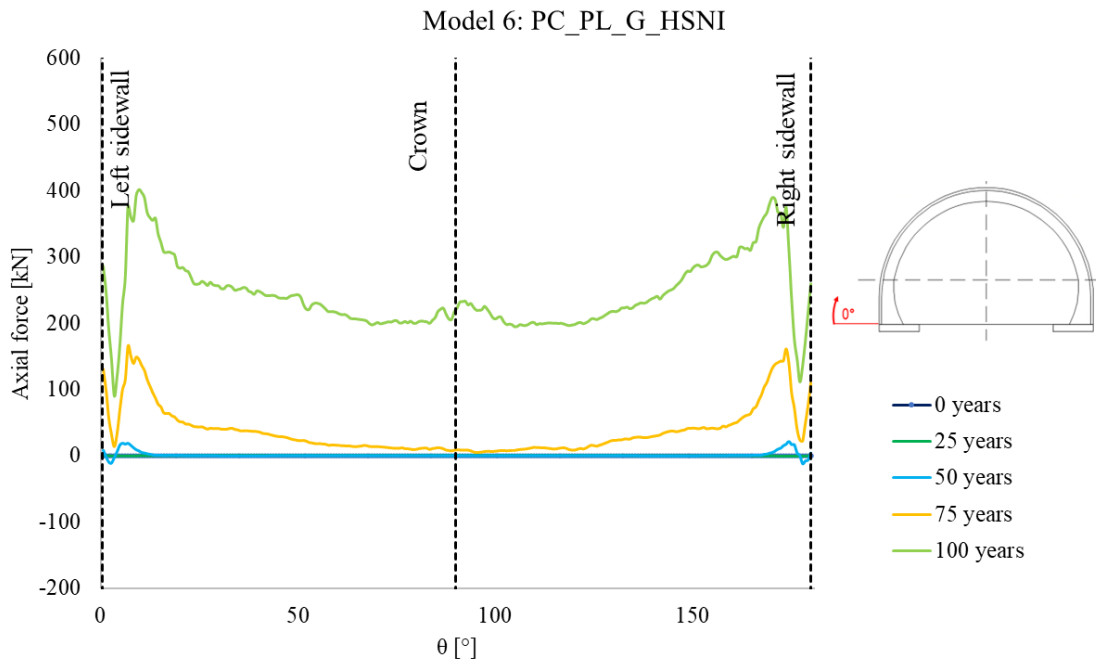


Figure 16: Axial force in the final lining of Model 6

In the case of the cross section with an invert arch, such as in Model 5, the axial forces are generally higher, particularly near the sidewalls where they reach a maximum of nearly 800 kN after 100 years of degradation. At the crown, axial forces increase over

time, reaching more than 500 kN for the 100-year mark. In addition, the forces in the middle invert arch are clearly visible and increased over time, which indicates that the invert arch plays a significant role in distributing these forces.

Differently, Model 6, which features a cross section without an invert arch, exhibits lower overall axial forces compared to Model 5. While axial forces are still substantial, they only reach about 400 kN in the sidewall area after 100 years of degradation. The crown in this model shows less accumulation of axial forces over time.

The presence of the invert arch in Model 5 greatly enhances the tunnel's stability by distributing axial forces more evenly and reducing the load at the crown. Without the invert arch, as in Model 6, the sidewalls bear the majority of the load. Although the forces are lower than in the continuous lining models (e.g., Model 5), the absence of the invert arch results in significantly higher displacements, potentially doubling those seen in tunnels with a continuous lining. By analyzing the bending moments, the values are significantly higher for the cross section without a continuous lining provided by the invert arch

In terms of tangential stresses and displacements, the degradation over time has little effect on the section without an invert arch. In contrast, for the cross section with an invert arch, bending moments noticeably increase after 50 years due to the deterioration of the primary lining.

It is important to note that, for a poor-quality rock mass, the difference between the two cross sections (with and without invert arch) is almost null along the years, with both exhibiting similar levels of stress and displacement while the degradation takes place. This highlights the critical role of rock mass quality in tunnel behavior, especially over long periods.

4.2. Degradation of primary lining and influence of the rock mass degradation

As previously mentioned, the deterioration of primary lining properties results in an inverse effect on the stresses and displacements in the final lining. Specifically, as the strength and deformability properties of the primary lining are reduced in time, the stresses and displacements in the final lining increase.

When analyzing the impact of the rock mass degradation, each type of model is conceived with and without the degradation of the geological material. For example, by comparing the axial force of two models under identical conditions except that one includes rock mass degradation (Model 3, Figure 17) and another does not (Model 7, Figure 18), a significant difference is observed.

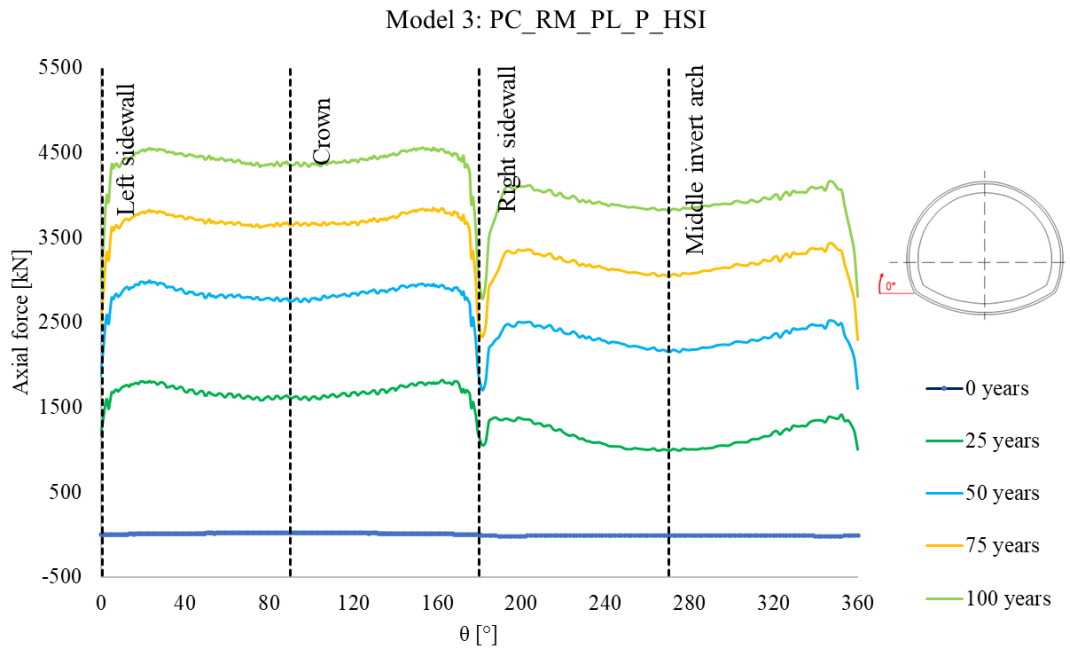


Figure 17: Axial force in the final lining of Model 3

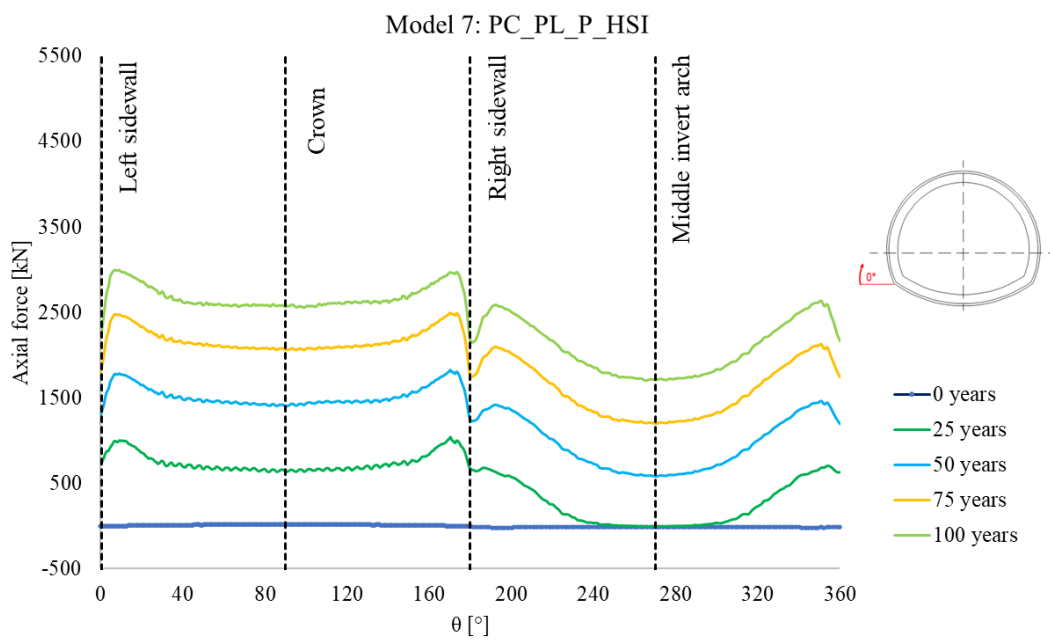


Figure 18: Axial force in the final lining of Model 7

For the case of Model 3, the forces increase progressively over time, where after 0 years the forces are null across all the section. Nevertheless at 100 years, the forces increase significantly, particularly at the sidewalls reaching up to approximately 4500 kN. The invert arch experiences less pronounced increases, though there is still a clear trend

of force growth with time, showing a strong degradation impact. In contrast, for Model 7 in which no rock mass degradation takes place, even though the force also increases progressively over time, the overall scale is significantly lower, since the forces range from 0 kN at 0 years to 3000 kN at 100 years, notably less than for Model 3. The sidewalls still bear the highest forces, but the overall magnitude of force increase is less severe compared to when degradation is considered.

In terms of stress, displacements and bending moments, which are also analyzed in this study the trend is similar. However, the importance of the rock mass quality plays a major role in the effects of the degradation of this material, since for a good-quality rock mass the increase of stresses is minimum over the years, especially for a horse-shoe-shaped excavation without invert arch. This analysis will be deeply explained in the following subchapters. The detailed results used for the analysis can be found in the excel files provided in Appendix B.

4.3. Influence of the rock mass quality

To analyze the effect of rock mass quality on the lining as the primary lining degrades, we consider Model 2 (Figure 19) and Model 4 (Figure 20), as both models are identical except for the rock mass properties. This comparison highlights one of the most significant impacts of rock mass quality on tunnel degradation. In the case of good-quality rock mass, the effects of degradation only become noticeable after 50 years. In contrast, for poor-quality rock mass, there is a steady increase in degradation starting as early as year 25. This demonstrates how rock mass quality plays a crucial role in the rate and extent of degradation over time.

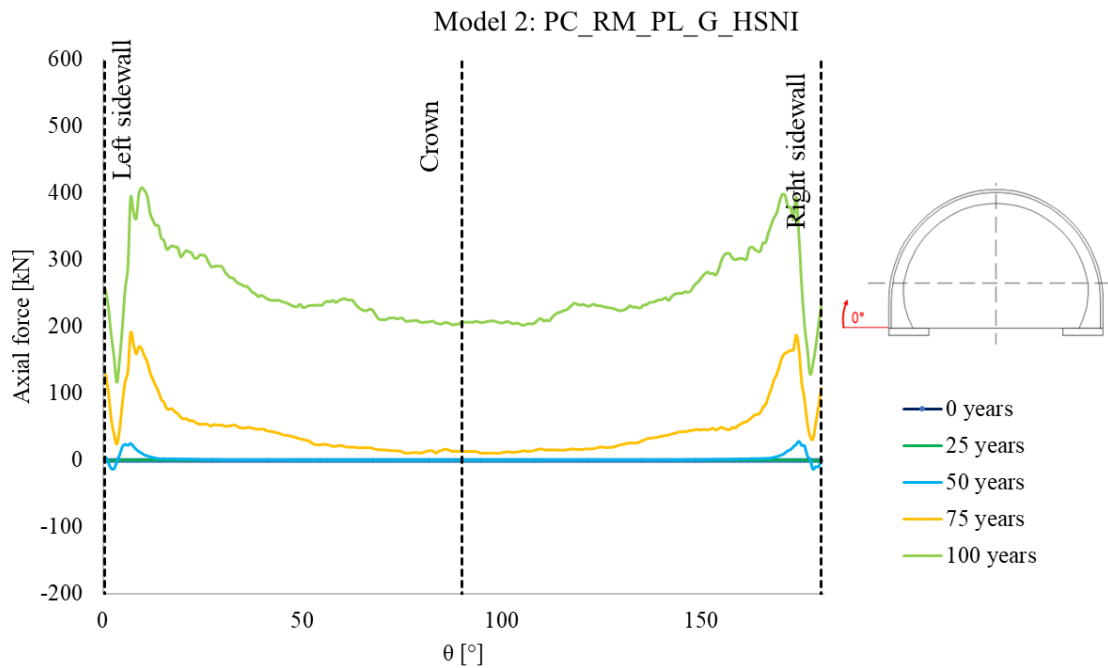


Figure 19: Axial force in the final lining of Model 2

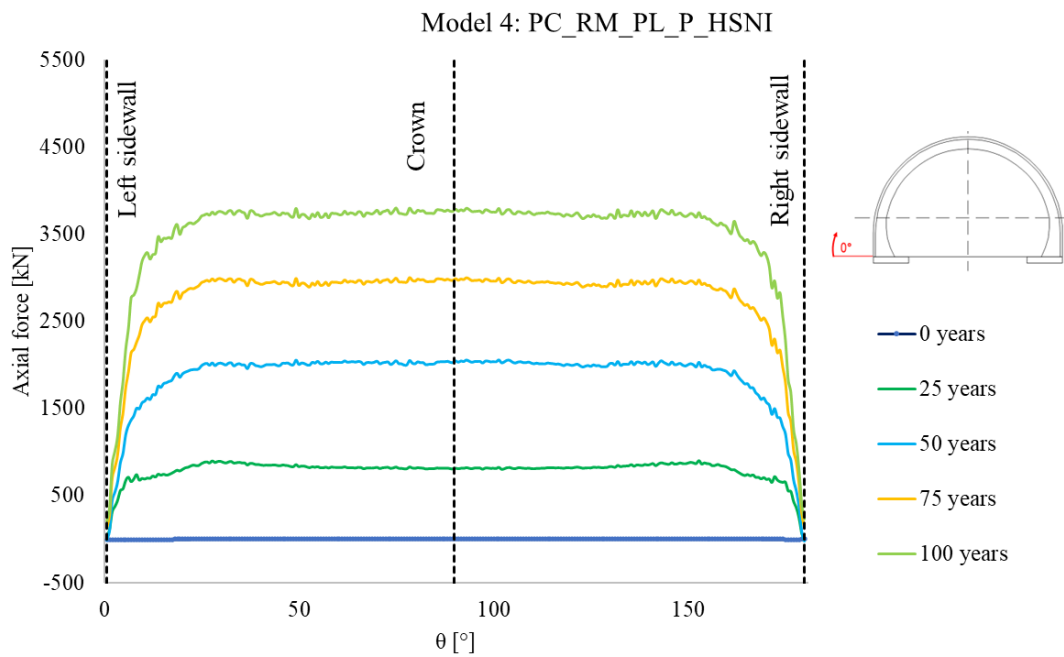


Figure 20: Axial force in the final lining of Model 4

In detail, Model 2 having a good quality rock mass, the axial forces in the tunnel lining are much smaller in magnitude reaching 400 kN on the sidewalls after 100 years. The sidewalls experience the highest forces, but even at 100 years the forces remain moderate compared to the poor-quality rock mass model. Indeed, for model 4 the axial

forces increase dramatically, reaching values as high as 3500 kN at the sidewalls after 100 years, even at 25 years the forces are already significantly larger compared to the good rock mass model.

The key differences between the two models lie primarily in the magnitude of forces. In Model 4, which represents a poor-quality rock mass, the axial forces are significantly higher at every time interval compared to the good-quality rock mass. This highlights the substantial impact of rock mass quality on the stress distribution within the tunnel lining, with poor-quality rock masses leading to much higher forces and more effect of long-term degradation.

When it comes to bending moments, the influence of rock quality is even more pronounced. In rock masses with low GSI, bending moments increase exponentially over time, specifically at the sidewalls, where the degradation over time is most evident. Although small fluctuations occur at the crown, the bending moment there is almost negligible compared to those at the sidewalls, which bear a significant portion of those forces. This abrupt increase in bending moments along the cross section is mostly observed in tunnels without an invert arch. In contrast, for tunnels with a continuous lining (i.e., including an invert arch), bending moments are significantly lower, even in poor-quality rock masses.

The type of rock mass also has a notable effect on circumferential displacements. For poor quality rock, displacements increase as degradation progresses, reaching values up to three times higher than those in good-quality rock, even at the 100-year mark. On the contrary, for high-GSI rock mass, displacement changes are almost negligible in time, particularly in tunnels without an invert arch.

Similarly, tangential stresses behave as displacements. In poor-quality rock, the evolution of tangential stresses is more pronounced, with values potentially tripling by 100 years, evidencing much higher impact on tunnel stability in poor-quality rock masses. More detailed data implemented in the analysis for bending moments, stresses and displacements is available in Appendix B.

4.4. Influence of the presence of steel reinforcement

The presence of steel reinforcement in the final lining is briefly analyzed to determine under which conditions the final lining is verified under the degradation conditions of the primary one. For the case of a plane concrete (i.e. no steel reinforcement), which applies to the first eight models in this analysis, the verification is carried out according to NTC 2018 standards, where the resisting axial and shear forces computed must exceed the acting ones. A simplification was performed for the verification of the shear force, since

it requires calculating the axial force at every point along the lining, therefore, the maximum axial force was implemented to compute the minimum requested shear force.

For instance, Figure 21 and Figure 22 illustrate the axial and shear force verifications, respectively, for the cross section with an invert arch (H.S.I) after 100 years of degradation, representing the worst scenario. A continued line represents the results of acting forces for each model, while the red dotted one is the resistant force that is verified.

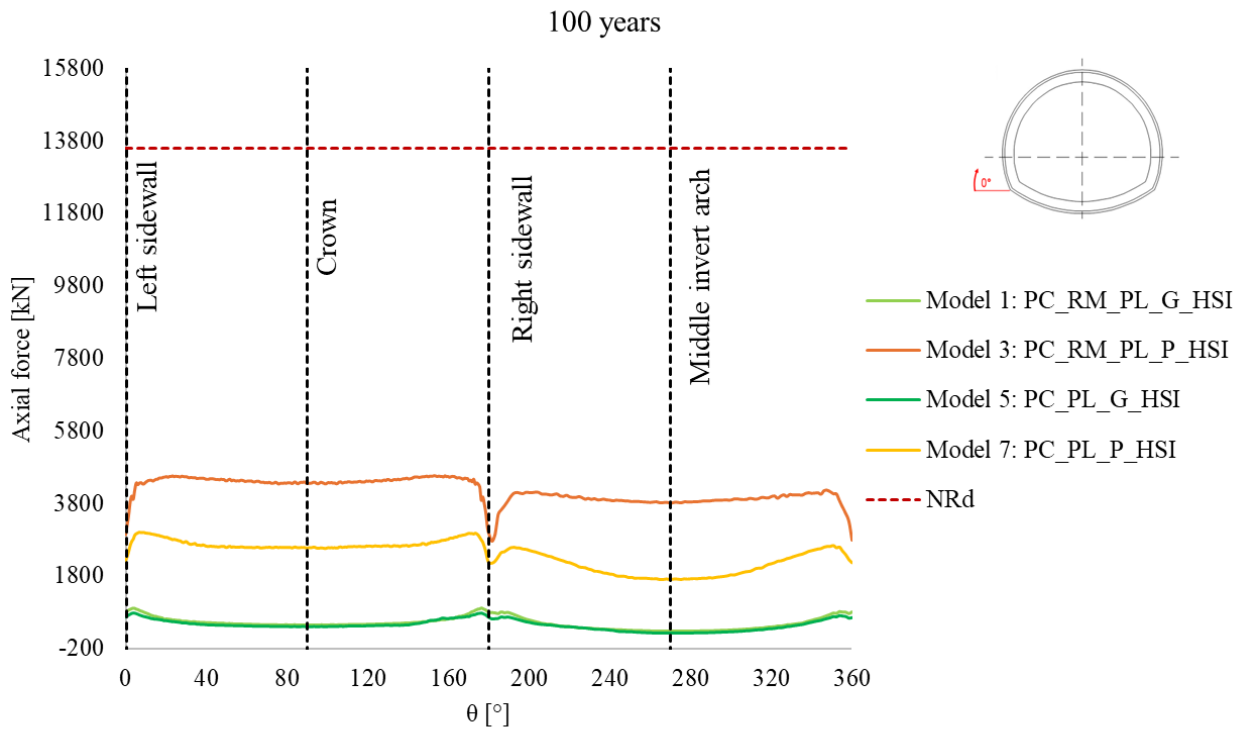


Figure 21: Verification of Axial force at 100 years of degradation for the H.S.I. section

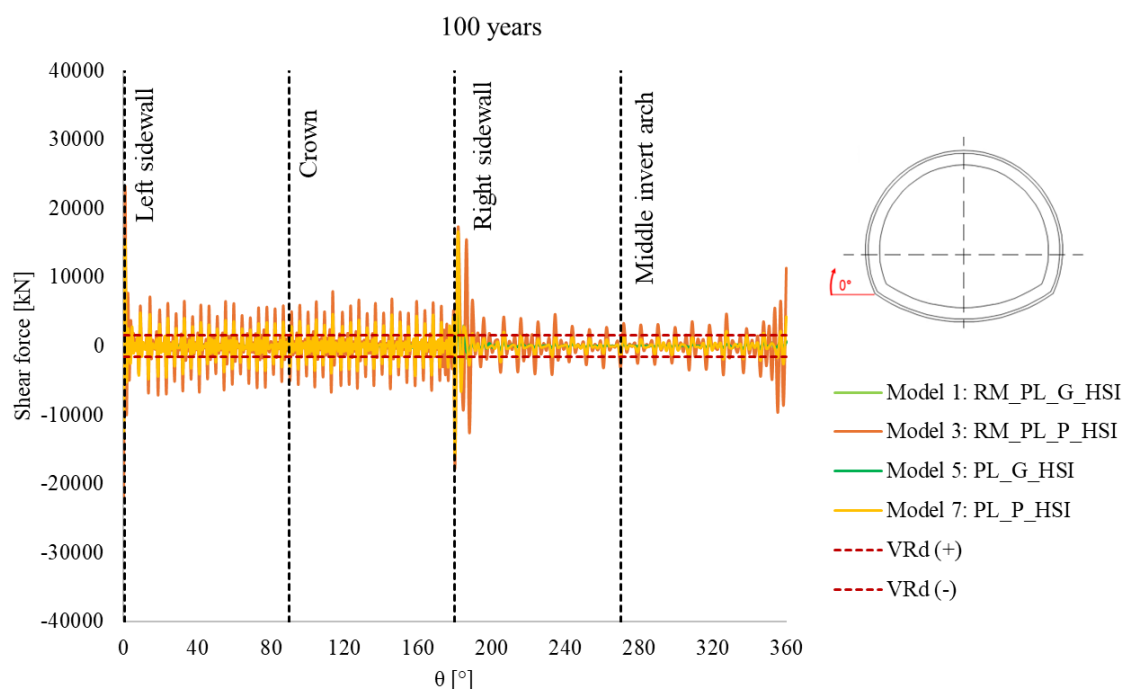


Figure 22: Verification of Shear force at 100 years of degradation for the H.S.I. section

For the case of axial forces, the section is fully verified across all the models and conditions. In contrast, for shear forces Model 3 and Model 7, both involving poor-quality rock mass, do not comply with the verification across the section. This issue occurs after 25 years of degradation in both cross-section geometries with poor rock mass quality.

On the other hand, in models under equal conditions, a reinforced concrete final lining is placed, and its verification is performed through interaction diagrams. The results analyzed every 25 years evidence that the section is verified for all the models throughout the lining with one exception: at the base of the sidewalls in Model 11 which involves poor-quality, degraded rock mass in a horseshoe section with invert arch. As illustrated in Figure 23, the final lining in this case is not verified after 25 years of degradation.

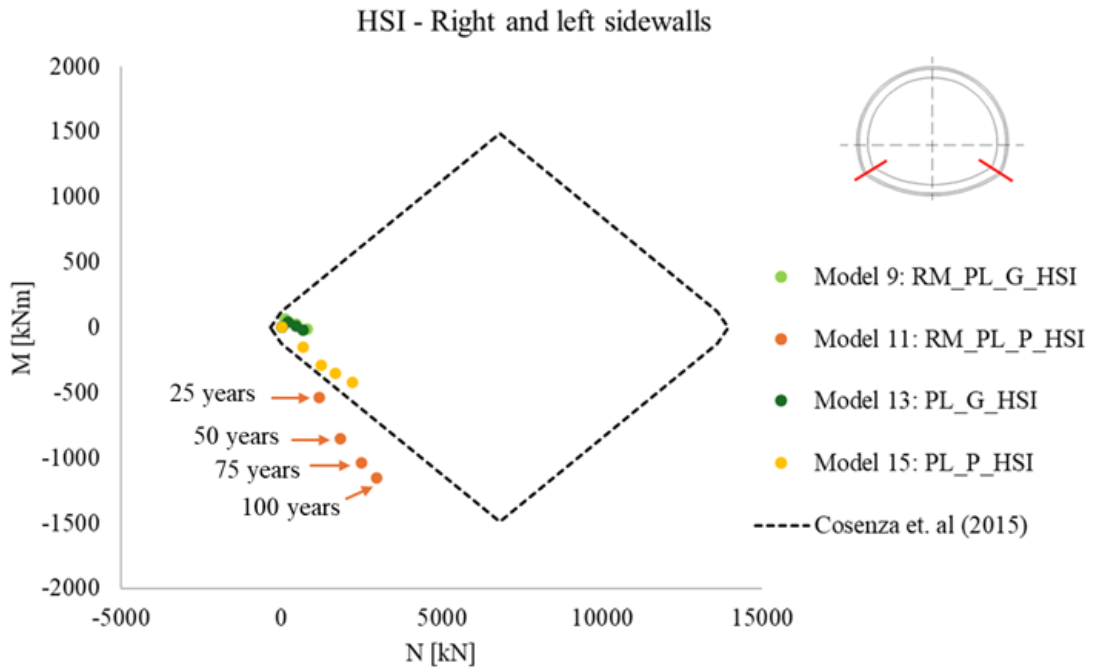


Figure 23: Interaction diagram for the HSI section at the beginning of sidewalls

4.5. Results overview

To provide a clear visualization and comparison of all the analyzed models, Figure 24 and Figure 25 are presented. These plots display the axial forces in the final lining over time under rock mass degradation in some cases and primary lining degradation, focusing on the sidewall and crown, which were previously identified as the most critical areas along the cross-section. The dotted lines in blue represent the models regarded as the horseshoe with invert arch (H.S.I.) cross section and the ones in green constitute the geometry of horseshoe without invert arch (H.S.N.I.).

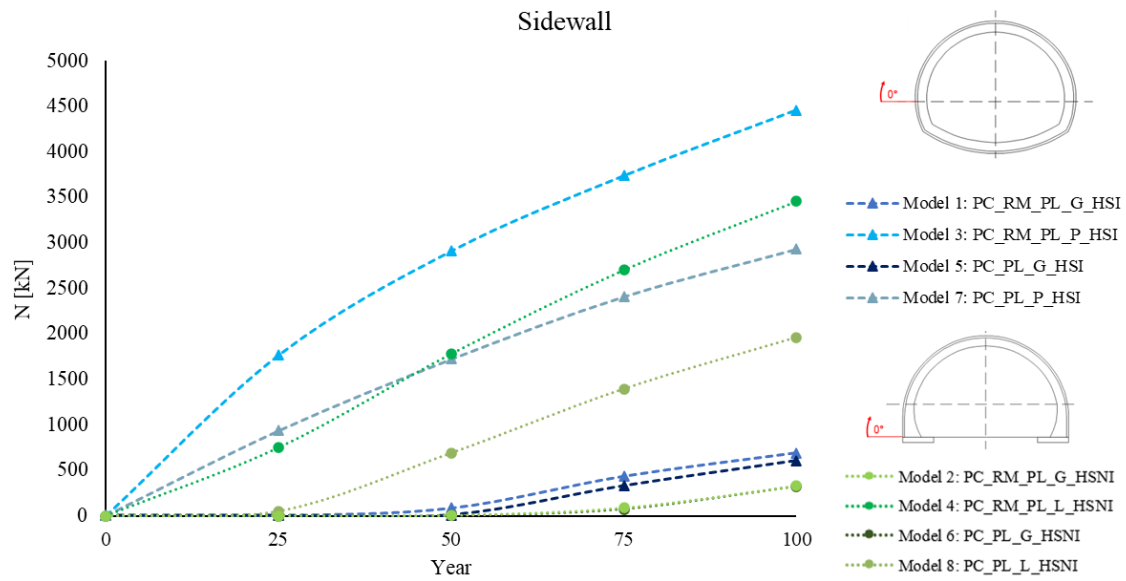


Figure 24: Evolution of axial force in time at the sidewall

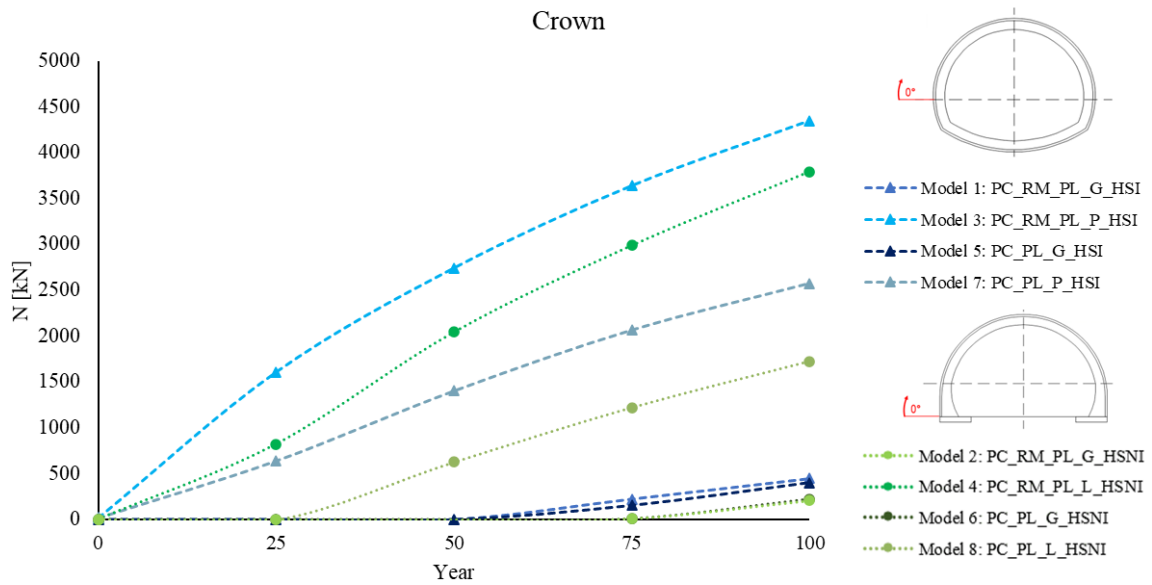


Figure 25: Evolution of axial force in time at the Crown

A similar behavior is observed in both graphs where models with a continuous final lining (H.S.I) experience higher axial forces compared to H.S.N.I models under similar conditions. For instance, Model 3 shows higher axial forces than Model 4 where the only difference of conditions between them is the cross section. However, this trend differs when displacements are analyzed, since the absence of the invert arch causes the final lining to experience displacements even at the earliest stages of degradation.

This highlights the role that geometry plays in determining the influence of primary lining degradation on the axial forces experienced by the final lining, as well when load transfer begins. For example, in Models 7 (H.S.I) and 8 (H.S.N.I) which share the same condition except for geometry, axial forces in the final lining begin to increase at 0 and 25 years respectively.

Furthermore, the quality of the rock mass has an even more significant impact on increasing forces in the lining than rock mass degradation itself. This is evident in Models 7 and 8 which feature low quality but non-degraded rock mass and experience the second-highest stresses with only the low quality degraded rock mass models experiencing the highest stresses. Alternatively, Models 1 and 2 which feature good-quality degraded rock mass show minimal force increase over the 100-year analysis period. This suggests that rock mass degradation has influence only if the rock mass is low-quality.

It is important to remark that regardless of degradation or geometry, models with a good-quality rock mass exhibit minimal force changes, and that the influence of primary lining degradation becomes significant only after 50 years. In contrast, models with lower-quality rock mass experience increased axial forces much earlier, suggesting that primary lining degradation has a limited impact on load transfer between linings in high quality rock conditions.

To further demonstrate the influence of the primary lining degradation across all variables (e.g. stress, displacement, axial force and bending moments), Tables from Table 12 to Table 15 are provided. These tables offer a qualitative representation for both sections having plain concrete as final lining, highlighting the impact of primary lining degradation as each variable is measured. Table 11 illustrates the legend used in these tables, which categorizes the after-stage at which each variable begins to increase. This categorization is based on the stage when most of the final lining notice significant changes. For instance, a section in dark red, indicates that for that geometry, the effects are visible immediately after the 0 year-stage, light red indicates changes at 25 years, yellow after 50 years, light green section experiences effects in terms of this variable after 75 years and dark green experience any significant changes even after 100 years.

Table 11. Legend of tables 13 to 16








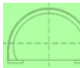

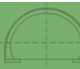
	H.S.I	H.S.N.I
Very high influence		
High influence		
Medium influence		
Low influence		
Very low influence		

Table 12: Influence of degradation on the Axial Force across the different models


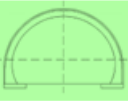






Axial force		Rock mass quality			
		Good		Poor	
Rock mass degradation	Present				
	Not present				

Table 13: Influence of degradation on the Bending Moment across the different models







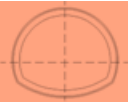

Bending moment		Rock mass quality			
		Good		Poor	
Rock mass degradation	Present				
	Not present				

Table 14: Influence of degradation on Stress across the different models




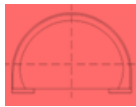
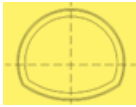
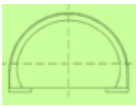
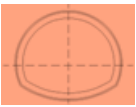

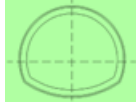
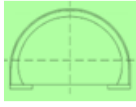
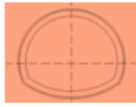
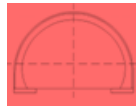
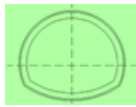
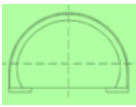


Stress		Rock mass quality			
		Good		Poor	
Rock mass degradation	Present				
	Not present				

Table 15: Influence of degradation on displacement across the different models

Displacement		Rock mass quality			
		Good		Poor	
Rock mass degradation	Present				
	Not present				

In this way, it becomes clearer that the bending moment is only affected by the rock mass quality regardless of its degradation. In contrast, tangential stress is influenced by both cross section and rock mass quality. However, in the case of sections without an invert arch, the rock mass quality influences highly the stresses due to the primary lining degradation, underscoring the importance of a continuous lining in this geotechnical scenario. The rock mass deterioration does not play an important role when change of stresses over time are analyzed.

In addition, displacement is significant in sections with poor-quality rock mass, especially in the H.S.N.I section. In such cases, the rock mass degradation considerably affects the impact of primary lining degradation. It is important to note that at none of the cases the variable remains intact (dark green section), meaning that at some point, even after 100 years the load transfer takes place and the effects are visible.

By joining all the matrices, it is possible to observe that the most vulnerable section among all is the non-invert arch one at low quality-degraded rock mass.

Chapter 5

Conclusions

The main objective of this research is to investigate the long-term degradation of primary linings and rock mass in tunnels implementing numerical modeling techniques. The analysis focused on the behavior of tunnels over a span of 100 years, considering the degradation of primary linings, variations in rock mass quality, and different tunnel cross-sectional geometries. The results of this study have important implications for tunnel design, particularly in relation to the overall stability of the aging infrastructure.

One of the most significant findings of this study is the impact of primary lining degradation on the structural behavior of tunnels. The results demonstrate that as the primary lining deteriorates, load transfer to the secondary lining increases. This is particularly evident from the axial forces and bending moments in models with degraded primary linings. For instance, in Model 1, which represents a horseshoe-shaped tunnel with an invert arch in good-quality rock mass, the axial force increased progressively over 100 years. After construction, the axial forces were minimal, however by 100 years, they had increased significantly, especially at the sidewalls, where forces reached 4500 kN. This load redistribution is crucial because it highlights that the secondary lining must be designed to bear significantly higher loads as the primary lining deteriorates. The evolution of displacements observed in this model (Figure 13 in Chapter 4) confirms that the primary lining loses its ability to effectively distribute loads, particularly after 75 years.

This finding validates the hypothesis that long-term deterioration of primary linings results in a progressive shift of load to the final lining. Moreover, this progressive degradation suggests that engineers should prioritize less conservative yet reliable secondary lining designs, accounting for the actual rate of degradation rather than assuming complete primary lining failure after a specific period.

The quality of the rock mass plays a crucial role in determining tunnel stability. In models with poor-quality rock masses, degradation effects are more pronounced and occur sooner compared to tunnels in good-quality rock masses. Model 3, for example, which considers the degradation of both the primary lining and the rock mass in poor-quality rock, shows a dramatic increase in axial forces, reaching 4500 kN by 100 years (Figure 15). In contrast, Model 7, which simulates the same tunnel but without rock mass degradation, shows significantly lower axial forces, maxing out at around 3000 kN.

This comparison underscores the importance of accounting for the rock mass's initial quality when designing tunnels. In poor-quality rock, even at the 25-year mark, noticeable degradation occurs, affecting both the rock and the tunnel structure. On the other hand, tunnels in good-quality rock masses experience much less degradation over time, with significant structural impacts only becoming apparent after 50 years or more.

The degradation model used in this study, adapted from Showkati et al. (2021), captures these changes in rock mass properties and provides a practical framework for estimating long-term rock mass behavior. In particular, the degradation of the rock mass is modeled to reduce both strength and deformability parameters by up to 40% and 30%, respectively, over a period of 100 years.

The cross-sectional geometry of the tunnel also plays a significant role in determining how degradation affects the tunnel structure. Tunnels with an invert arch (e.g., Model 1) demonstrate better overall stability and lower displacements compared to tunnels without an invert arch. In Model 2, which represents a tunnel without an invert arch, the critical zones are observed at the sidewalls and the invert. Over time, displacements in the invert can reach as high as 5.4 mm by the 100-year mark, which is a significant increase compared to the same model with an invert arch (Figure 14). In this case, the absence of the invert arch leads to an uneven distribution of forces, causing higher stresses and earlier structural deterioration. This finding suggests that the invert arch plays a critical role in enhancing the long-term stability of tunnels, particularly in cases where the rock mass is of low quality. In good-quality rock mass, the invert arch helps reduce the concentration of stresses, prolonging the tunnel's service life. The results are consistent across multiple models and show that geometries with invert arches perform better under long-term degradation conditions.

Reinforcement in the final lining is shown to significantly enhance tunnel stability, particularly in models where the primary lining has degraded considerably. In this study, reinforced concrete (RC) was compared to plain concrete (PC) in the secondary lining. Models with RC, such as Model 9, demonstrated better resistance to increased forces caused by primary lining degradation compared to those with PC.

For example, in Model 9, where RC was used in the final lining of a tunnel with good-quality rock, the increase in axial force over 100 years was much less dramatic than in models with PC linings. The reinforcement allowed for better force distribution, with the RC lining experiencing lower displacements and less stress concentration compared to the PC lining in a similar model (Model 5).

The reinforcement provided by steel bars in the RC linings (as specified in Table 6) was particularly effective in mitigating the effects of long-term degradation, especially in

the final 25 years of the analysis. This suggests that, where possible, reinforced linings should be favored in tunnel design to ensure long-term structural integrity.

The practical implications of this study are clear: tunnel designs must account for the long-term degradation of both the primary lining and the rock mass, particularly in poor-quality rock mass conditions. The results demonstrate that without adequate reinforcement and consideration of tunnel geometry, degradation can lead to significant structural issues that could compromise tunnel safety.

Furthermore, the use of advanced numerical models, such as the ones implemented in this thesis, allows for a more accurate representation of the long-term interactions between the tunnel lining and the surrounding rock mass. By using a combination of degradation models, such as those proposed by Showkati et al. (2021) for rock mass and Ziller & Cont (2018) for primary lining, engineers can create more realistic models of tunnel behavior over time. Consequently, for engineers assessing the current condition of a primary lining in an aging tunnel, the following steps are recommended to ensure a complete evaluation:

- Classify the tunnel cross-section and rock mass quality: This will help in identifying the case of study based on the specific interaction between the lining and the surrounding rock.
- Evaluate the potential rock mass deterioration: Assess whether the rock mass is degrading due to factors such as weathering or time-dependent behavior. Consider how these degradation mechanisms can affect the performance of the primary lining, since whether the deterioration is considered or not, can define varied results under similar loads.
- Based on the previous conditions (i.e. cross-section, rock mass quality and possible rock mass degradation), analyze how the primary lining may be affected and degraded over time.
- Assess the current condition of the final lining: if possible, compare its present state to the initial design specifications. Quantifying the change in stresses will help in forecasting future performance and estimating the potential decrease in lining capacity over time.

The findings of this research are particularly relevant for aging tunnel infrastructures, many of which were constructed decades ago and are now experiencing the effects of long-term degradation. The ability to predict when and how these structures will degrade is crucial for planning maintenance and reinforcing strategies. This study provides a robust framework for understanding these phenomena, contributing to safer and more sustainable tunnel designs.

References

- AITES. (2024). *Support systems*. <https://tunnel.ita-aites.org/en/how-to-go-underground/design/support-systems>
- Atkinson, A., & Hearne, J. A. (1989). Mechanistic Model for the Durability of Concrete Barriers Exposed to Sulphate-Bearing Groundwaters. *MRS Online Proceedings Library (OPL)*, 176, 149–156.
- Aziz, N., Craig, P., Nemcik, J., & Hai, F. (2014). *Rock bolt corrosion – an experimental study*. 123(2), 69–77. <https://doi.org/10.1179/1743286314Y.0000000060>
- Bae, G. J., Chang, S. H., Kim, D. G., & Park, H. G. (2006). Prediction of corrosion of fully cement-grouted rockbolts by chloride diffusion. *Tunnelling and Underground Space Technology*, 21, 450.
- Boidy, E. (2002). *Modélisation numérique du comportement différé des cavités souterraines*. L'UNIVERSITE JOSEPH FOURIER.
- Carranza-Torres, C. (2004). *Modeling composite sections (e.g., steel sets and shotcrete) with FLAC and Phase 2*. 1(February), 1–5.
- Carranza-Torres, C., & Fairhurst, C. (2000). *Application of the Convergence-Confinement Method of Tunnel Design to Rock Masses That Satisfy the Hoek-Brown Failure Criterion*. 15(2), 187–213.
- Colman, S. M. (1981). Rock-weathering rates as functions of time. *Quaternary Research*, 15, 250–264.
- Galler, R., & Lorenz, S. (2018). Support elements in conventional tunneling – Focus on long-term behavior. *Underground Space (China)*, 3(4), 277–287. <https://doi.org/10.1016/j.undsp.2018.01.009>
- Granata, M. F., Margiotta, P., & Arici, M. (2013). Simplified Procedure for Evaluating the Effects of Creep and Shrinkage on Prestressed Concrete Girder Bridges and the Application of European and North American Prediction Models. *Journal of Bridge Engineering*, 18(12), 1281–1297. [https://doi.org/10.1061/\(asce\)be.1943-5592.0000483](https://doi.org/10.1061/(asce)be.1943-5592.0000483)

- Huisman, M., Robert, H., Kenneth, G., & Nieuwenhuis, J. A. N. D. (2006). *Predicting Rock Mass Decay in Engineering Lifetimes : The Influence of Slope Aspect and Climate. XII*(1), 39–51.
- Kamel, T., Limam, A., Silvani, C., & Pellet, F. L. (2015). Modeling the degradation of old subway galleries using a continuum approach. *Tunnelling and Underground Space Technology*, 48, 77–93. <https://doi.org/10.1016/j.tust.2014.12.015>
- Kong, C., Wang, H., Zhao, K., & Gao, X. (2022). Numerical Simulation of Long-Term Deterioration of Rock Mass Supported by Shotcrete Lining. *Frontiers in Earth Science*, 10(May), 1–11. <https://doi.org/10.3389/feart.2022.891084>
- Kosmatka, S. H., Kerkhoff, B., & Panarese, W. C. (2002). Design and Control of Concrete Mixtures. *Design and Control of Concrete Mixtures*.
- Ladanyi, B. (1974). Use of the long-term strength concept in the determination of the ground pressure on tunnel lining. *3rd ISRM Congr*, 1150–1156.
- Liu, C., Zhang, D., Zhang, S., Fang, Q., & Sun, Z. (2023). Long-term mechanical analysis of tunnel structures in rheological rock considering the degradation of primary lining. *Underground Space (China)*, 10, 217–232. <https://doi.org/10.1016/j.undsp.2022.10.005>
- Modlhammer, H.-M. (2011). *Numerical Methods for Tunneling using ABAQUS and Investigations of Long-Time- Effects of the Shotcrete Shell and its Impact on the Combined Support System*. Montanuniversitat Leoben.
- Neville, A. M., & Brooks, J. J. (1987). *Concrete technology* (Longman Sc).
- Nguyen, V. H. (2005). Couplage degradation chimique-comportement en compression du be'ton. *Thesis Dedoctorat. Paris Ecole Nationale Des Ponts et Chaussées*.
- Panet, M. (1978). Stability analysis of a tunnel driven in a rock mass in tracking account of the post-failure behavior. *Rock Mechanics*, 8(1), 209–223.
- Panet, M. (1995). M. Calcul des Tunnels par la Methode de Convergence-Confinement. *Presses de l'Ecole Nationale Des Ponts et Chausse'es*.
- Panet, M., & Guenot, A. (1982). Analysis of convergence behind the face of a tunnel. *Tunnelling 82. In Proceedings of the 3rd International Symposium, Brighton, UK*.
- Sandrone, F., & Labiouse, V. (2010). *Analysis of the evolution of road tunnels equilibrium conditions with a convergence – confinement approach*. 201–218. <https://doi.org/10.1007/s00603-009-0056-y>

- Shimamoto, K., Yashiro, K., Kojima, Y., & Asakura, T. (2009). *Prediction Method of Tunnel Deformation Using Time-dependent Ground Deterioration Model*. 50(2), 81–88.
- Showkati, A., Salari-rad, H., & Hazrati, M. (2021). Predicting long-term stability of tunnels considering rock mass weathering and deterioration of primary support. *Tunnelling and Underground Space Technology Incorporating Trenchless Technology Research*, 107(October 2020), 103670. <https://doi.org/10.1016/j.tust.2020.103670>
- Ślusarek, J. (2010). *THE CORRELATION OF STRUCTURE POROSITY AND COMPRESSIVE STRENGTH OF HARDENING CEMENT MATERIALS STRUCTURE OF*. 85–92.
- Sulem, J. (1994). Analytical methods for the study of tunnel deformation during excavation. *Barla G (Ed) Gallerie in Condizioni Difficili MIR'94, Torino, Pp 301–317*.
- Tating, F., Hack, R., & Jetten, V. (2013). Engineering aspects and time effects of rapid deterioration of sandstone in the tropical environment of Sabah , Malaysia. *Engineering Geology*, 159, 20–30. <https://doi.org/10.1016/j.enggeo.2013.03.009>
- Tran-Manh, H., Sulem, J., & Subrin, D. (2016). Progressive degradation of rock properties and time-dependent behavior of deep tunnels. *Acta Geotechnica*, 11(3), 693–711. <https://doi.org/10.1007/s11440-016-0444-x>
- Trunda, V., & Hilar, M. (2020). Natm tunnels – consideration of the partly damaged primary lining impact for the secondary lining evaluation. *Acta Polytechnica*, 60(2), 145–150. <https://doi.org/10.14311/AP.2020.60.0145>
- Usman, M., & Galler, R. (2013a). Long-term deterioration of lining in tunnels. *International Journal of Rock Mechanics and Mining Sciences*, 64, 84–89. <https://doi.org/10.1016/j.ijrmms.2013.08.028>
- Usman, M., & Galler, R. (2013b). Long-term deterioration of lining in tunnels. *International Journal of Rock Mechanics and Mining Sciences*, 64, 84–89. <https://doi.org/10.1016/j.ijrmms.2013.08.028>
- Vlachopoulos, N., & Diederichs, M. S. (2009). *Improved Longitudinal Displacement Profiles for Convergence Confinement Analysis of Deep Tunnels*. 131–146. <https://doi.org/10.1007/s00603-009-0176-4>
- Vu, T. M., Sulem, J., Subin, D., & Monin, N. (2013). Semi-Analytical Solution for Stresses and Displacements in a Tunnel Excavated in Transversely Isotropic

Formation with Non-Linear Behavior. *Rock Mechanics and Rock Engineering*, 46, 213–229. <https://doi.org/10.1007/s00603-012-0296-0>

Wang, W., & Gong, J. (2019). New relaxation function and age-adjusted effective modulus expressions for creep analysis of concrete structures. *Engineering Structures*, 188, 1–10.

Yokozeki, K., Watanabe, K., Sakata, N., & Otsuki, N. (2004). *Modeling of leaching from cementitious materials used in underground environment*. 26, 293–308. <https://doi.org/10.1016/j.clay.2003.12.027>

Yoon, J.-U., Han, J.-W., Joo, E.-J., & Shin, J.-H. (2014). Effects of Tunnel Shapes in Structural and Hydraulic Interaction. *Tunnelling and Underground Space Construction for Sustainable Development*, 18(3), 735–741.

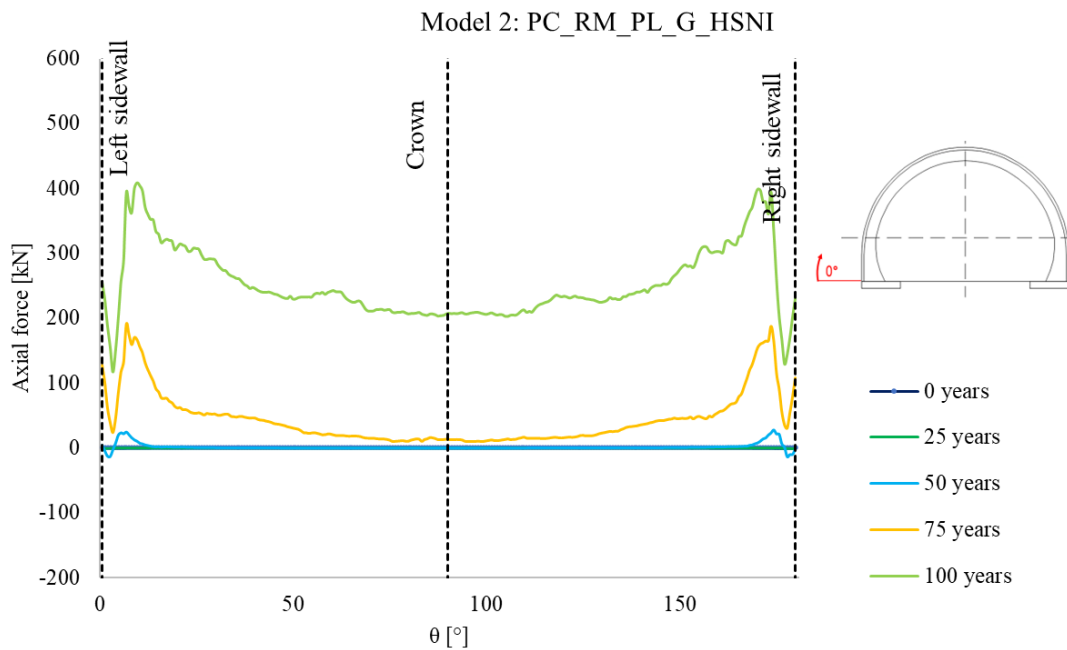
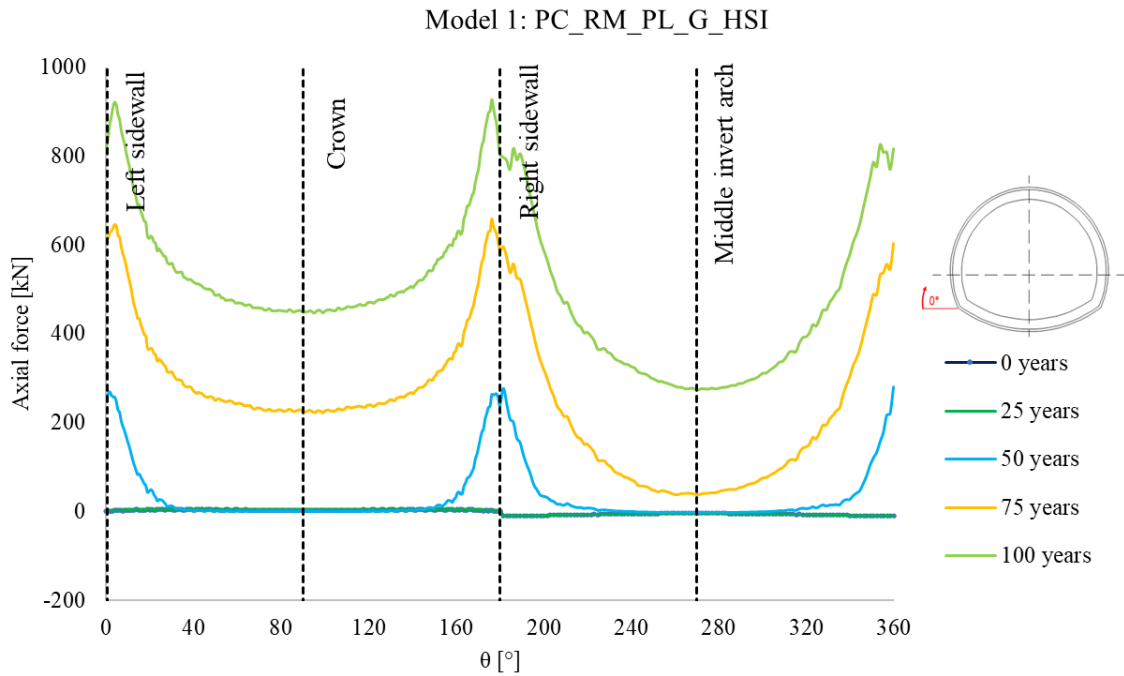
Yoshida, N., Morgenstern, N. R., & Chan, D. H. (1990). A Failure Criterion for Stiff Soils and Rocks Exhibiting Softening. *Canadian Geotechnical Journal*, 27, 195–202.

Ziller, L., & Cont, M. (2018). Evaluation of long-term ground load on conventional tunnel linings. *The World Tunnel Congress*.

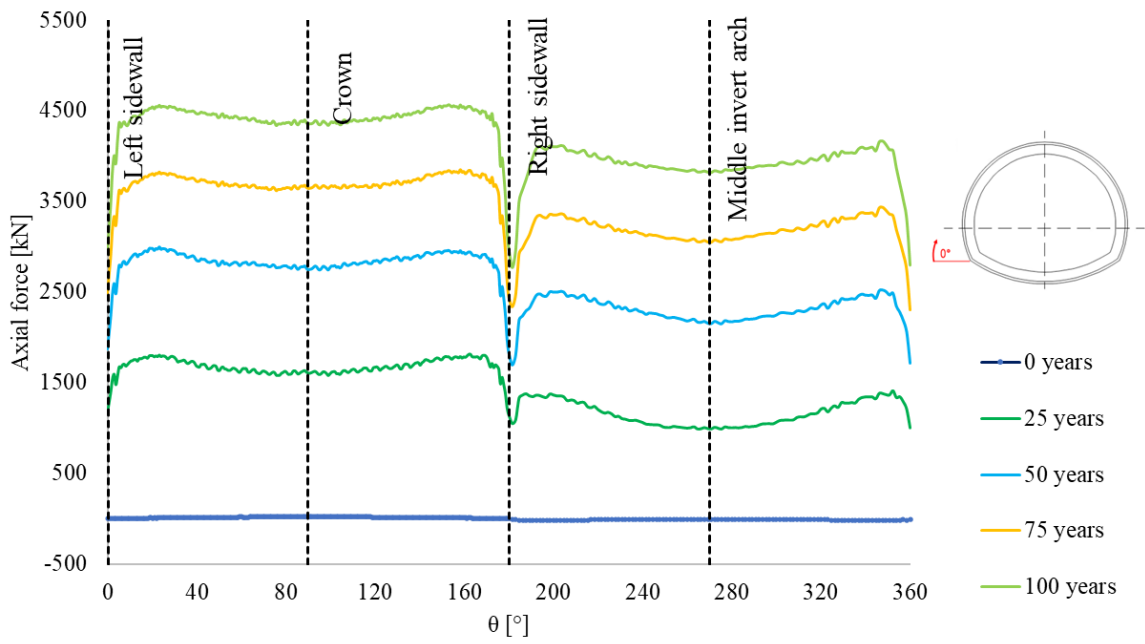
Appendix A. Summary modeling cases

Reference	Tunnel type	Dimension	Rock mass properties	Rock mass constitutive model	Support constitutive model	Model characteristics	Rock mass degradation model	Support degradation model	Results
Numerical Simulation of Long-Term Deterioration of Rock Mass Supported by Shotcrete Lining (Kong et al., 2022).	Horeshoe with invert arch.	Depth=50 m	$\gamma=21 \text{ kN/m}^3$, $E=15000 \text{ MPa}$, $\nu=0.3$, $\phi=24.93^\circ$, $c=0.2 \text{ MPa}$, $\sigma_{cr}=2.73 \text{ MPa}$, $A_0=1.46$, $S_0=0.16$.	Proposed by Yoshida et al., 1990. A, S, and S_0 parameters which depend on the cohesion and friction angle of the rock.	Mohr-Coulomb failure criteria	No vertical displacement in the top and bottom of the vertical boundaries and the top has a free restraint.	3 cases: 1. A, and S_0 decreased to a quarter of its original value in 10 years. 2. A, and S_0 decreased to a quarter of its original value in 100 years. 3. Parameters are equal to the original ones.	Deteriorated thickness (Xd) depends on time and factor a.	*Case 1: Support pressure gradually transferred to the secondary lining displacement and pressure increase relatively quick. *Case 2: Since the shotcrete was not able to sustain the pressure of the rock mass, the secondary lining displacement and pressure increase relatively quick. *Case 3: Support pressure and secondary lining mainly came from support pressure during construction. Pressure and displacement are relatively low compared to cases 1 and 2. *Deterioration of both rock mass and shotcrete will cause the increase of pressure in the secondary lining, increasing the displacement and reducing the safety factor by 85%.
Predicting long-term stability of tunnels considering rock mass weathering and deterioration of primary support (Shoukati, Salari-ezad, & Hazerati, 2021).	Horeshoe with invert arch.	Depth=60 m	$\gamma=27 \text{ kN/m}^3$, $E=4500 \text{ MPa}$, $\nu=0.24$, $\phi=33^\circ$, $c=0.65 \text{ MPa}$, $\text{CSI}=50$, $K_0=1$.	Isotropic Elastic-plastic	Elastic-Perfectly plastic	2D model with size of 130 m x 130 m with 6000 elements and restrain at the top and bottom sides of the model.	An expression in terms of time and an integral degradation rate (RD) is used for cohesion and Young's Modulus degradation. Imposing different values of time (e.g. 0, 10, 20, 50, 100 years).	BOITS: Reduction of both cross section areas in terms of SHOTCRETE: Degradation of Young's Modulus and compressive strength, whose gradual decrease depends on chemical characteristics	At early stages, the only forces simulated for the final lining is its self weight, however since the tunnel primary support system starts to deteriorate, tunnel loads are gradually transferred to the final lining, causing an increase in thrust and bending moments. Specially for the bending moments there is an important increase in the long-term at the tunnel sidewalls
Analysis of the evolution of road tunnel equilibrium conditions with a convergence-confinement approach (Santolone & Labrosse, 2010).	Circular	R=5 m Depth=250 m	CASE 1 (Poor quality sandstones): $\gamma=24 \text{ kN/m}^3$, $E=2000 \text{ MPa}$, $\nu=0.25$, $\phi=30^\circ$, $c=0.5 \text{ MPa}$, $\text{CSI}=50$. CASE 2 (Good quality mbs): $\gamma=25.4 \text{ kN/m}^3$, $E=8000 \text{ MPa}$, $\nu=0.4$, $\phi=20^\circ$, $c=1 \text{ MPa}$.	Mohr-Coulomb failure criteria (6 implementation) (GCC).	Elastic-Perfectly plastic	(-)	1. Aging: Lemaitre's law (evolution of primary creep) for cohesion and Young's Modulus degradation. 2. Weathering: Reduction of c and ϕ .	Reduction of Young's Modulus and compressive strength, based on the affirmation that reduction of the rock mass degradation. However, a good estimation of rock mass degradation must be done, so the tunnel safety factor is more appropriate. *For the evaluation of tunnel equilibrium it is important to consider the interaction between support and rock mass in which both factors can evolve in time	*Considering the degradation of final lining and rock mass in separate ways, it shows that the influence of reduction of lining properties is lower for the long term stability with respect to the rock mass degradation. However, a good estimation of rock mass degradation must be done, so the tunnel safety factor is more appropriate.
Long-term deterioration of lining in tunnels (Usman & Guler, 2013).	Horeshoe with invert arch.	Diameter of the arch in the top heading tunnel (2R) = 10 m Height=111 m and depth=250 m.	$\gamma=27 \text{ kN/m}^3$, $E=500 \text{ MPa}$, $\nu=0.4$, $\phi=35^\circ$, $c=3 \text{ MPa}$.	Mohr-Coulomb failure criteria.	Mohr-Coulomb for shotcrete and Elastic for liner	Other boundaries located to avoid boundary condition influence. Mesh is 4 to 5 times the tunnel diameter.	(-)	By reducing 10% at each year the compressive strength of shotcrete. *Only cohesion *Young's Modulus and cohesion *For the case where the three properties are reduced simultaneously, the shotcrete functionality stop at the point where it hardly supports any quantity of stress	*By only degrading the shotcrete's Young's Modulus, it not only caused a transfer of loads into the liner liner but the rock mass in the surroundings had to carry the redistribution of stresses. *Decreasing both Young's Modulus and cohesion of shotcrete there was a significant increase in the effect of deterioration, causing sufficient damage of the material at the point where the secondary lining had to carry the stresses. *For the case where the three properties are reduced simultaneously, the shotcrete functionality stop at the point where it hardly supports any quantity of stress
Evaluation of long-term ground load in conventional tunnel linings (Ziller & Corn, 2018).	Horeshoe without invert arch.	Area of excavation=60 m ² Depth=700 m.	$\gamma=40 \text{ MPa}$, $\nu=12$, $E_1=40 \text{ GPa}$, $\text{OSI}=40$.	Elastic-plastic behavior with Hook and Hovort failure criteria.	Plastic shotcrete model and Mohr-Coulomb failure criteria	Triangular elements for volume reduction. Beam elements of linear components. Size and boundary conditions of the model established to prevent border effects.	(-)	For the Mohr-Coulomb case it was represented as a decrease of cohesion (in terms of UCS) and elastic modulus. For the Plastic Shotcrete Model was evaluated with the decrease of E_{30} and σ_{30} .	Axial forces in the secondary lining after full degradation is lower than the one for the primary lining at initial stage due to stress redistribution in the rock. The DPL (Degraded Primary Lining) model proposed in this paper used more realistic assumptions, especially for good GSI values and high depths. The final pressure applied in the lining with DPL method is about 50% less than the one evaluated with the traditional approach (direct application of total loads in the secondary lining).
Numerical Methods for Tunneling using ABAQUS and Investigations of Long-Term Effects of the Shotcrete Shell and its Impact on the Combined Support System (Mollhammer, 2011).	Circular	R=10 m Depth=250 m	$\gamma=27 \text{ kN/m}^3$, $E=500 \text{ MPa}$, $\nu=0.4$ to 0.5.	Mohr-Coulomb failure criteria.	Linear elastic perfectly plastic	Size model 55 m x 55 m in anisotropic conditions with finite elements as representation of liners.	(-)	Deterioration of Young's Modulus and compressive strength reducing steps by 10% each, both parameters are reduced independently and then simultaneously.	*Some results are obtained comparing the case where only the degradation of Young's Modulus and the case where both are degraded. *Stresses in the liner are higher when degrading E than reducing E. *At 90% of deterioration the stresses are similar when the degradation is modelled for E and ϕ independently. *When K=1 it leads to tangential stresses in the liner higher in the springline than at the tunnel crown.
Practical modelling approaches to determine the long term behaviour of tunnel construction (Pantelis, Popoulos et al., 2012).	Circular.	R=6 m Depth=600 m.	$E=30 \text{ MPa}$, $\nu=0.26$, $\phi=15^\circ$, $c=0.76 \text{ MPa}$, Bulk Modulus=1.1E10 Pa, Shear Modulus=1.2E10 Pa.	Mohr-Coulomb and CVISC model	Linear elastic perfectly plastic	Mesh: Graded. Boundary: Rollers constraints with corner pins.	No decrease in the properties, only the stress released caused by the excavation.	(-)	For the Mohr-Coulomb model the conventional excavation sequence employed in 3D models was trending to a 2D solution. For K=1: Main difference between Mohr-Coulomb and Burger models is the magnitude (variance of +/- 3 cm). Also when MC sees equilibrium larger falls. For K=0.5: CVISC model exhibits higher radial displacements (variance of +/- 10-15 cm) in comparison to MC model.
Long-term behavior of lined tunnels excavated in squeezing ground (Y. Liu et al., 2020).	Circular.	R=5.5 m Depth=105 m	ROCK MASS: $\phi=26^\circ$, $c=0.63 \text{ MPa}$, tensile strength=8.3 kPa, Bulk Modulus=250 MPa, Shear Modulus=250 MPa. HOISTS: $\phi=23^\circ$, $c=0.38 \text{ MPa}$, tensile strength=8.5 kPa.	CVISC model (Burger model) as a plastic component simulating the contribution of Mohr-Coulomb failure criteria).	Elastic	3D model with 4-noded elements. Size of 220 m.	(-)	No decrease in the properties, the coordinates of the nodes were updated step by step (Large-strain mode). Re-profiling process.	CVISC proved that is accurate to describe time dependent and anisotropic behavior of squeezing conditions.
Study on the Progressive Deterioration of Tunnel Lining Structures in Cold Regions Experiencing Freeze-Thaw Cycles (Xu et al., 2021).	Horeshoe with invert arch.	(-)	Lining concrete: $E_c=30 \text{ GPa}$, $\nu_c=0.2$.	ANSYS only to simulate flow expansion in the material.	Linear elastic	Model with software ANSYS only to simulate the effect of freeze and flow expansion in the material.	(-)	Decrease in the Young's Modulus and Poisson ratio	1. At first, there is no deterioration immediately after the construction. 2. Slight deterioration of 5 cm (1000 freeze-thaw cycles=10 years). 3. 20 years (2000 freeze-thaw cycles) this 5 cm have moderate deterioration and between 5-10 cm into deterioration. 4. 30 years (3000 freeze-thaw cycles) for the first 5 cm of lining having severe deterioration, while within 5-10 cm moderate deterioration and into deterioration for 10-15 cm of the lining surface.

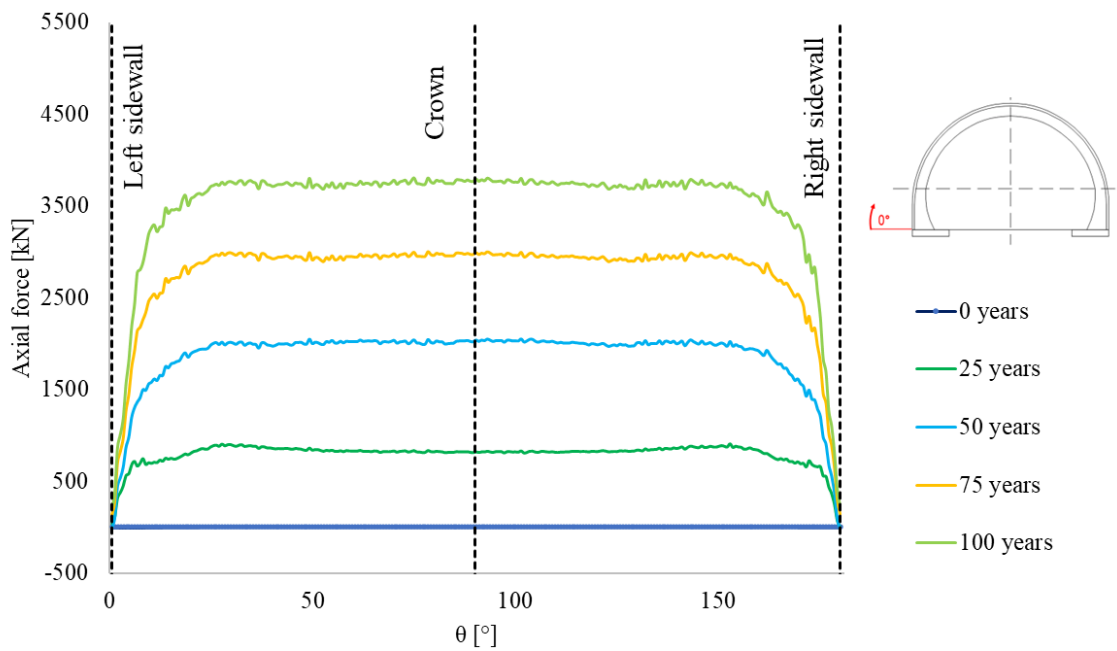
Appendix B.1. Axial forces

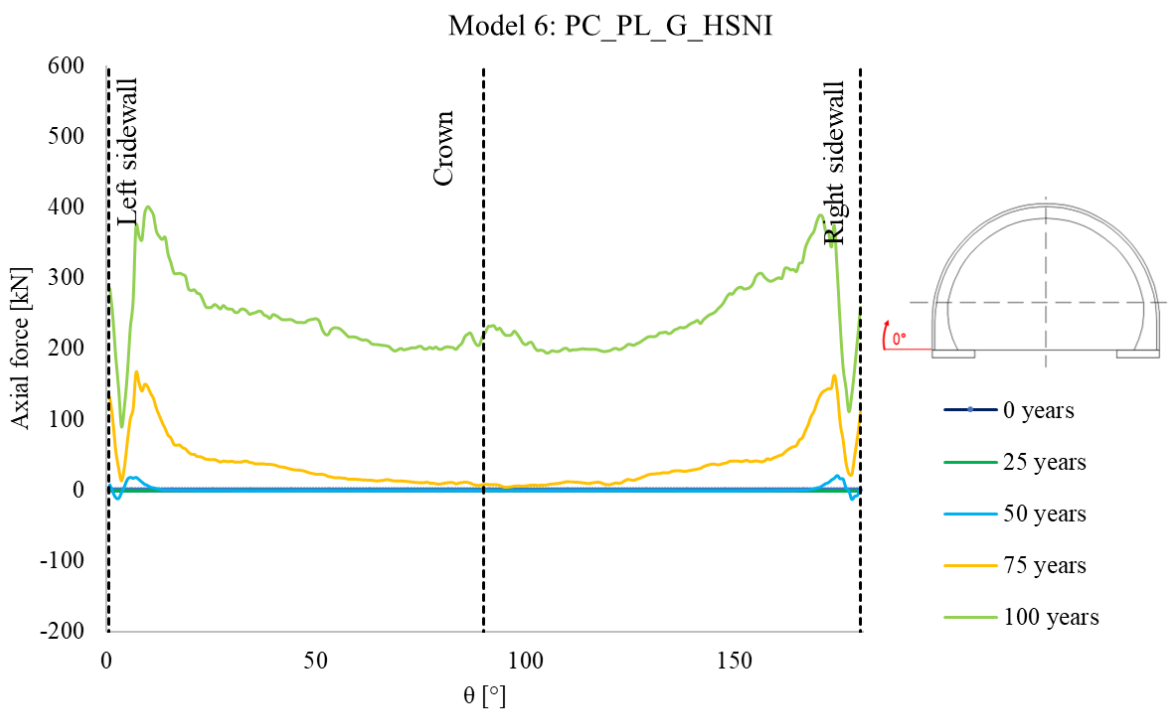
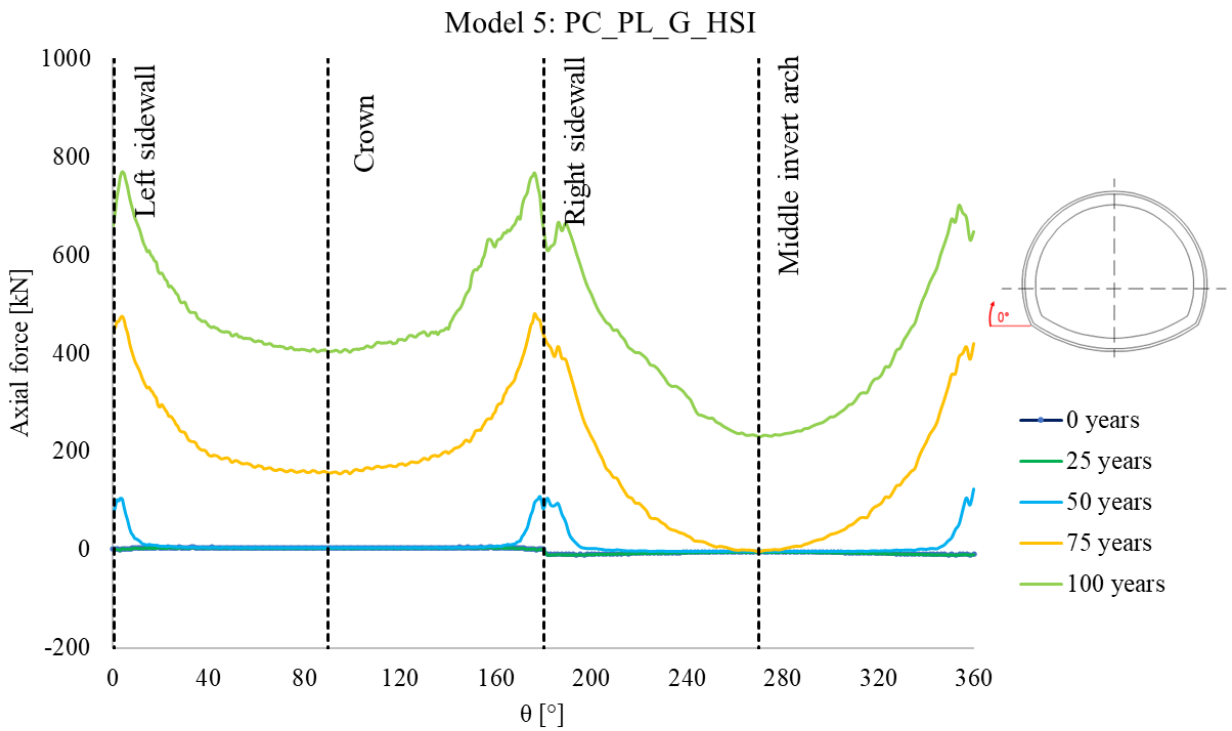


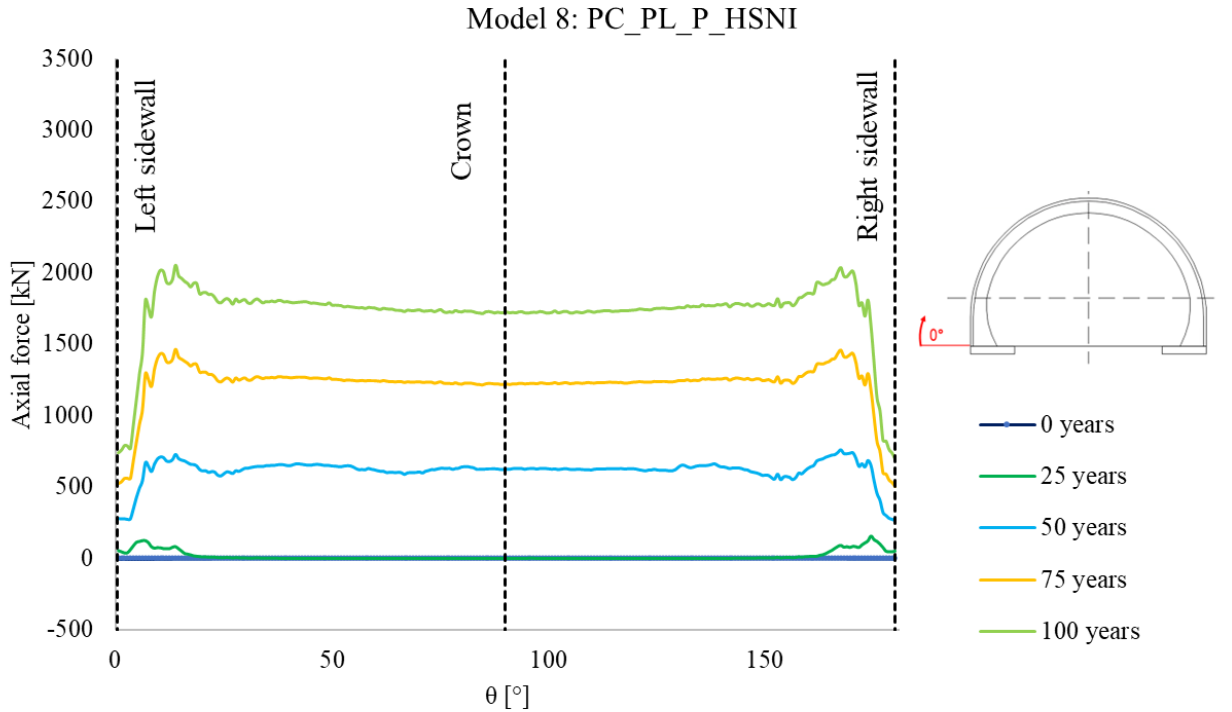
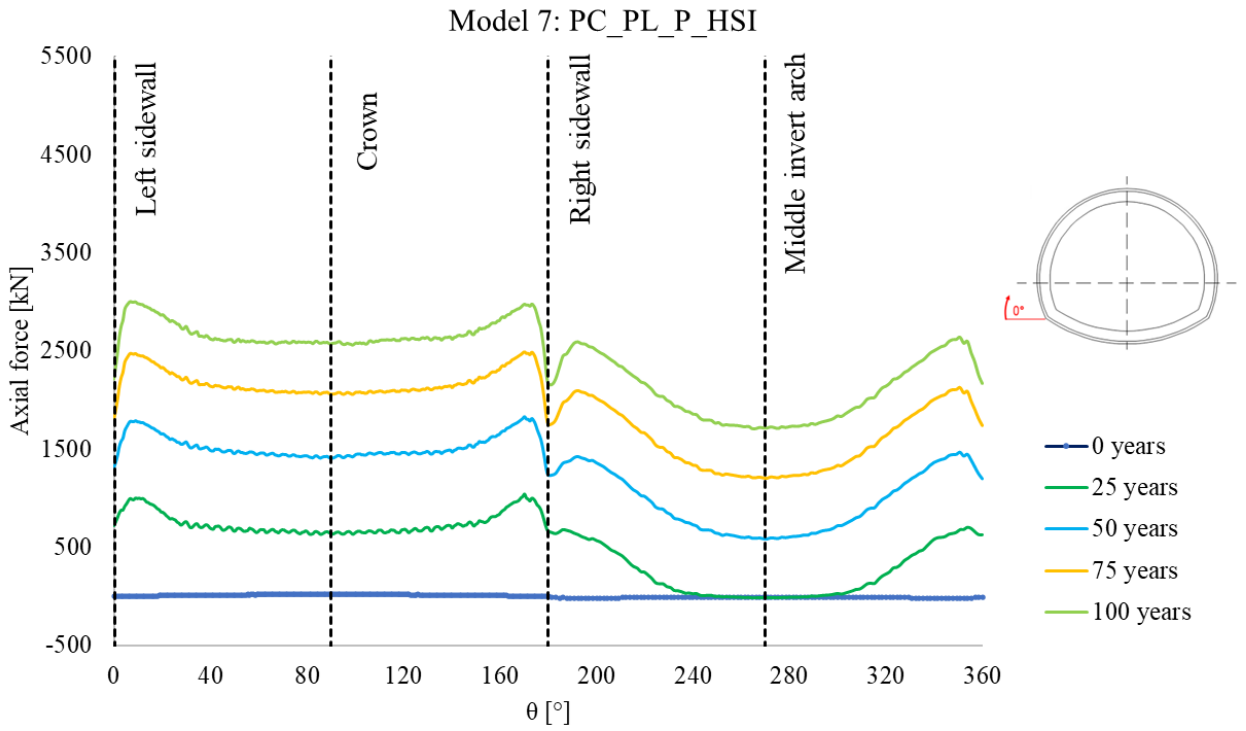
Model 3: PC_RM_PL_P_HSI



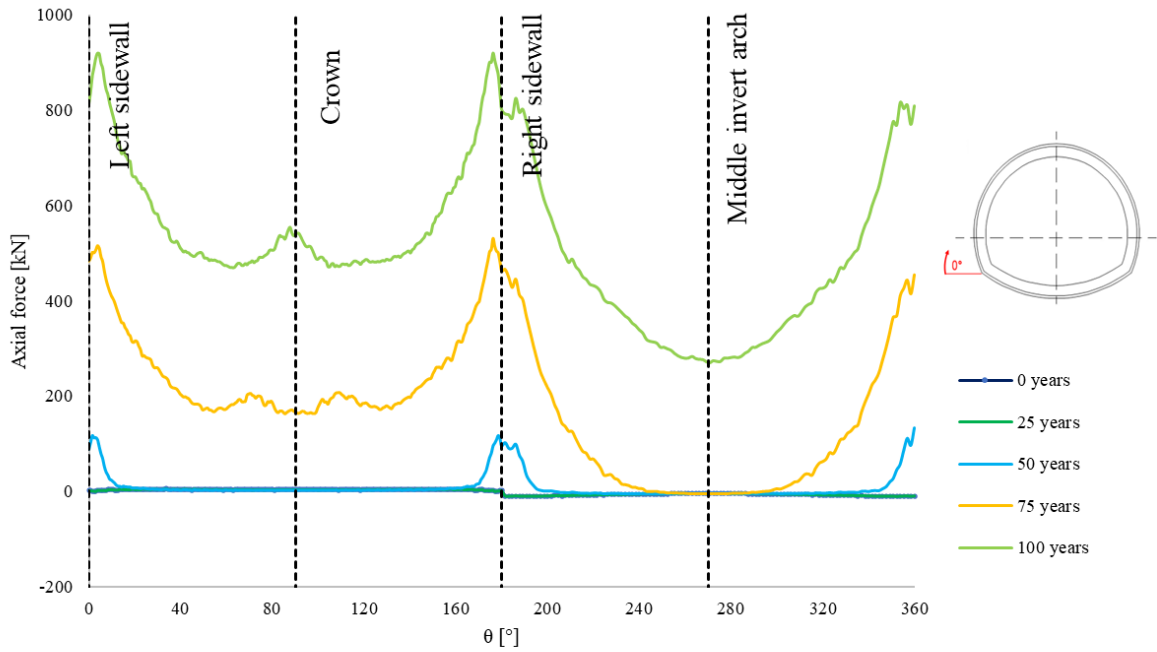
Model 4: PC_RM_PL_P_HSNI



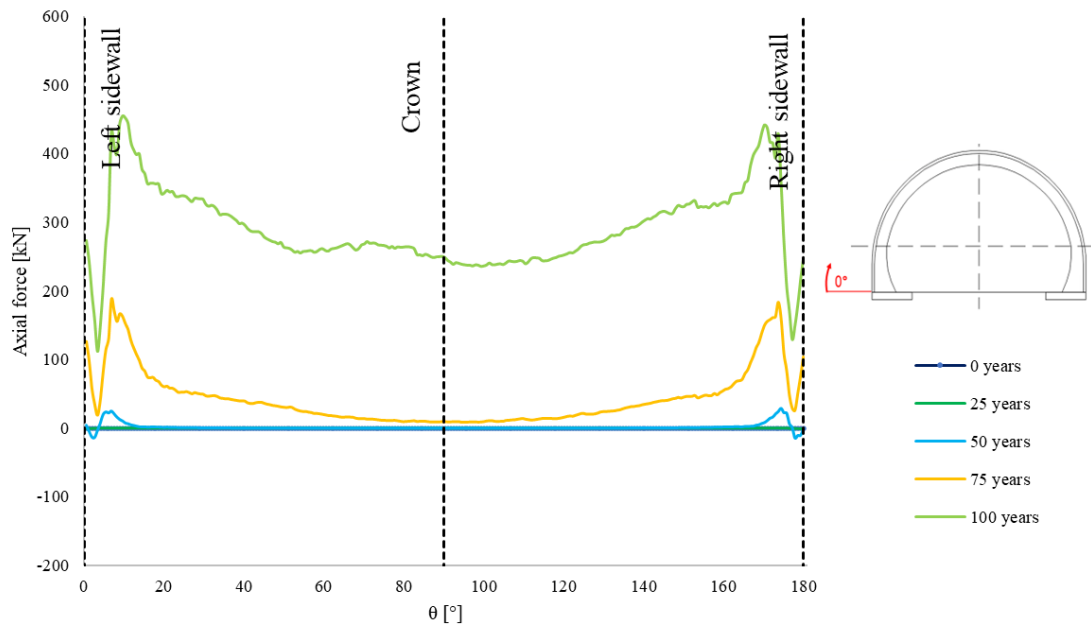




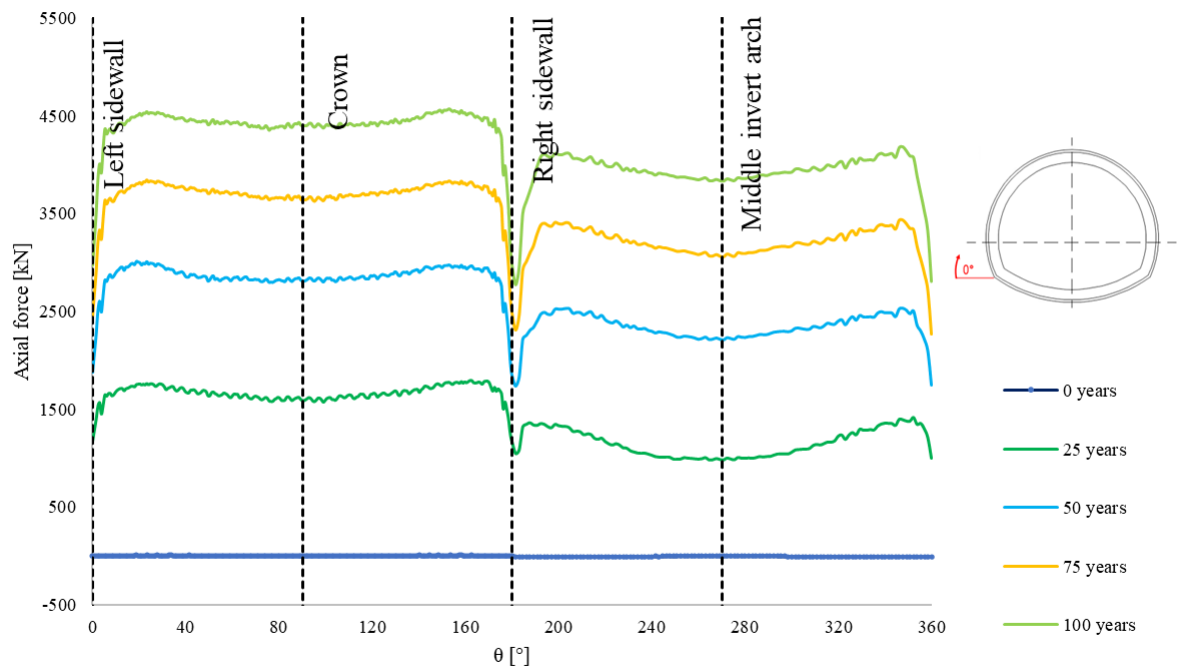
Model 9: RC_RM_PL_G_HSI



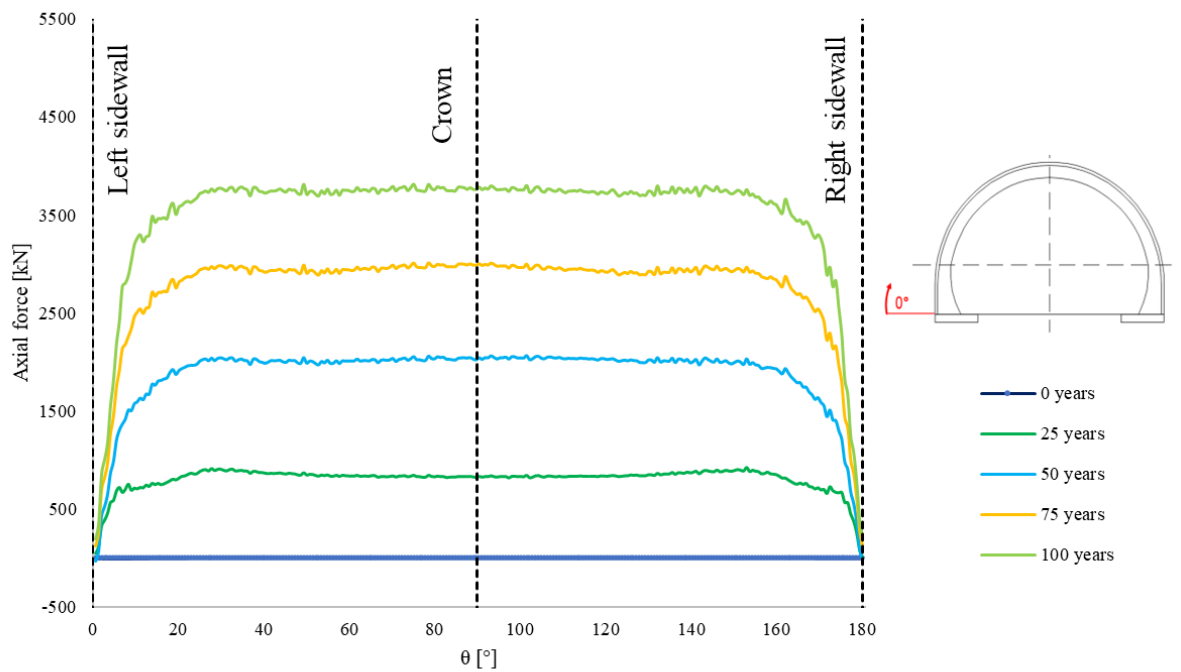
Model 10: RC_RM_PL_G_HSNI

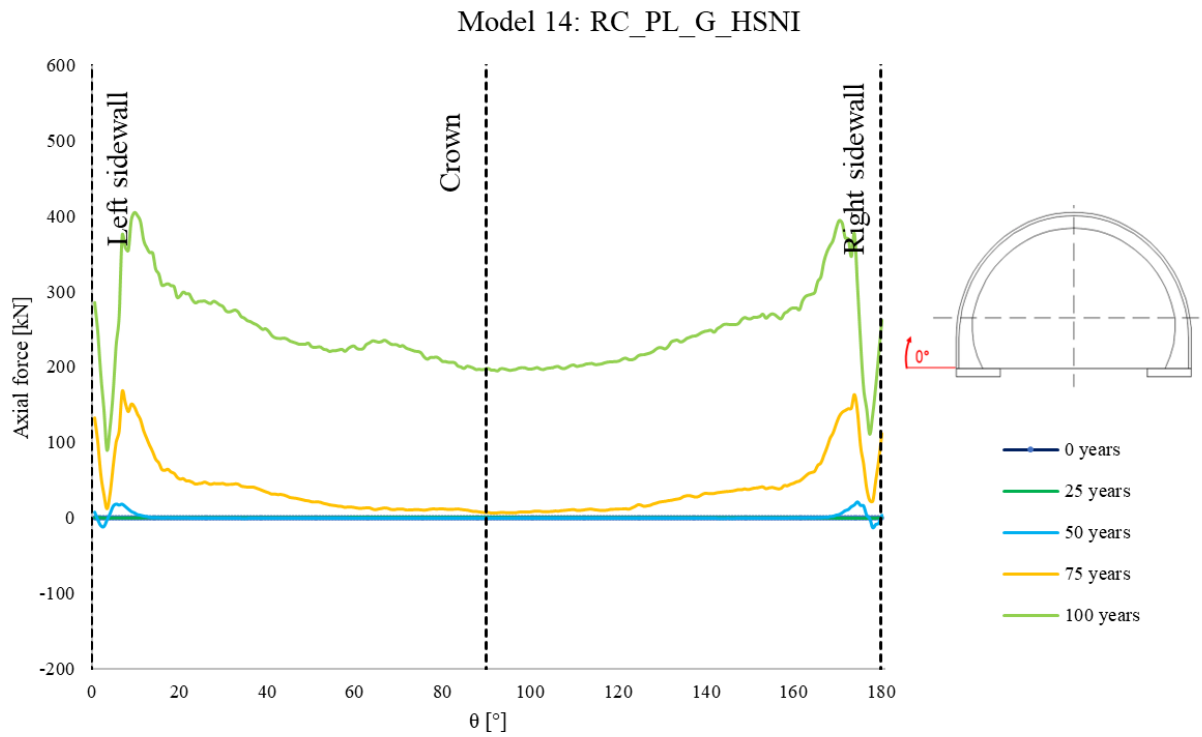
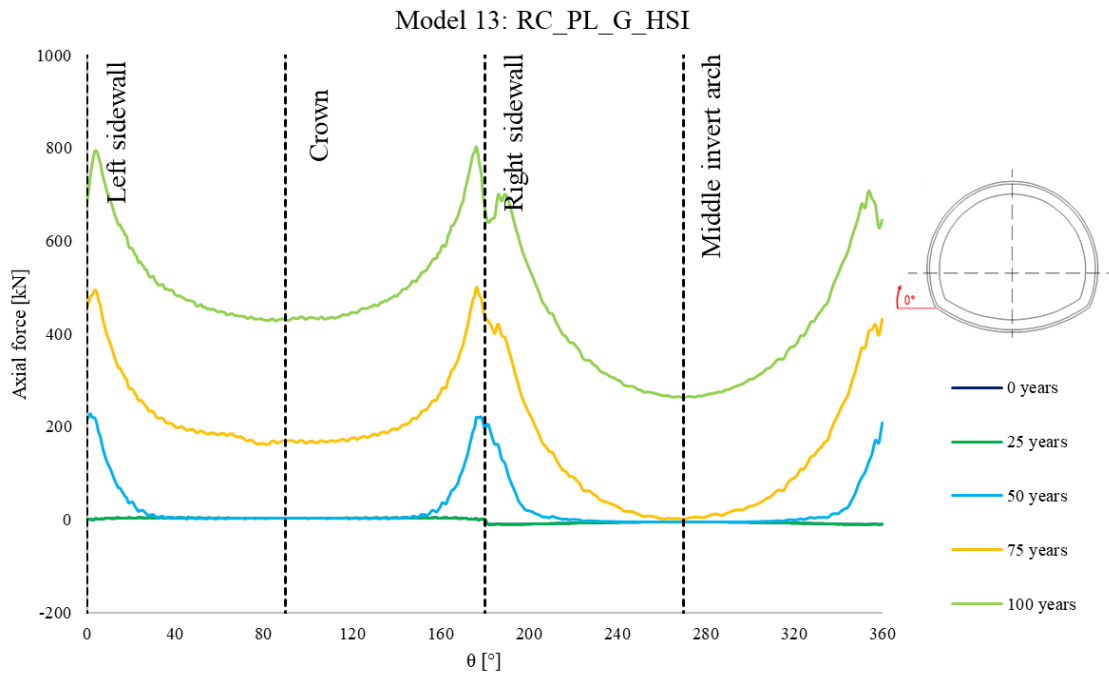


Model 11: RC_RM_PL_L_HSI

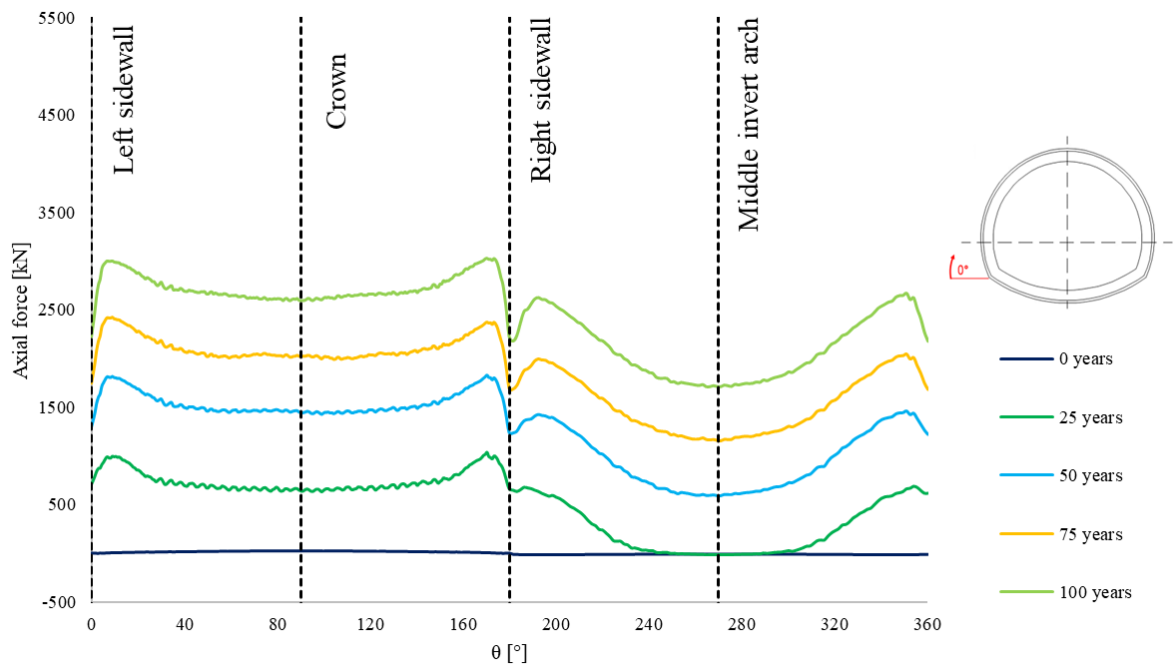


Model 12: RC_RM_PL_L_HSNI

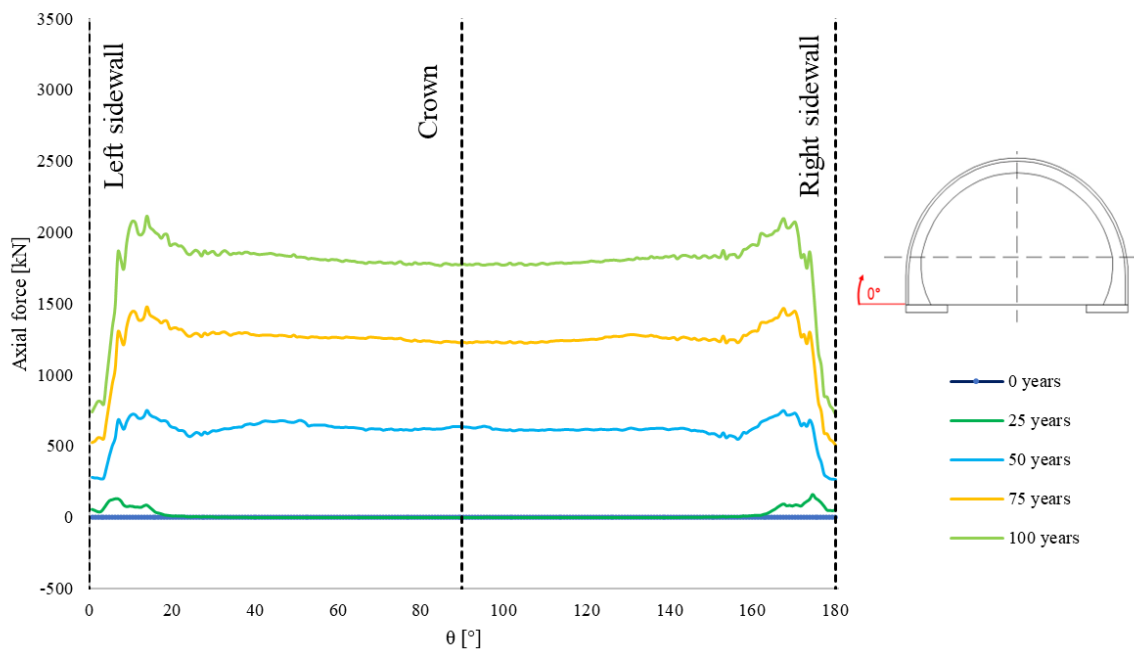




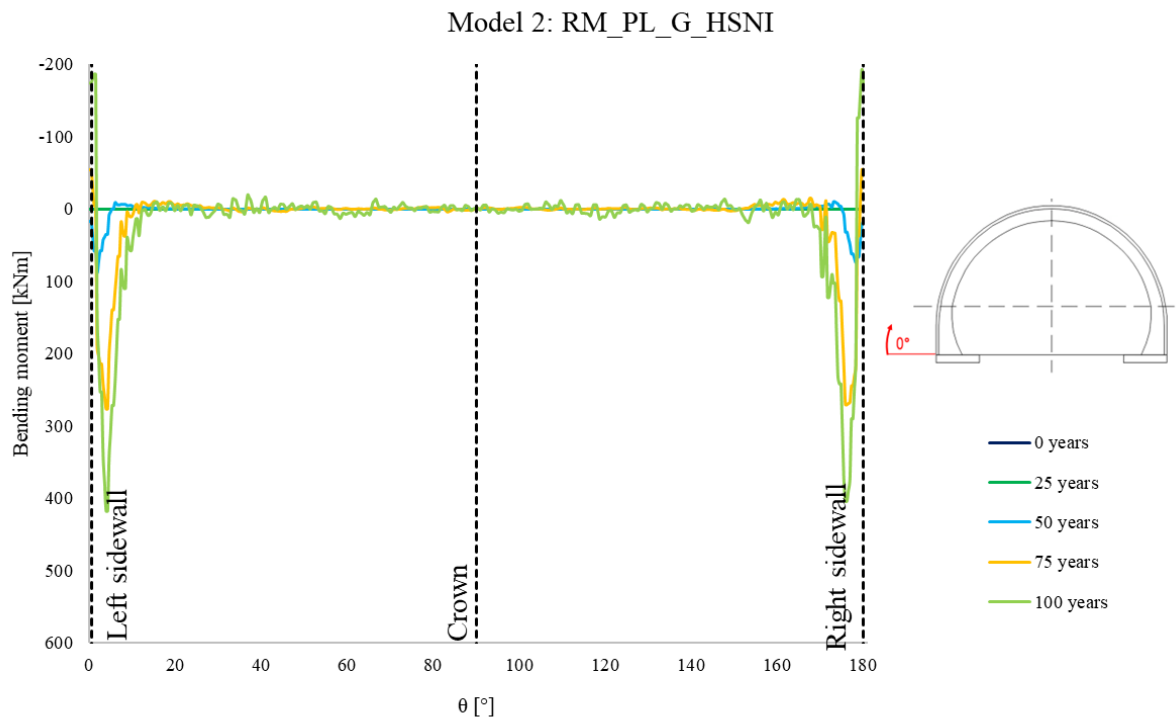
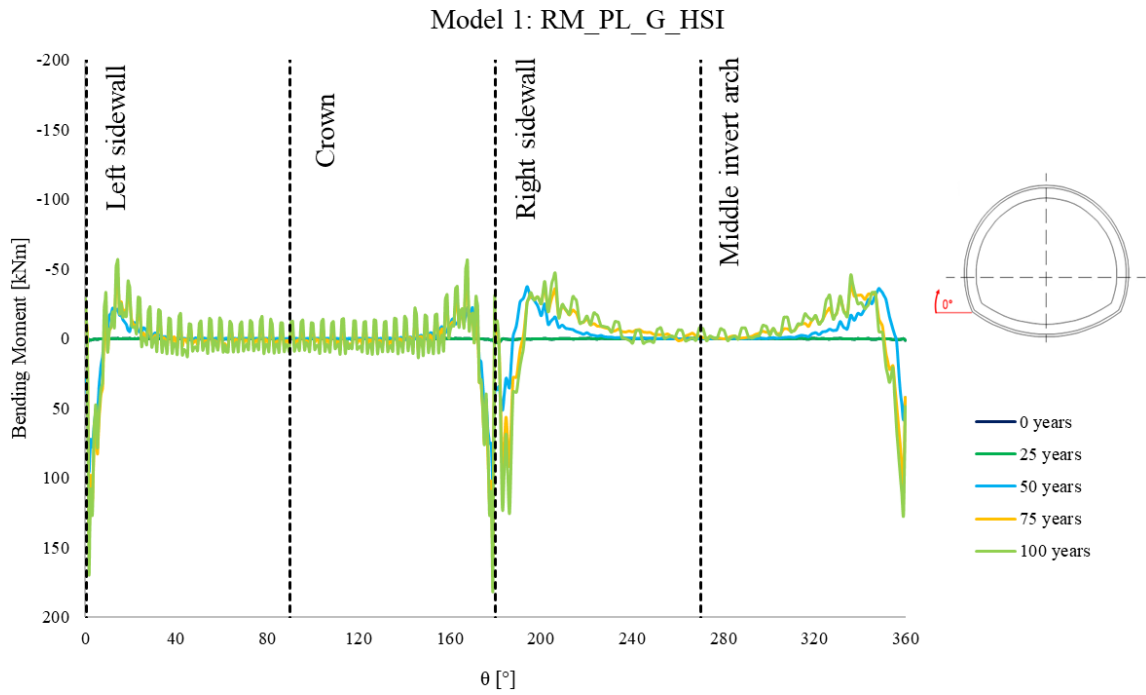
Model 15: RC_PL_L_HSI



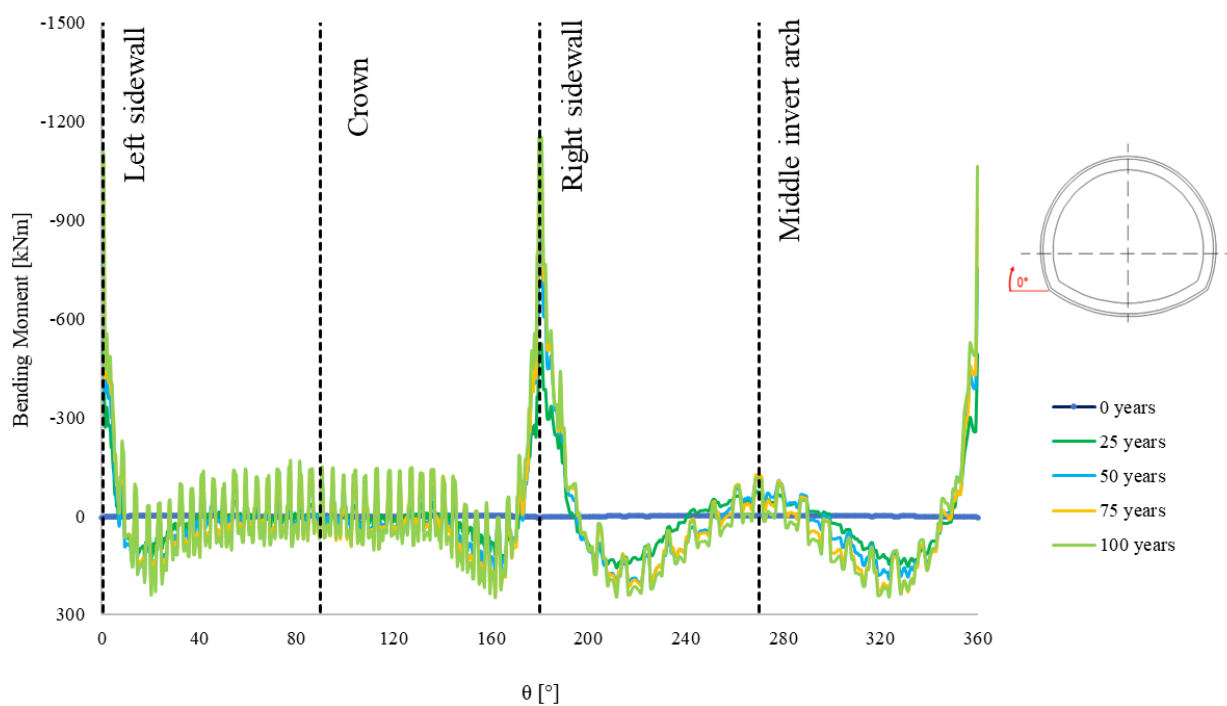
Model 16: RC_PL_L_HSNI



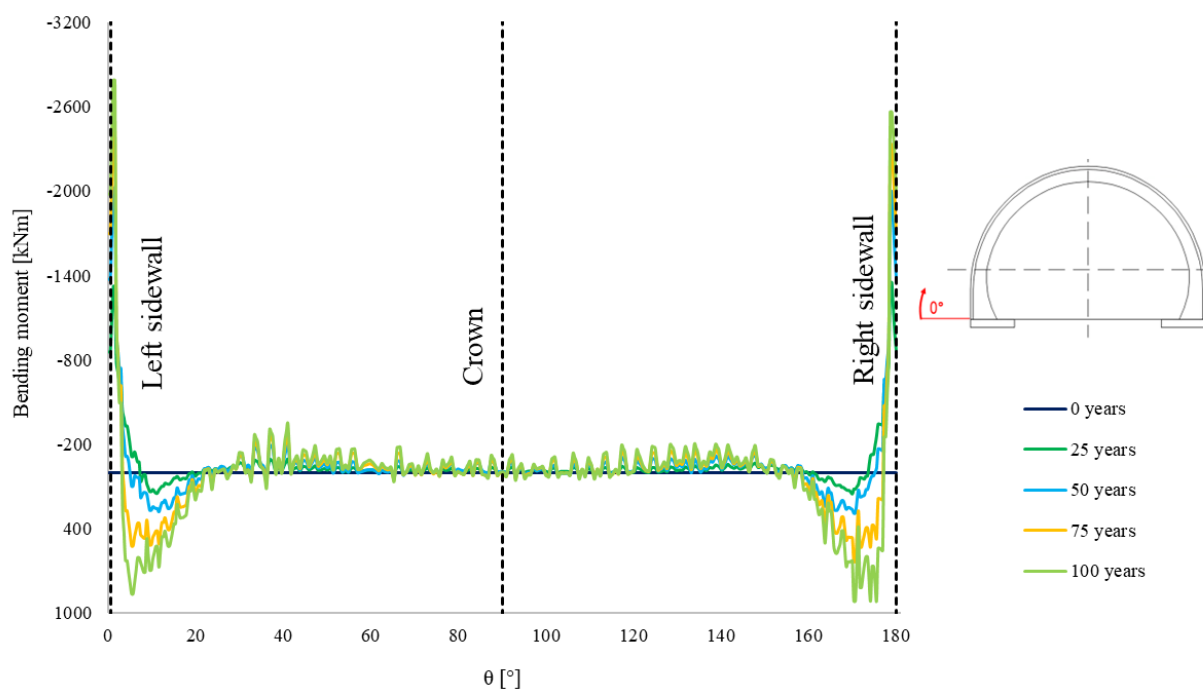
Appendix B.2. Bending moments



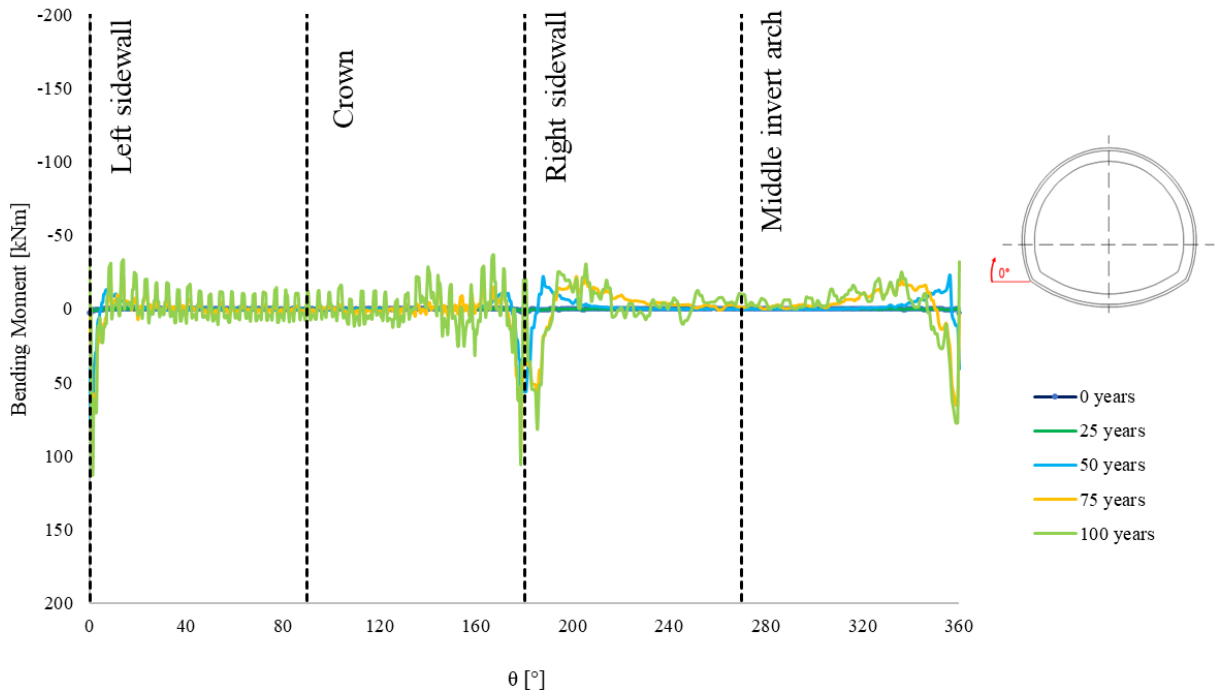
Model 3: RM_PL_L_HSI



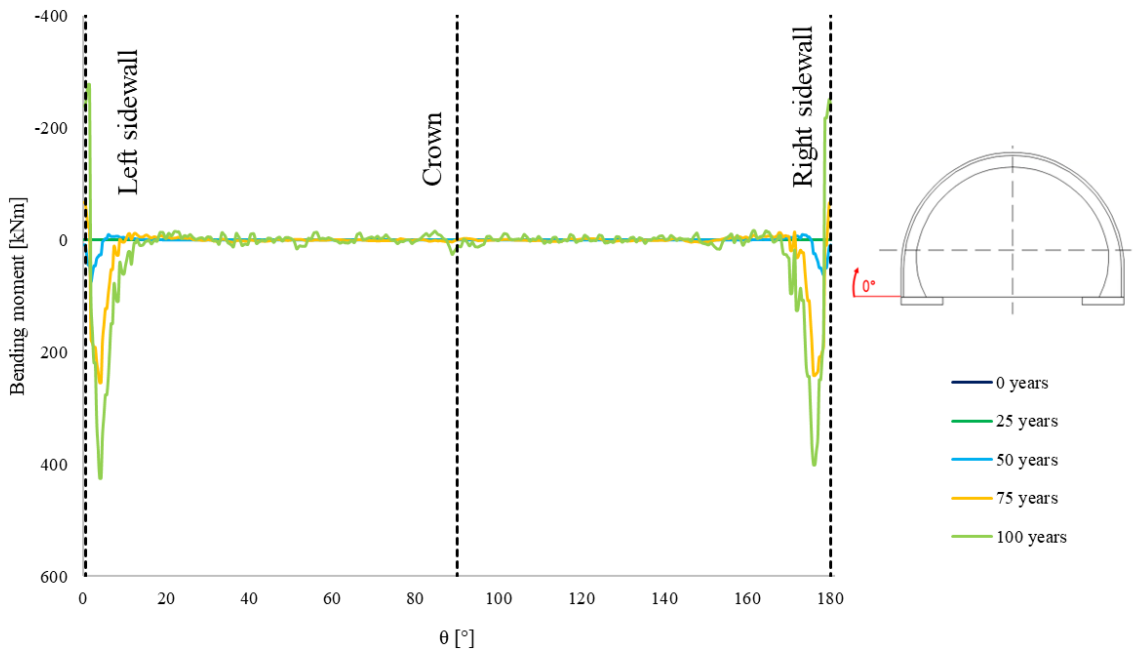
Model 4: RM_PL_L_HSNI



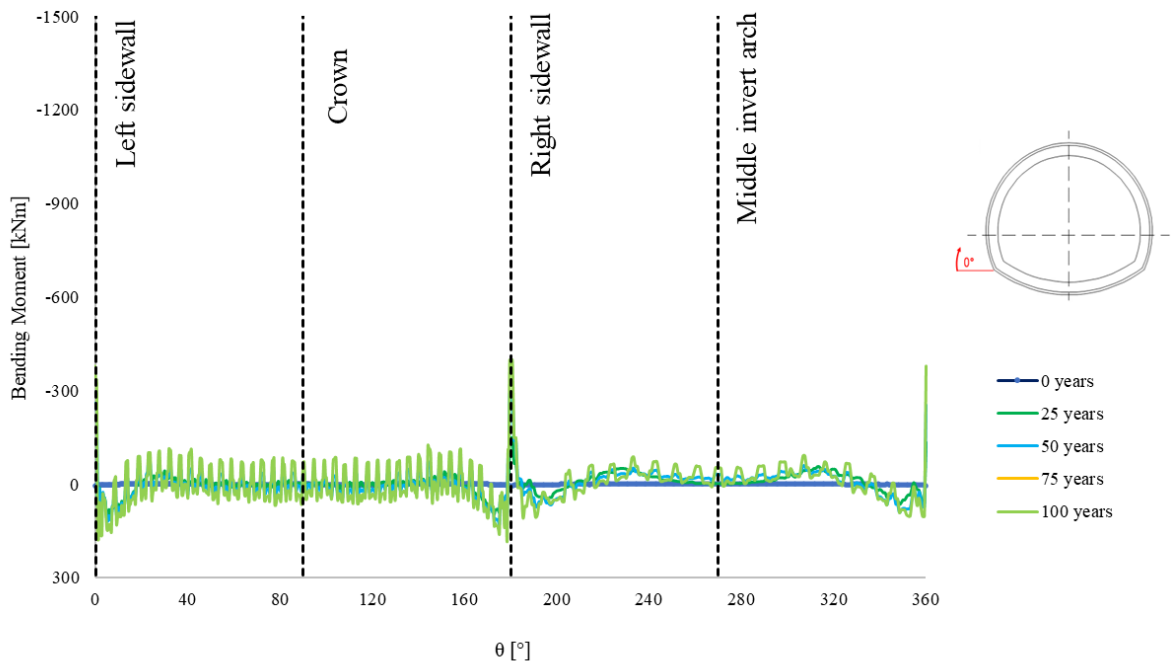
Model 5: PL_G_HSI



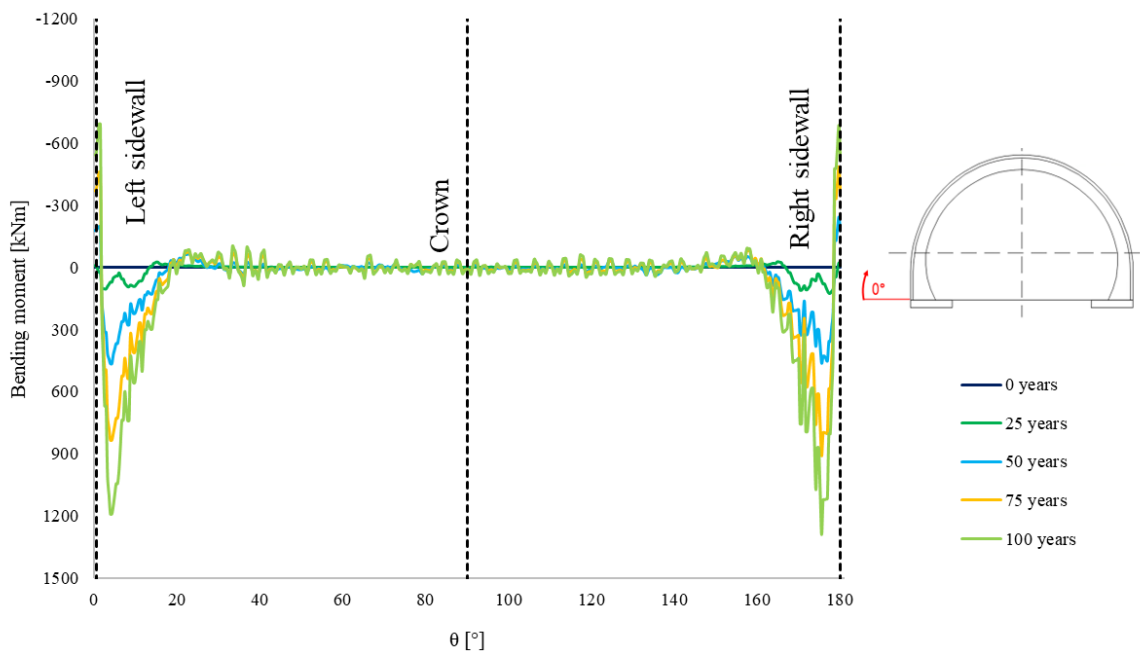
Model 6: PL_G_HSNI



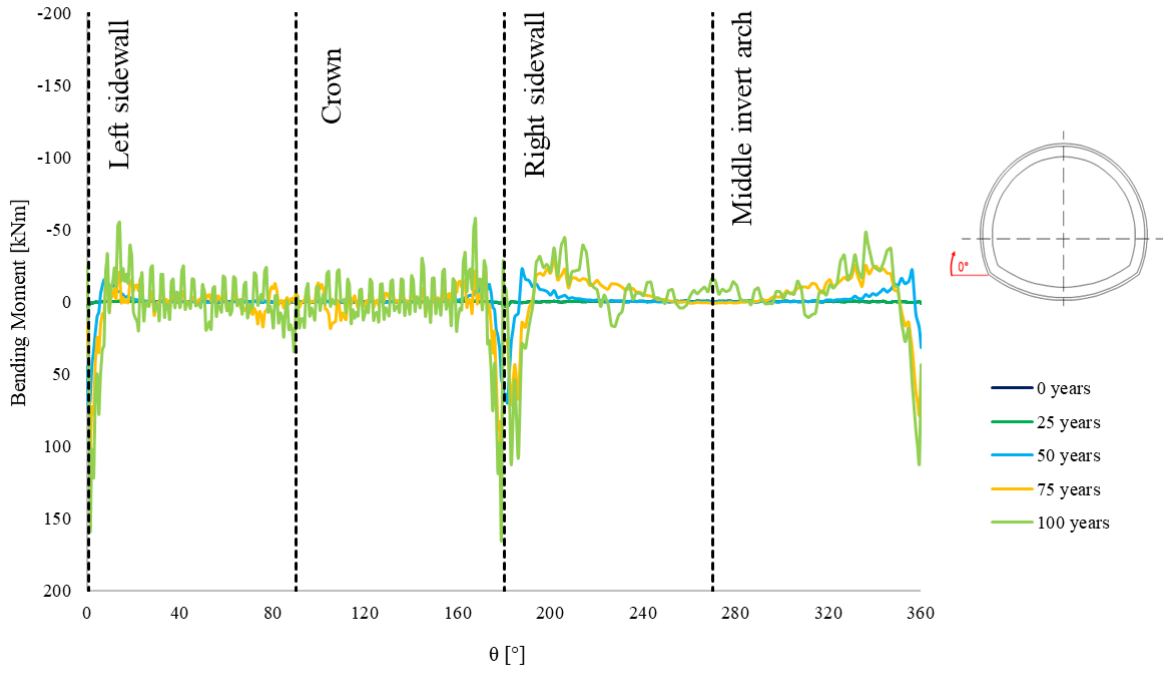
Model 7: PL_L_HSI



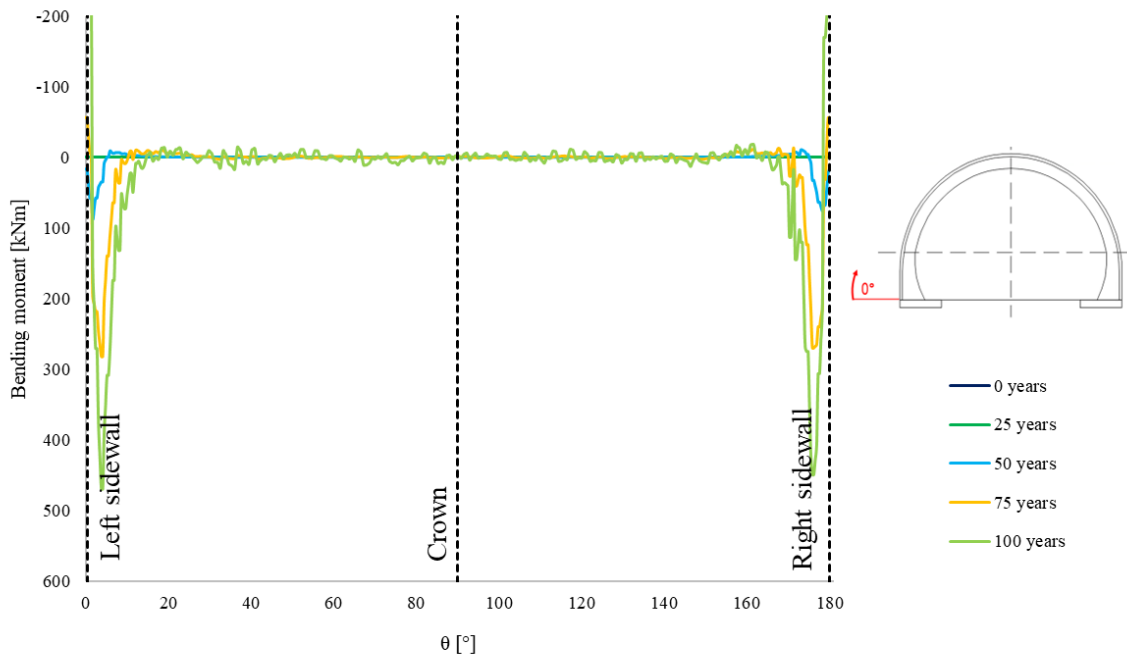
Model 8: PL_L_HSNI



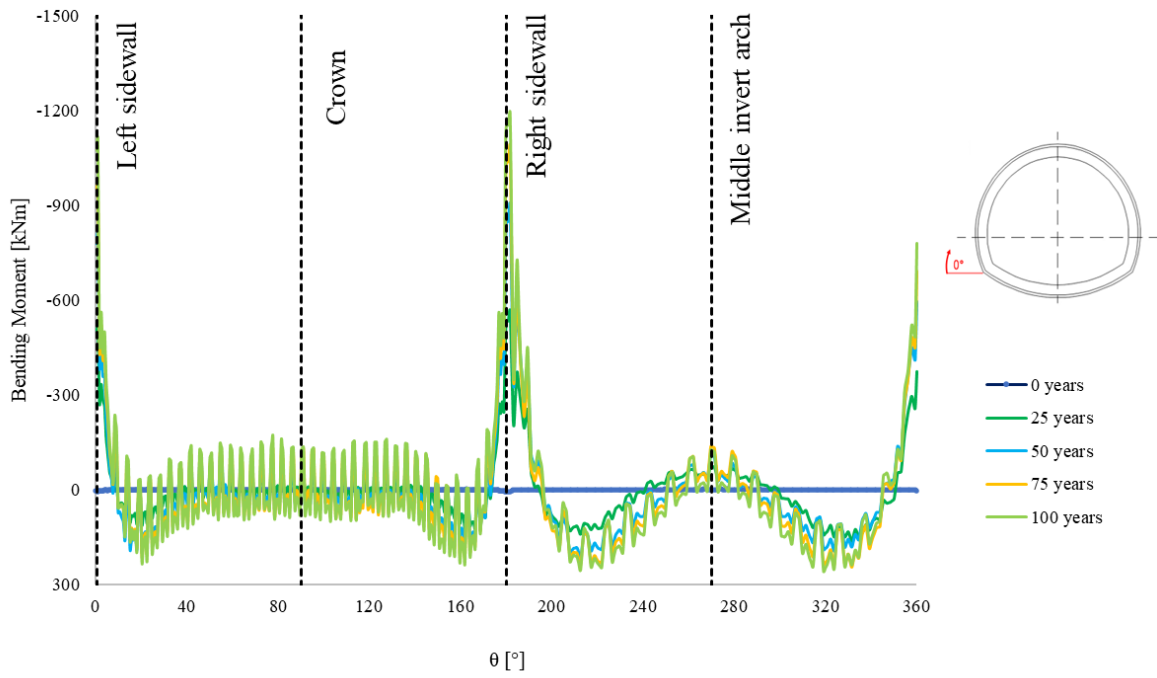
Model 9: RC_RM_PL_G_HSI



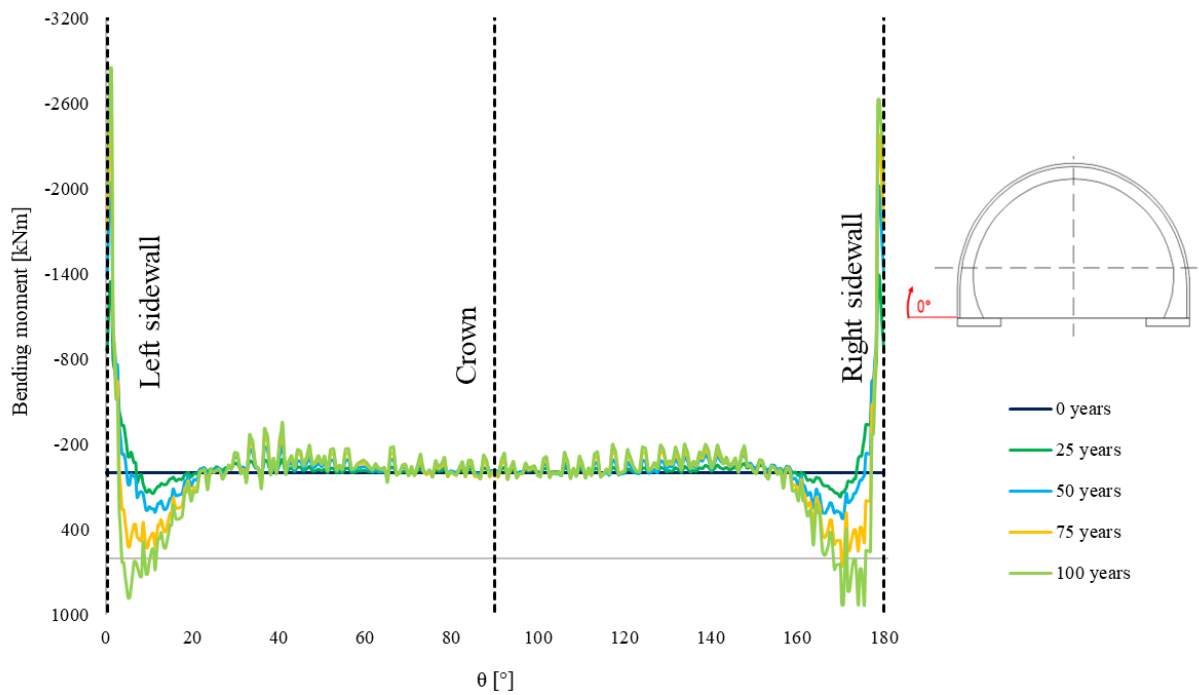
Model 10: RC_RM_PL_G_HSN1



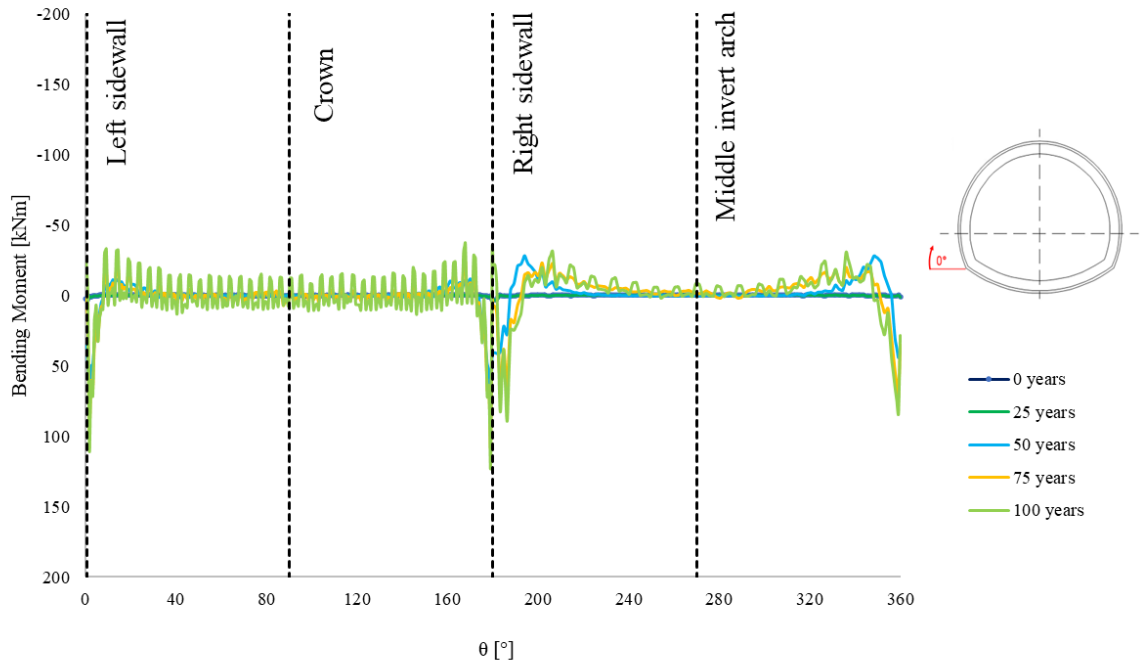
Model 11: RC_RM_PL_L_HSI



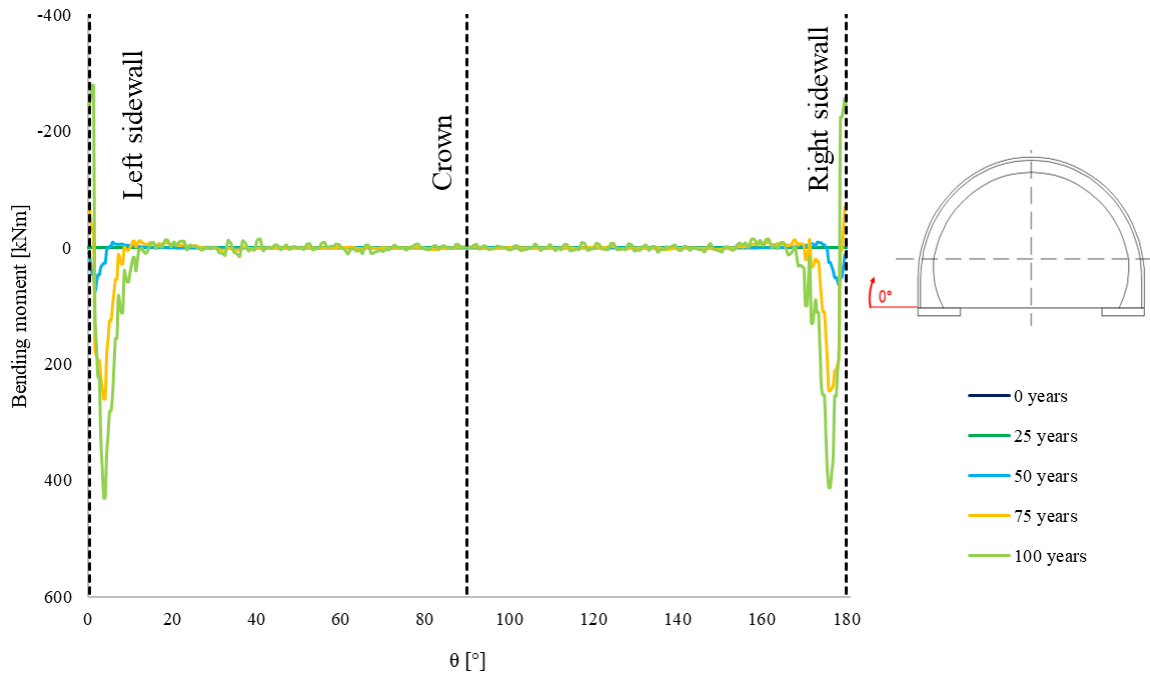
Model 12: RC_RM_PL_L_HSNI



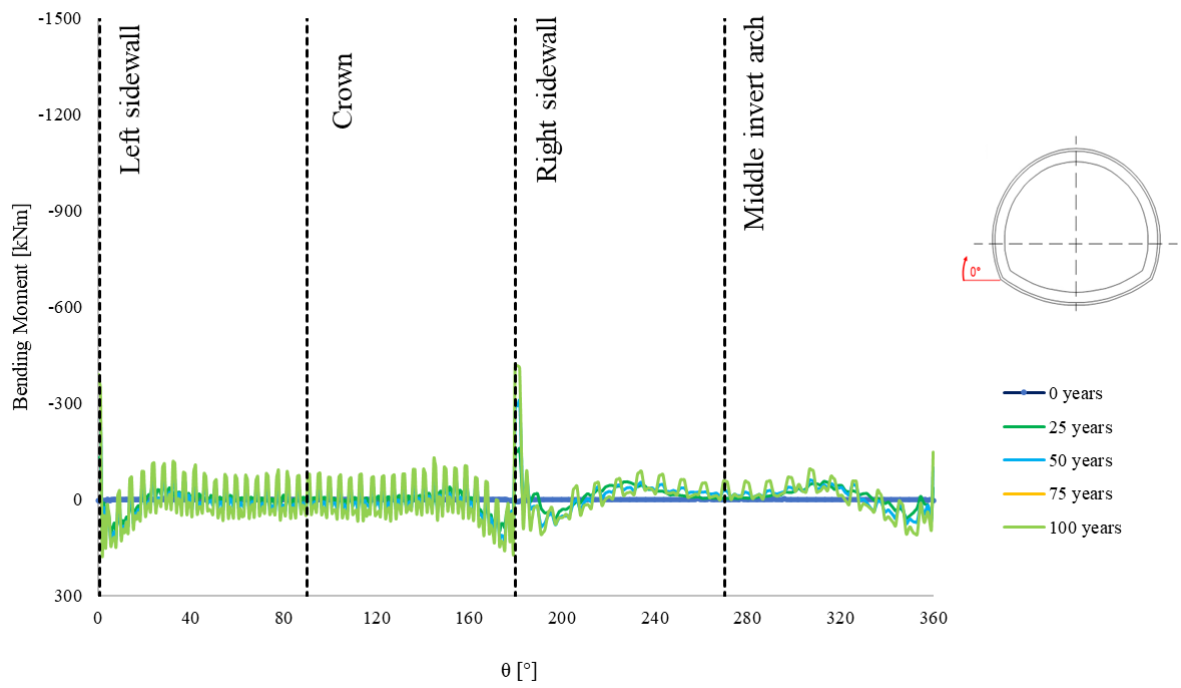
Model 13: RC_PL_G_HSI



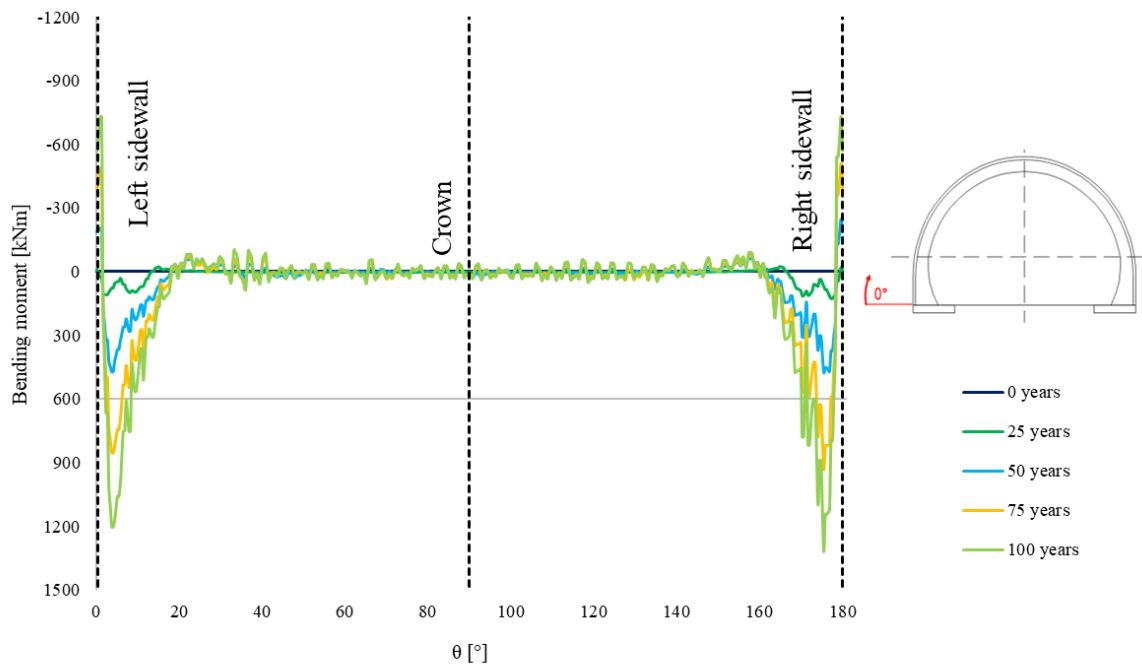
Model 14: RC_PL_G_HSNI



Model 15: RC_PL_L_HSI

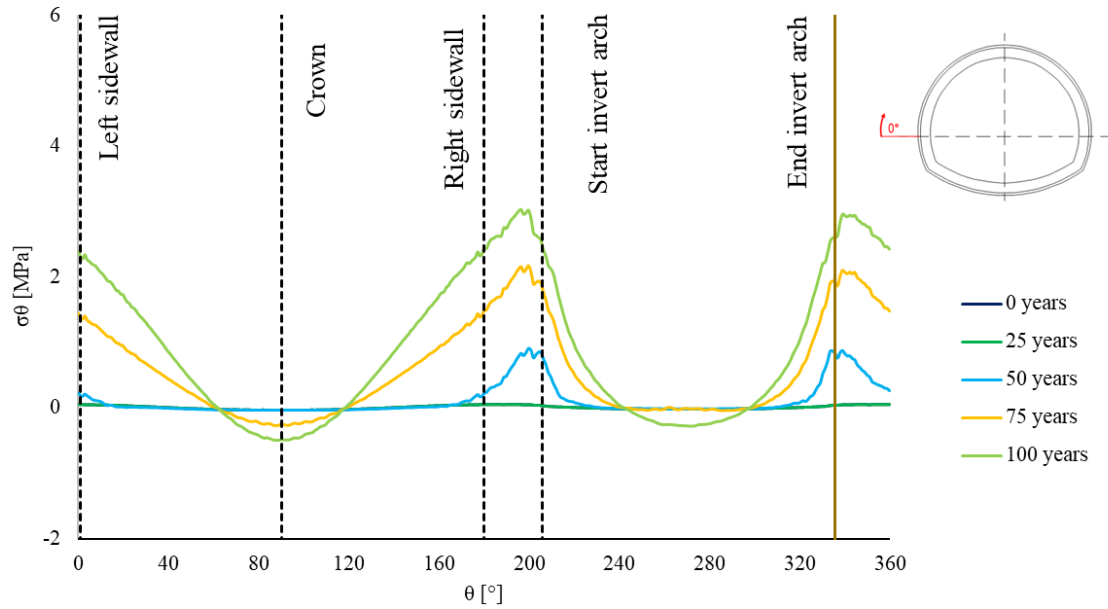


Model 16: RC_PL_L_HSNI

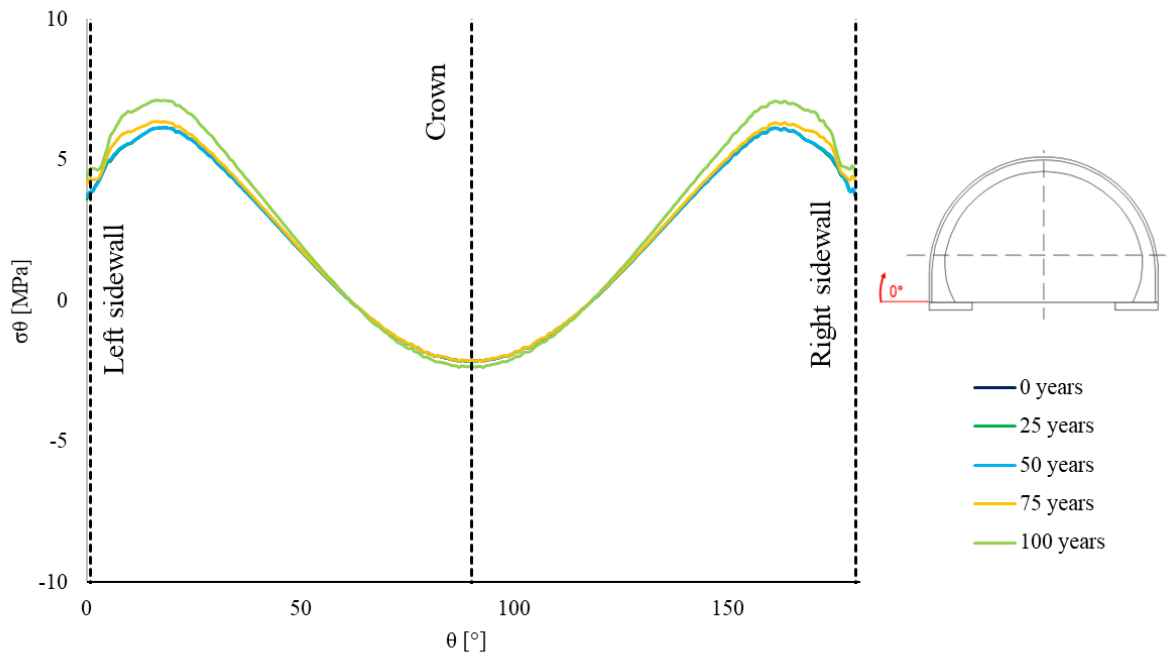


Appendix B.3. Stresses

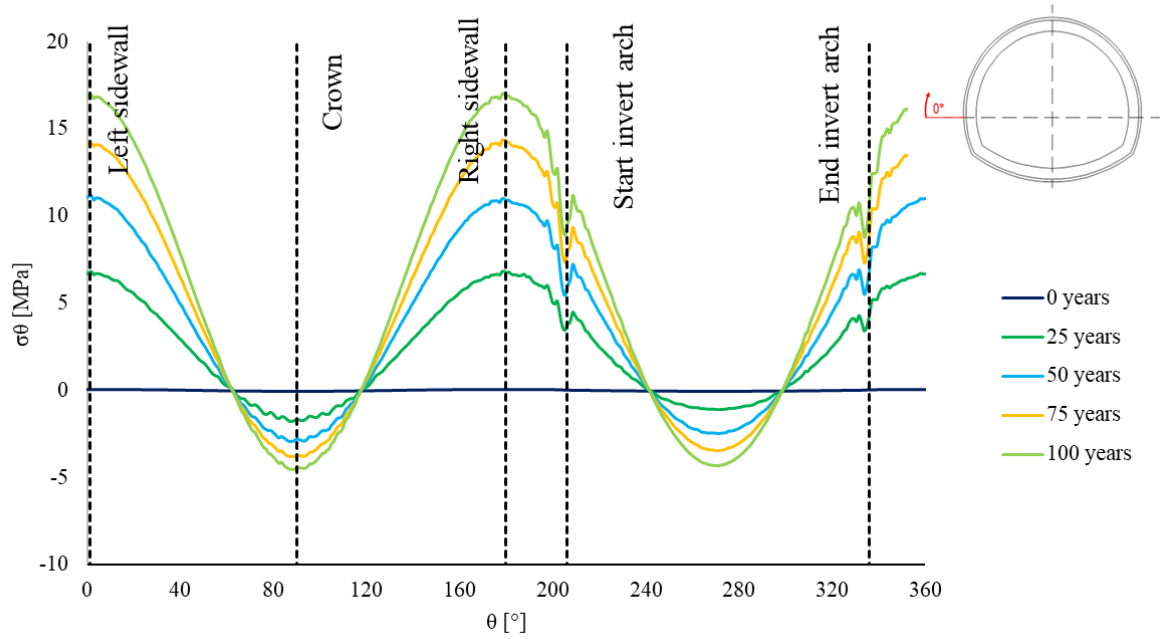
Model 1: PC_RM_PL_G_HSI



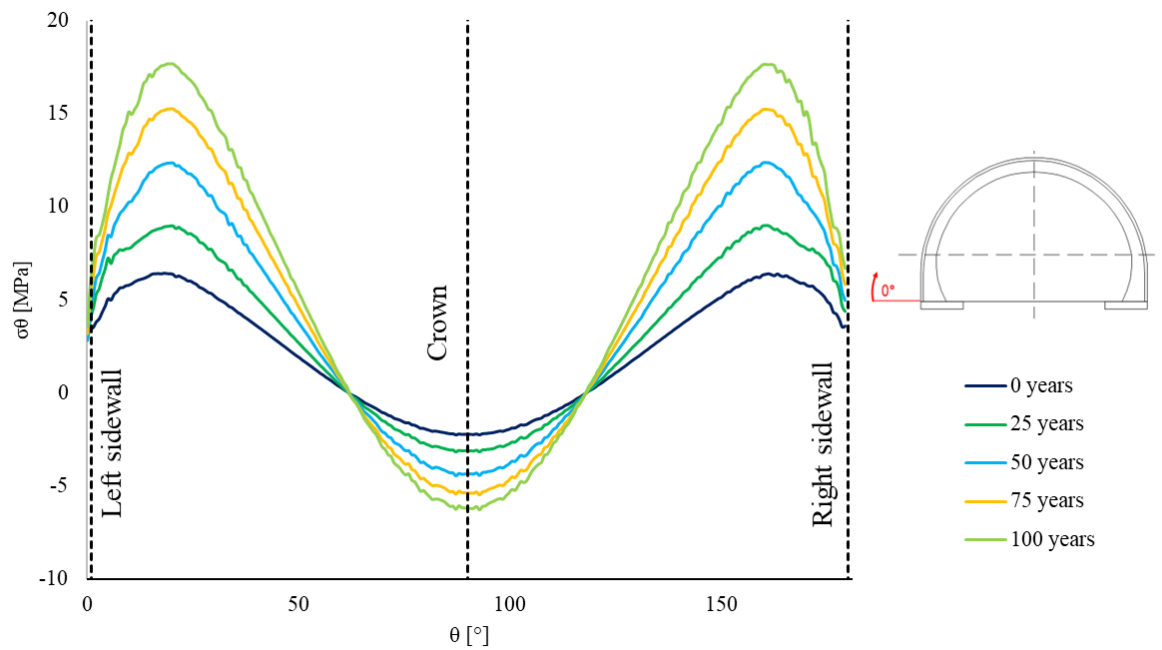
Model 2: PC_RM_PL_G_HSNI



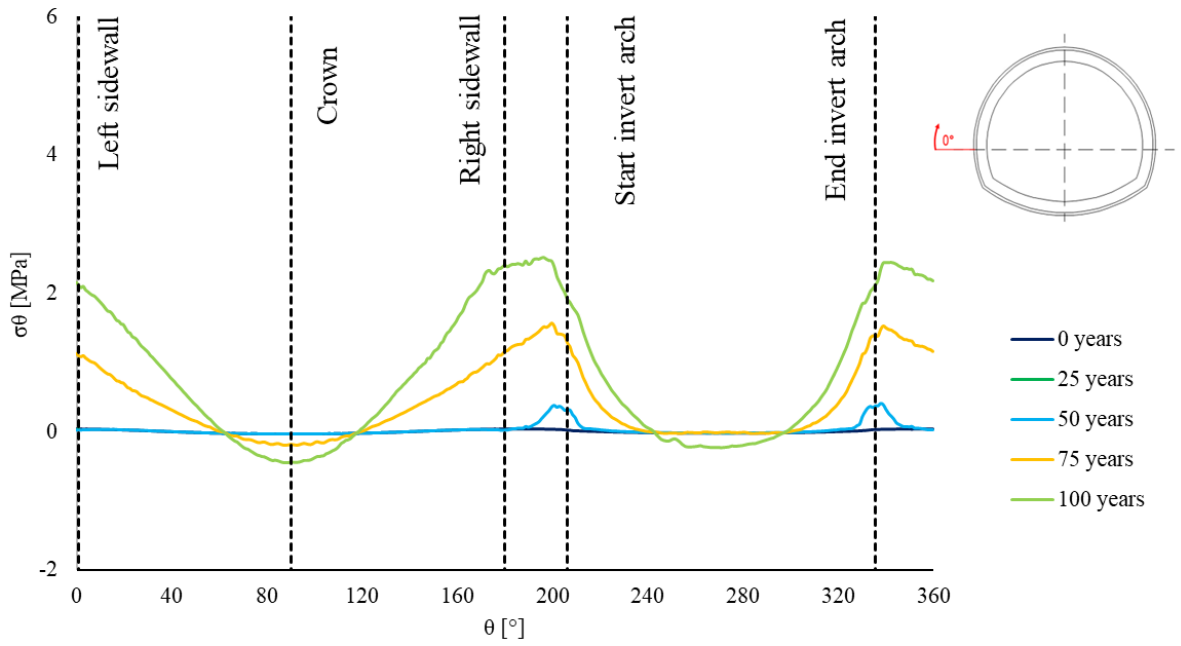
Model 3: PC_RM_PL_L_HSI



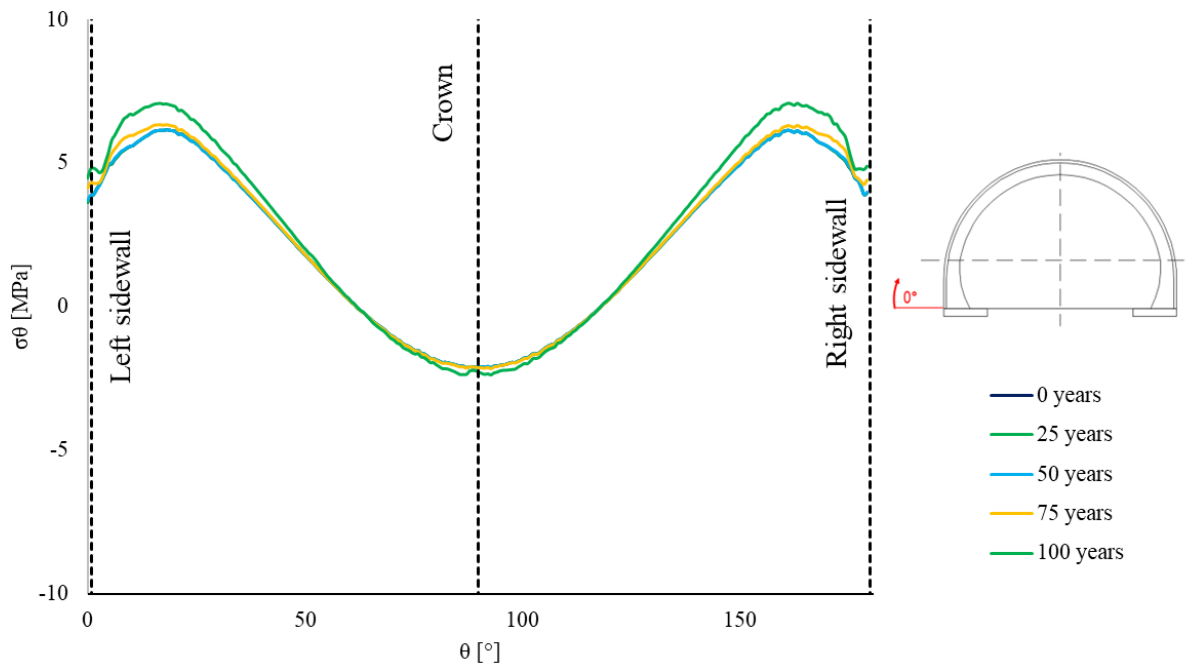
Model 4: PC_RM_PL_P_HSNI

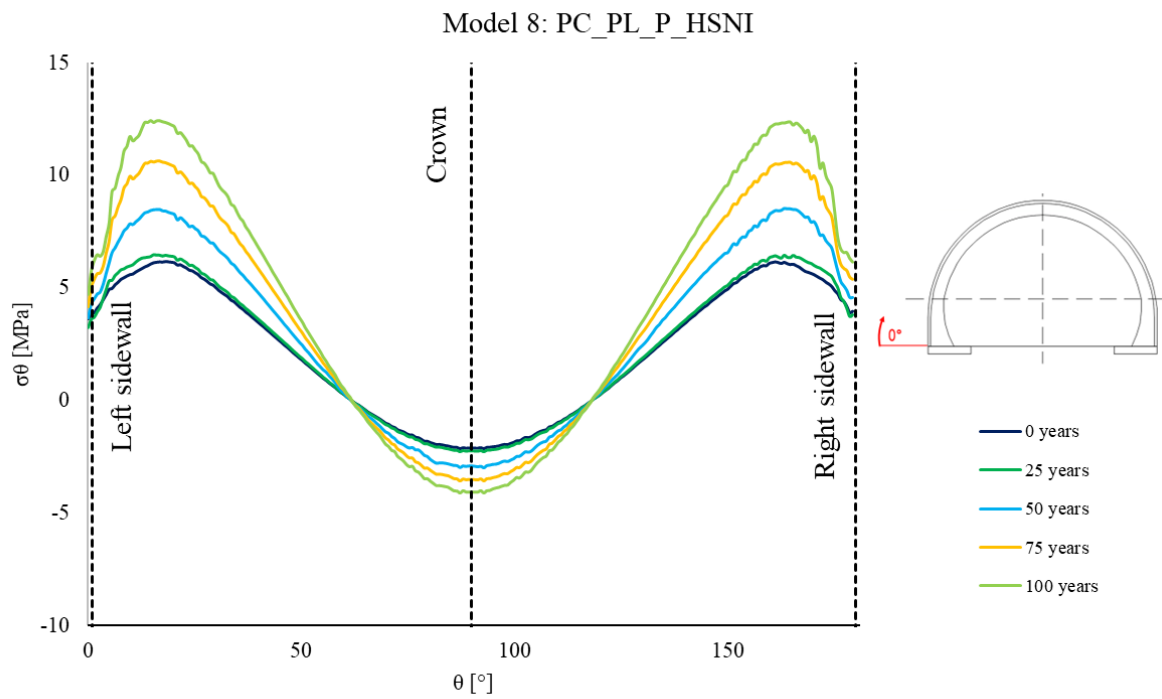
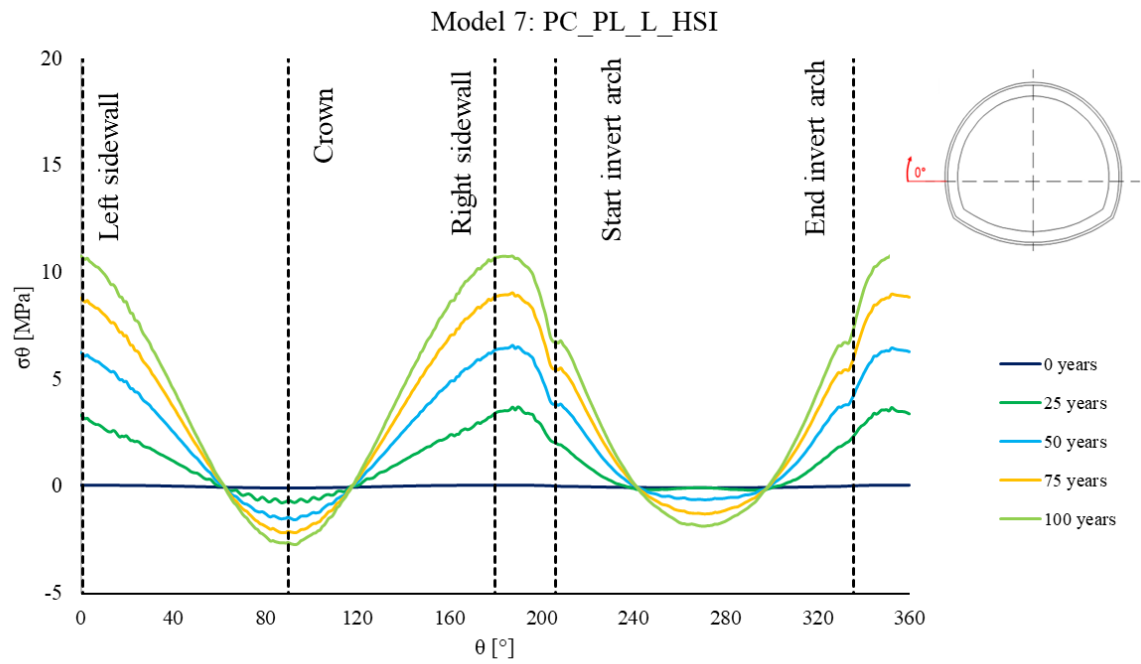


Model 5: PC_PL_G_HSI

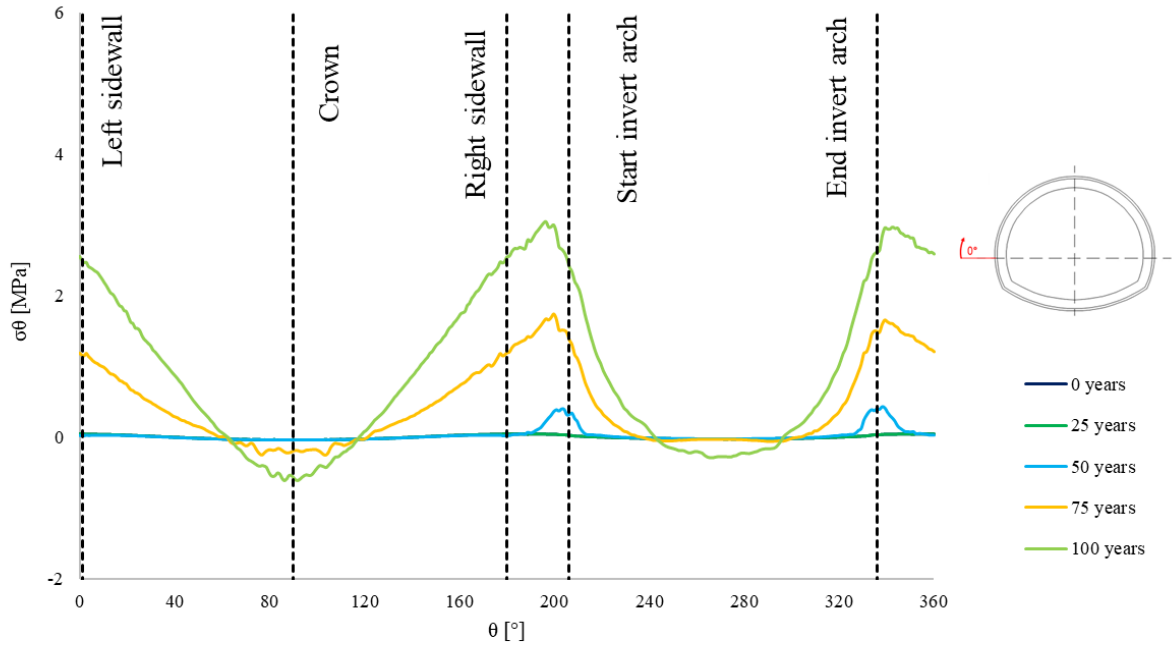


Model 6: PC_PL_G_HSNI

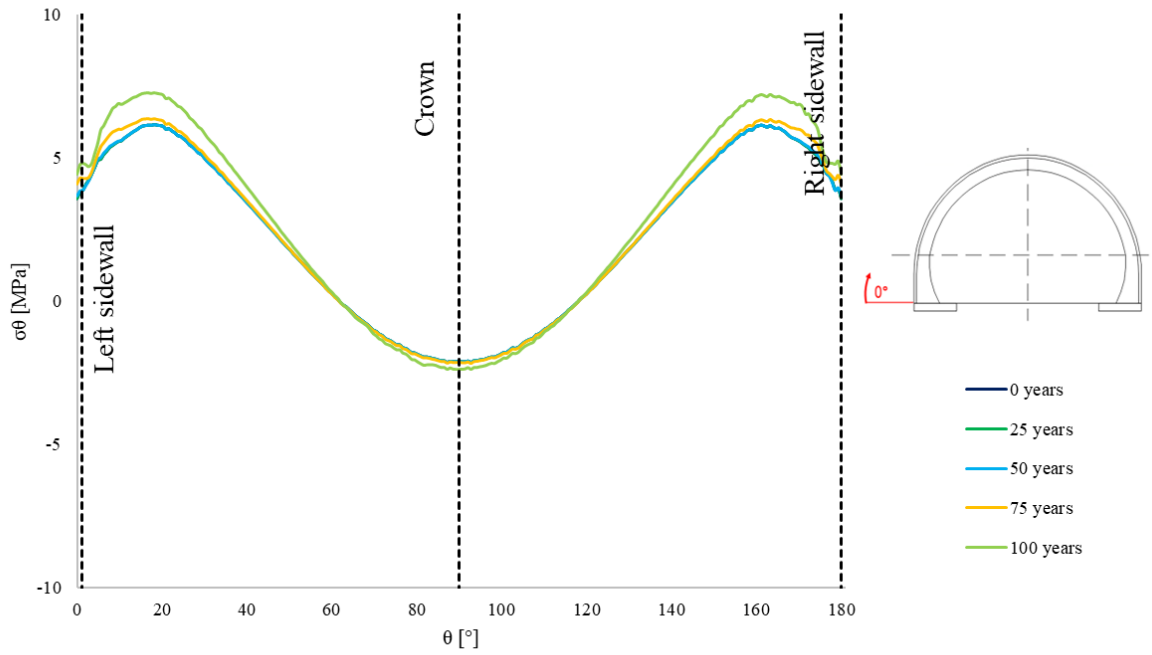




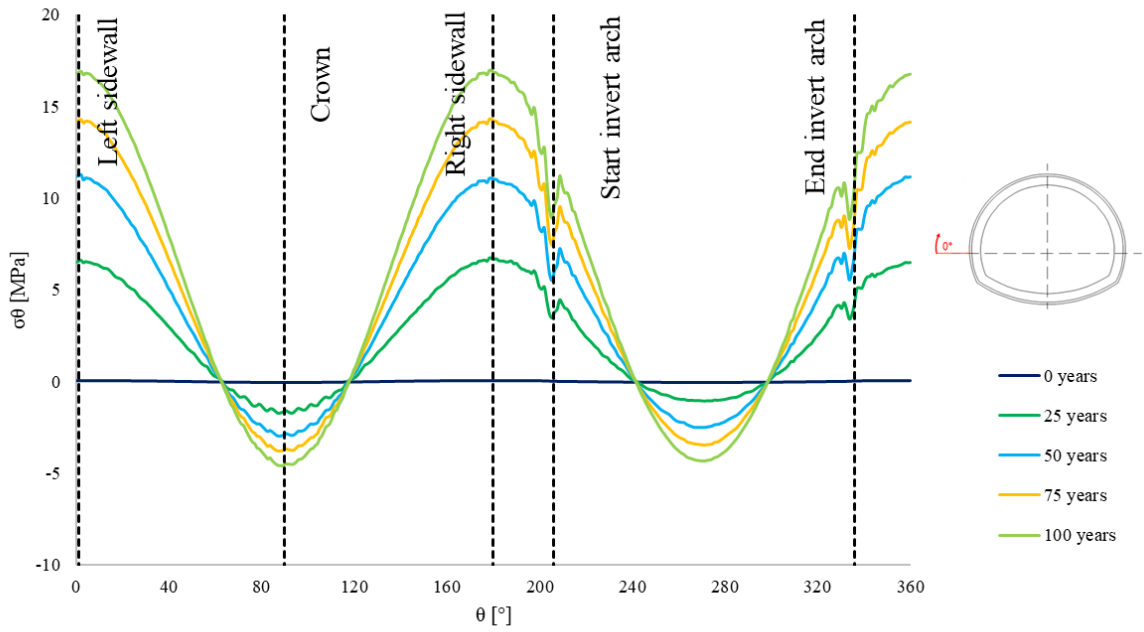
Model 9: RC_RM_PL_G_HSI



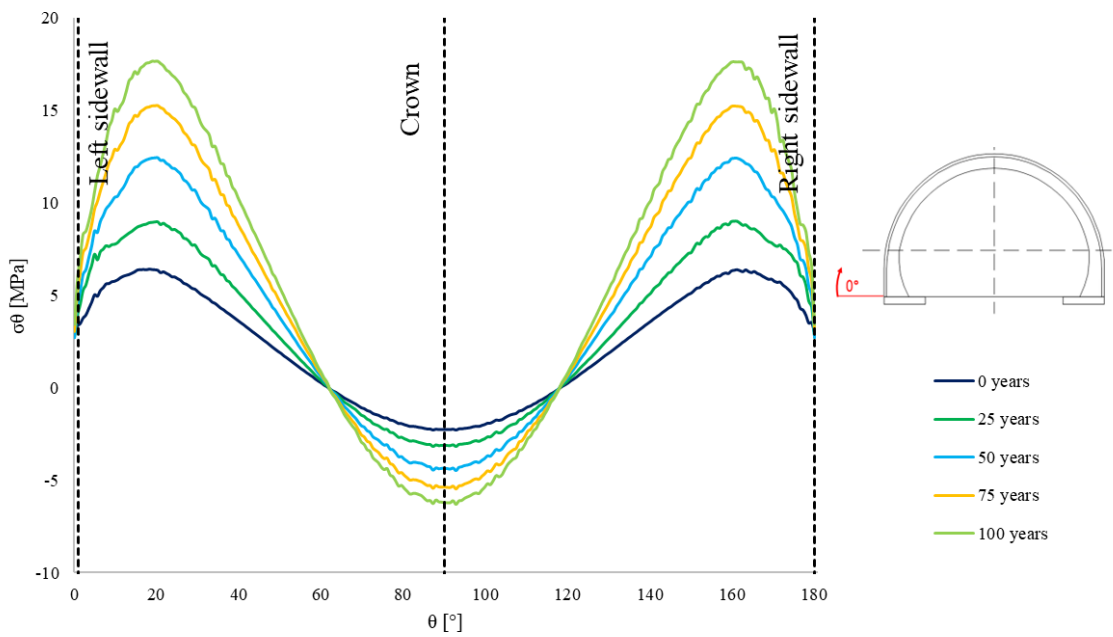
Model 10: RC_RM_PL_G_HSNI



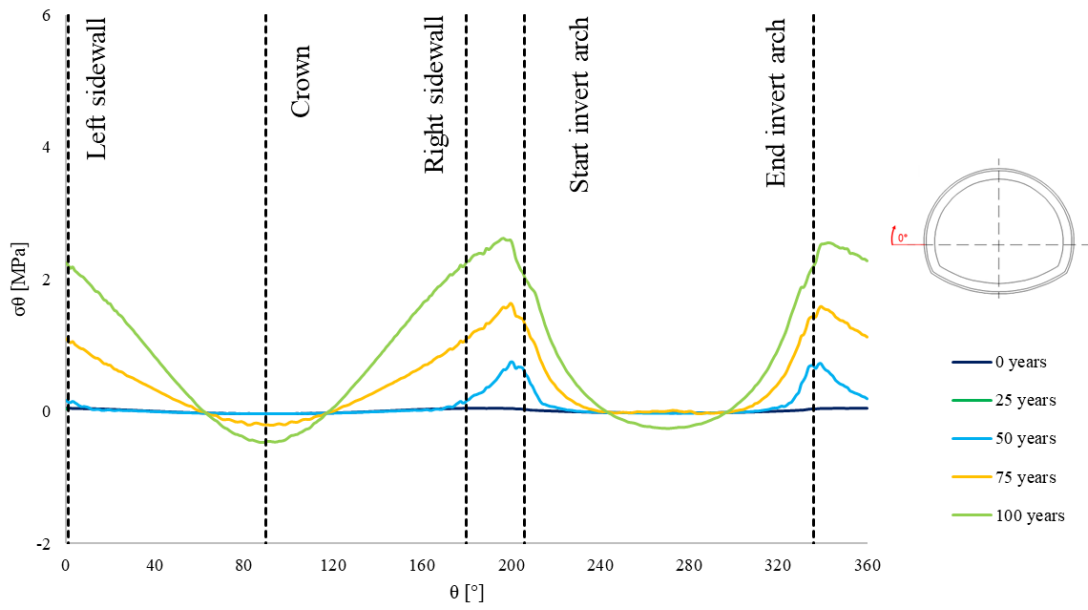
Model 11: RC_RM_PL_L_HSI



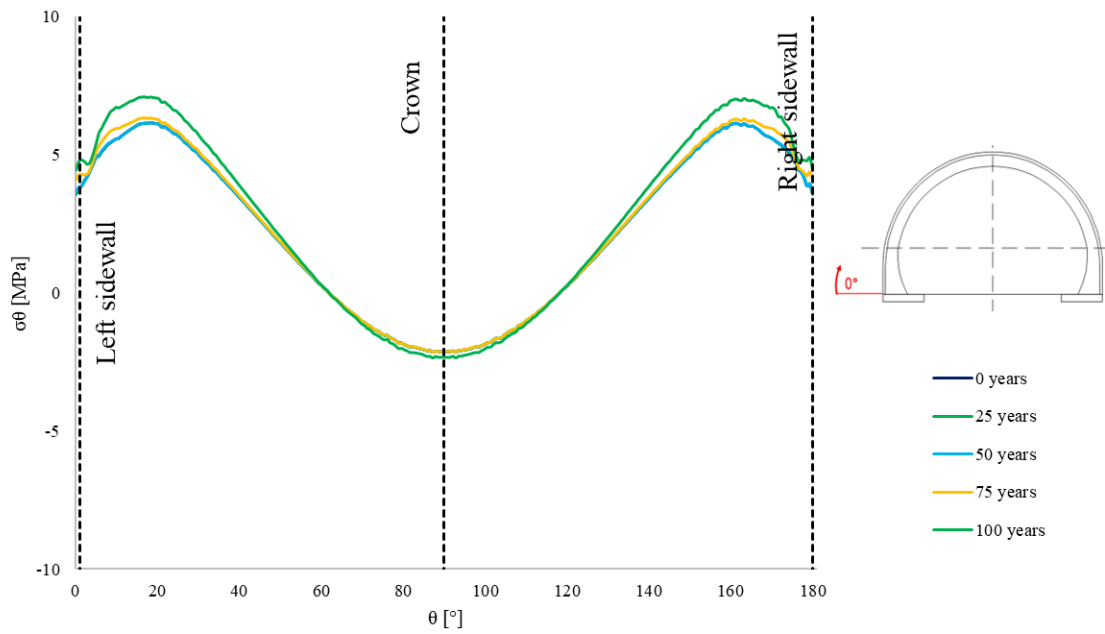
Model 12: RC_RM_PL_P_HSNI



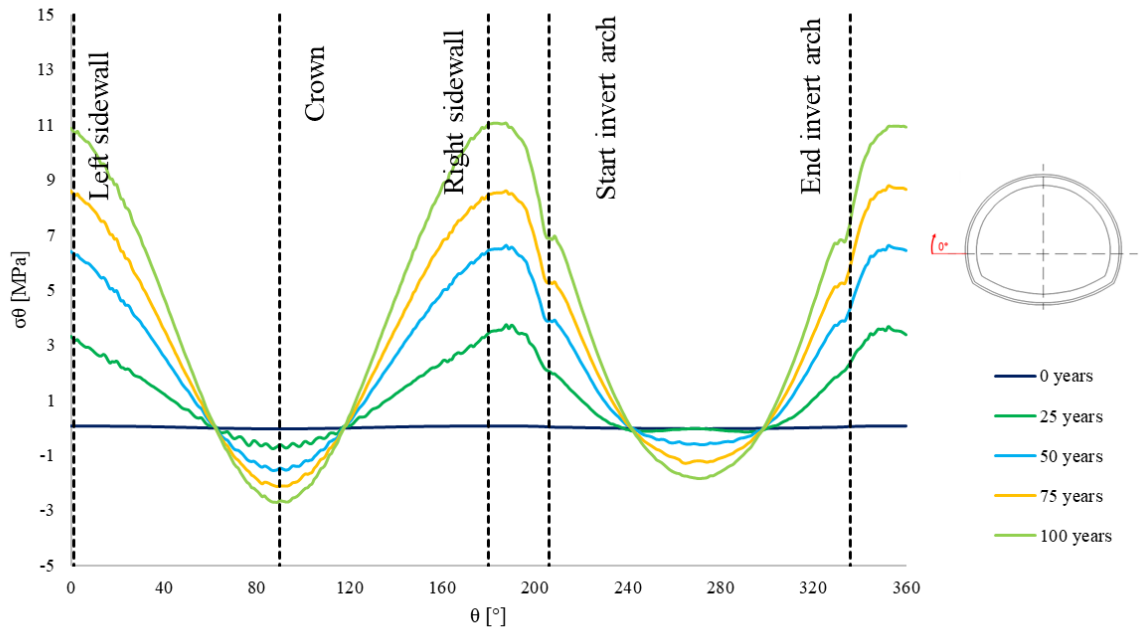
Model 13: RC_PL_G_HSI



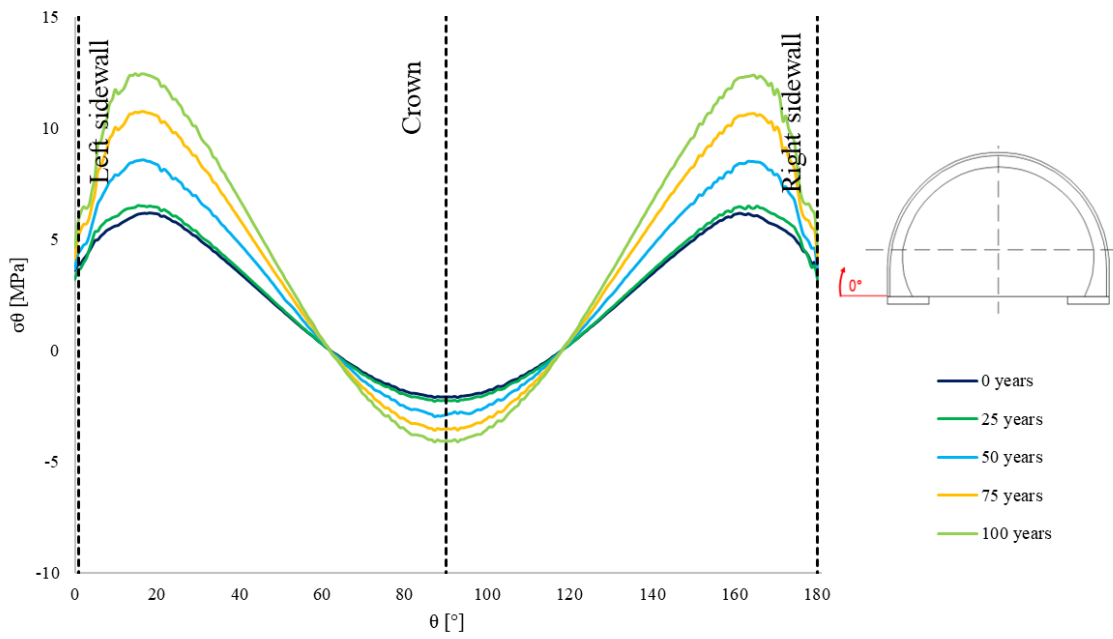
Model 14: RC_PL_G_HSNI



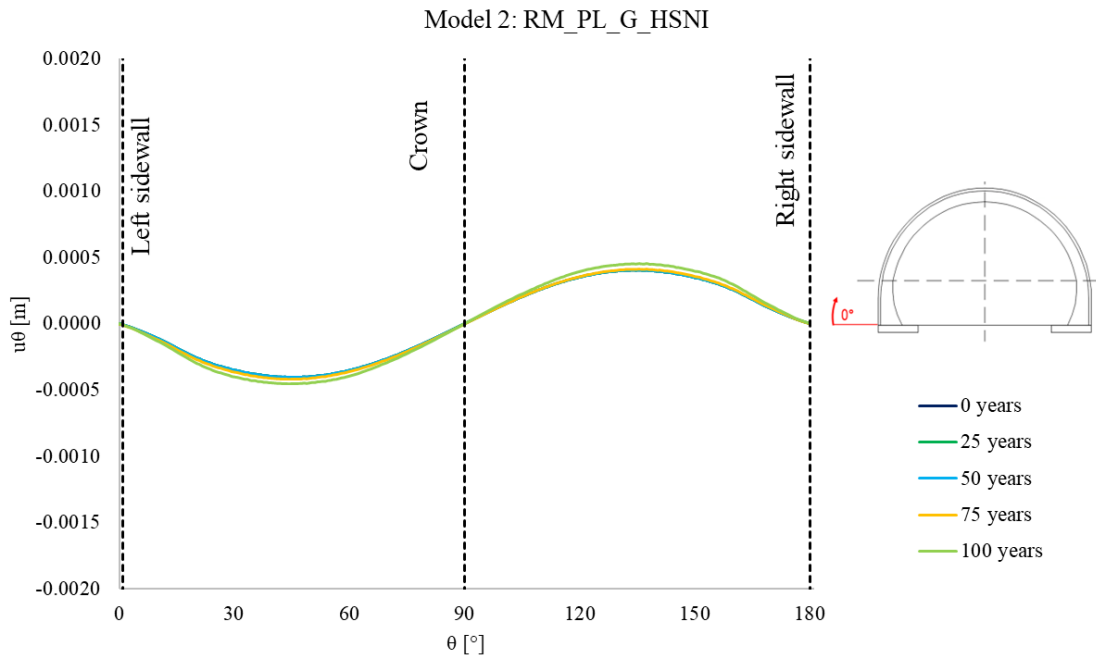
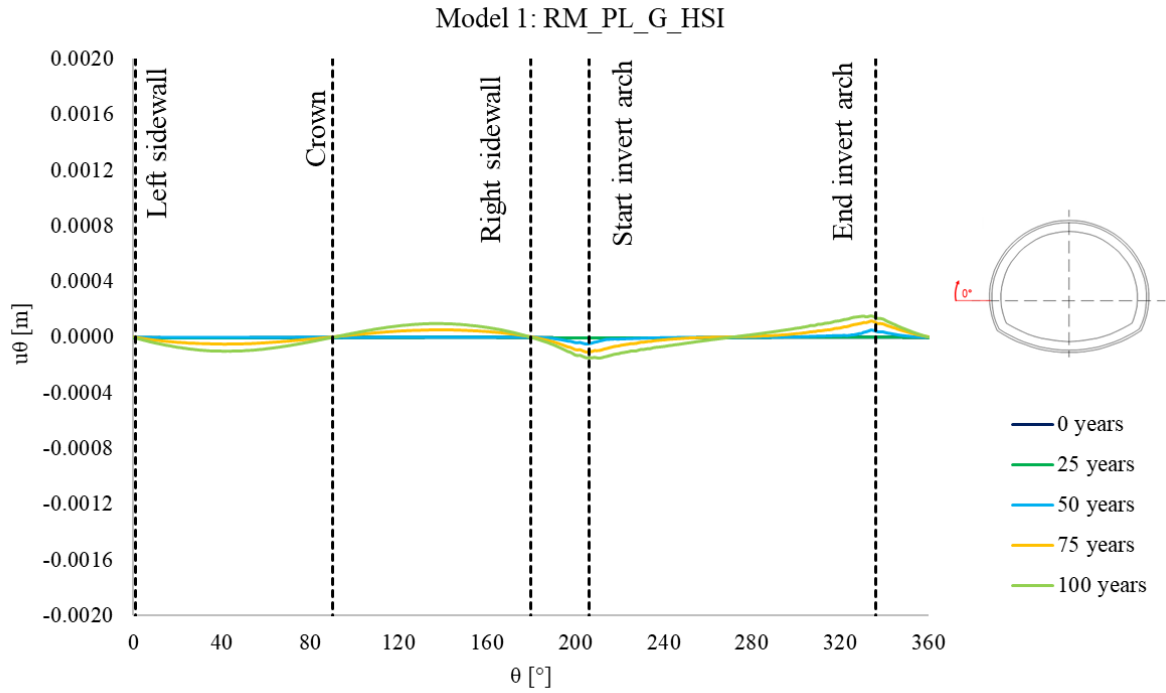
Model 15: RC_PL_L_HSI

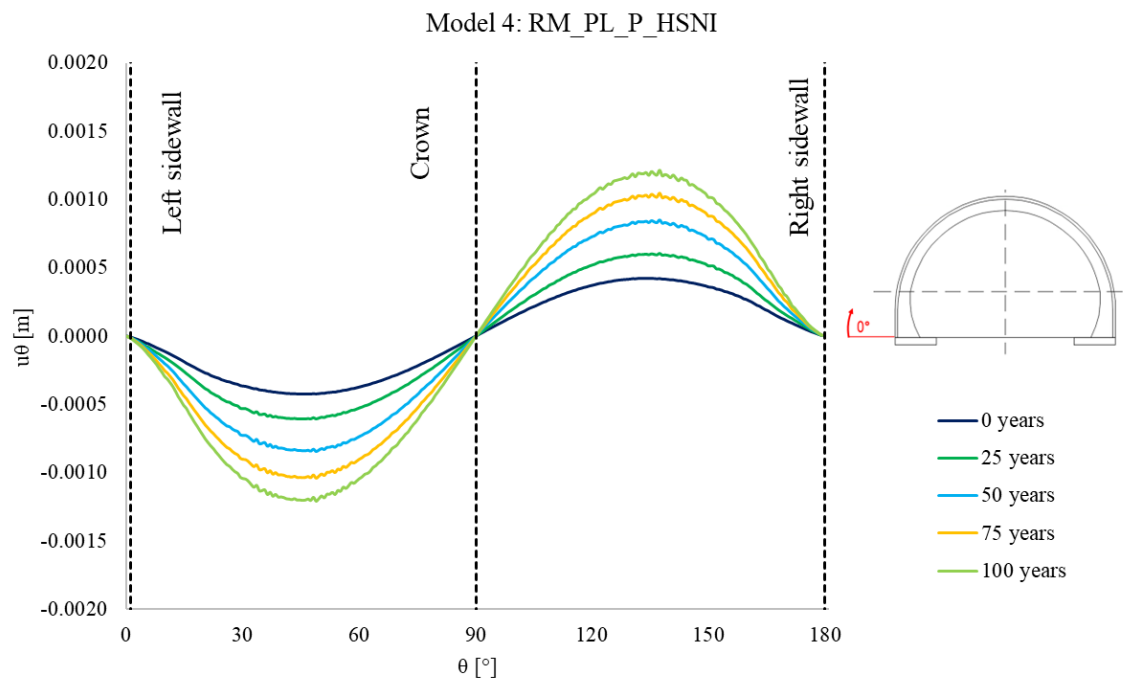
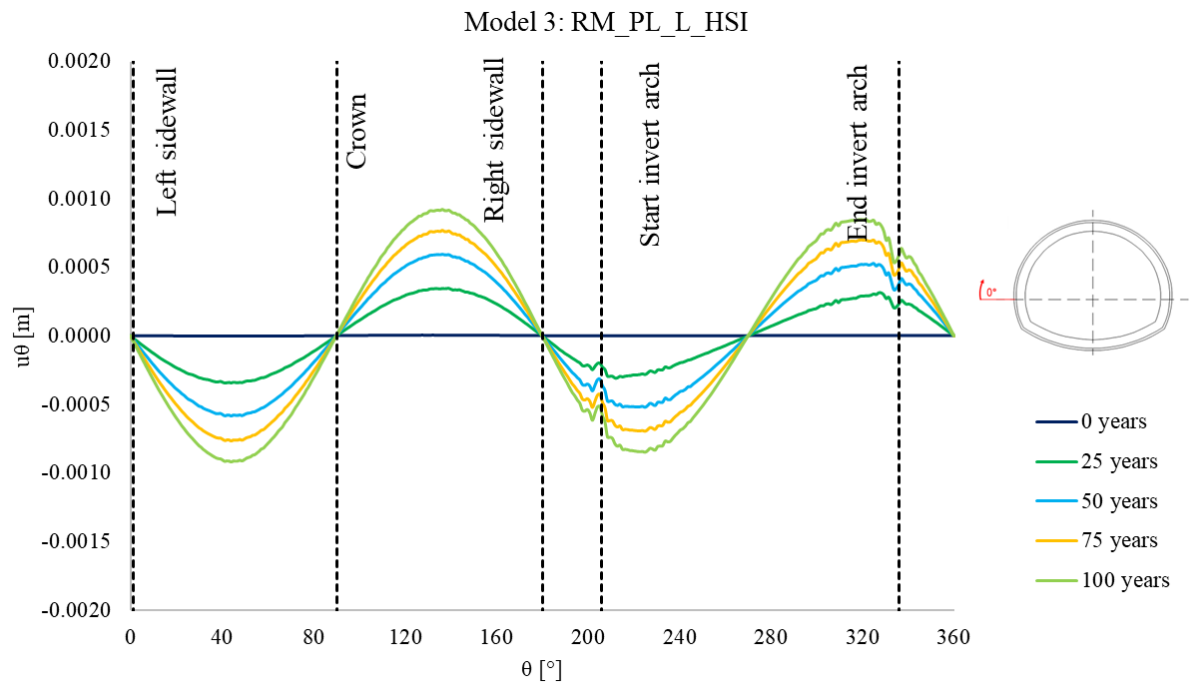


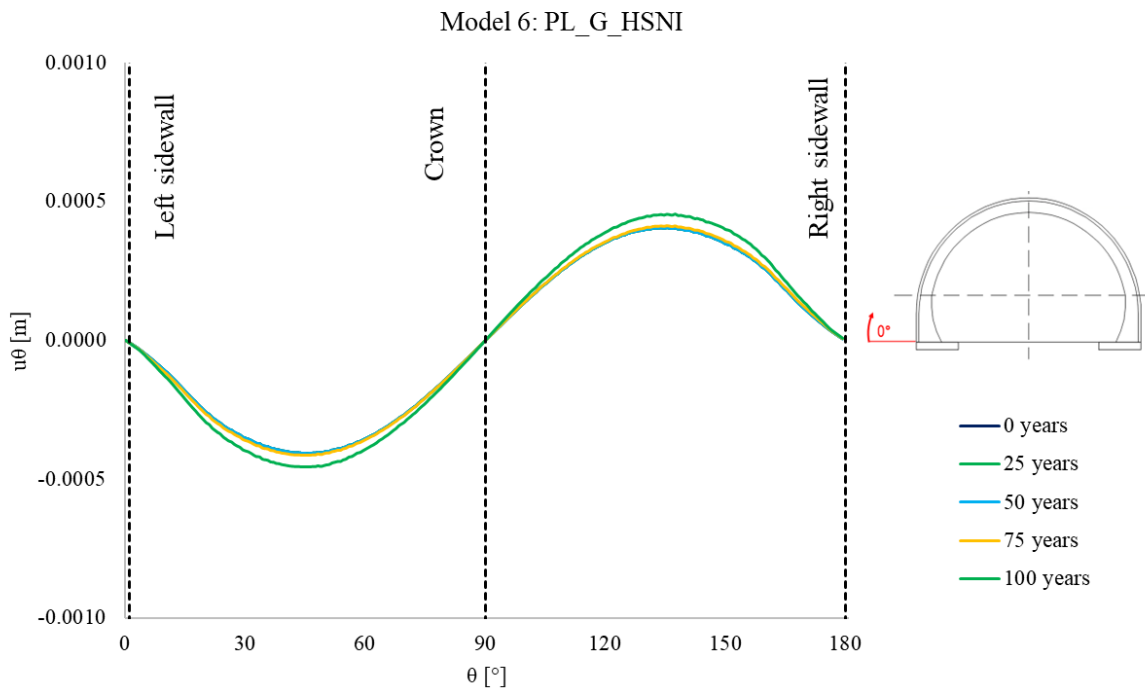
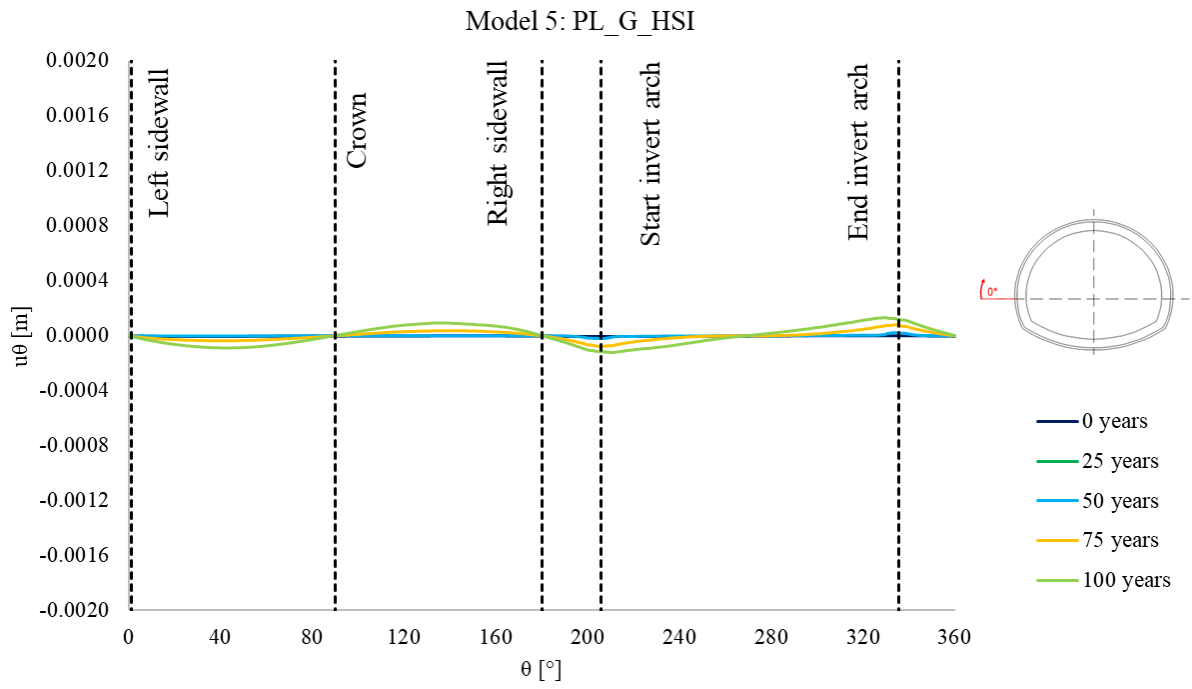
Model 16: RC_PL_P_HSNI

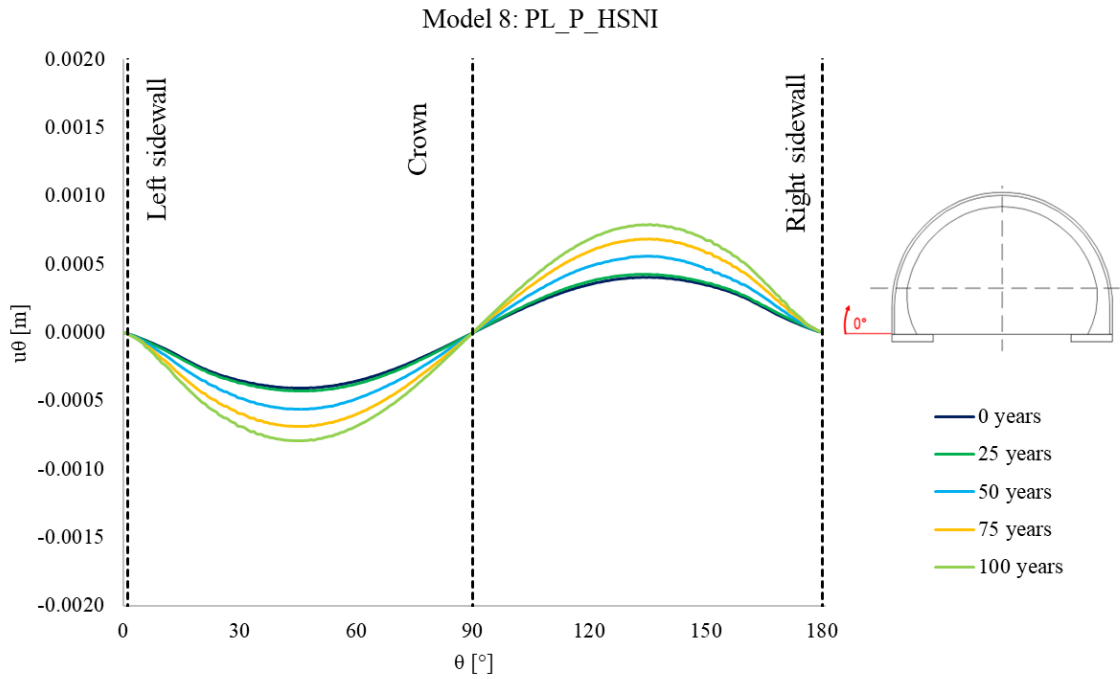
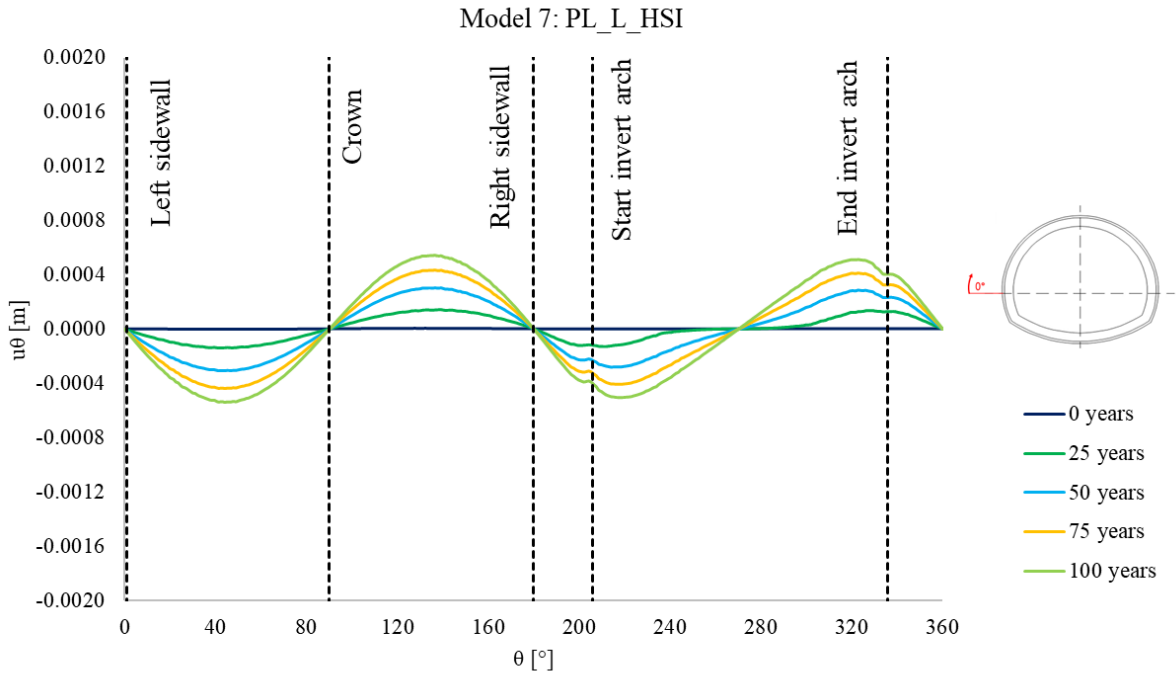


Appendix B.3. Stresses

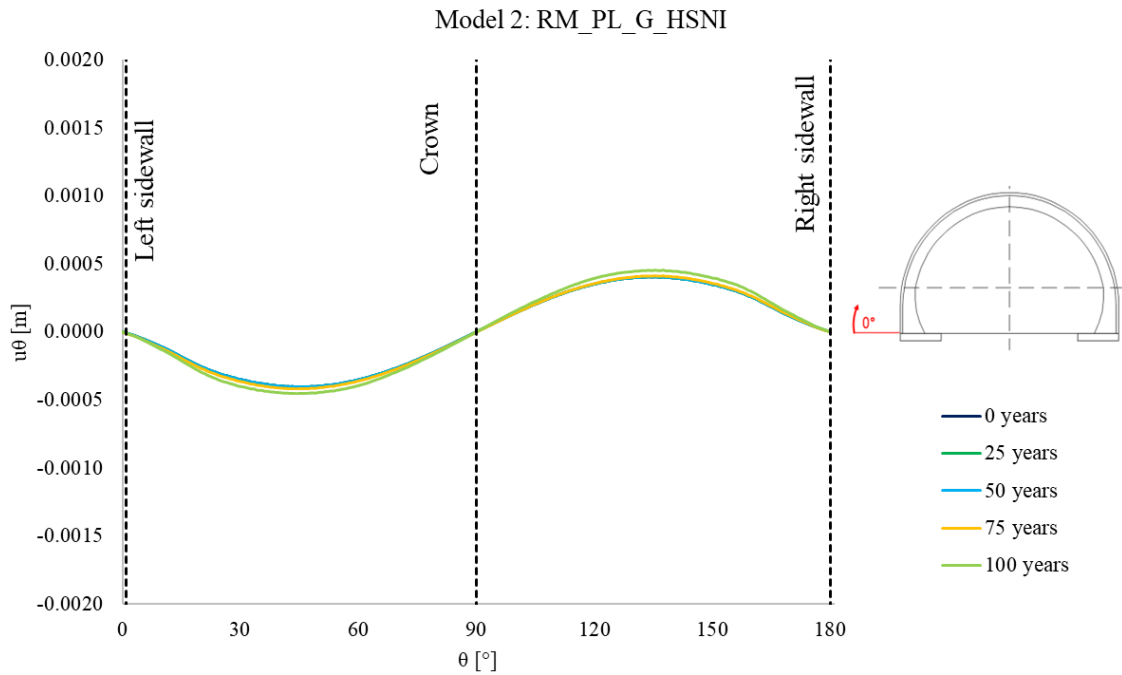
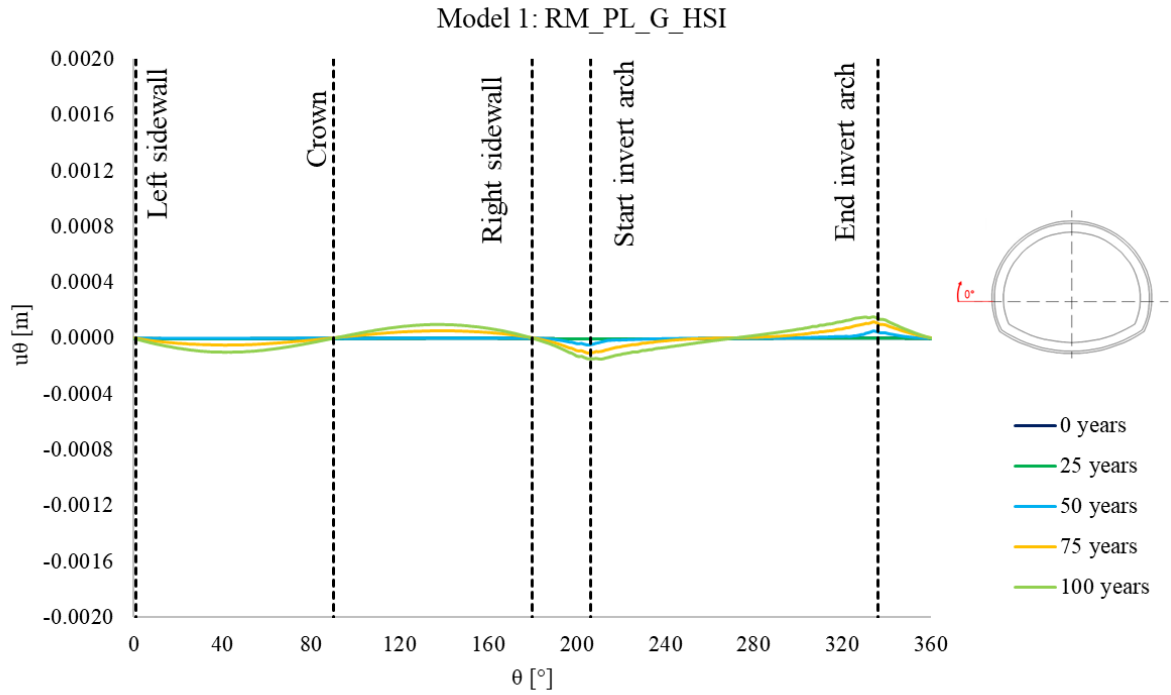


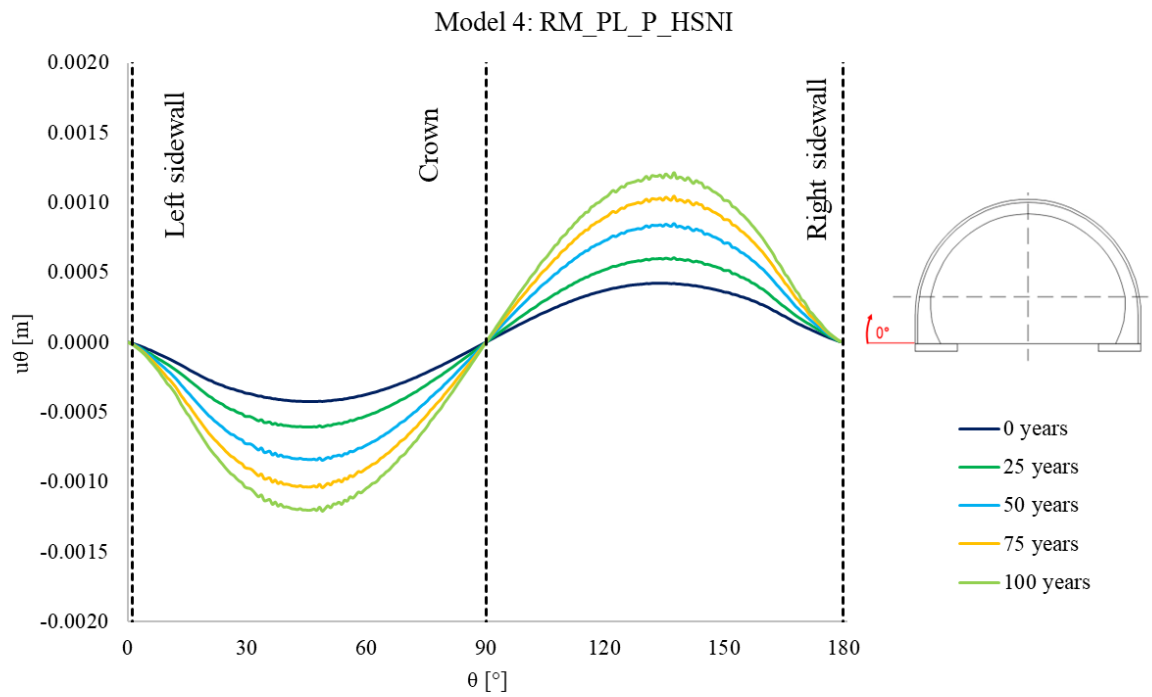
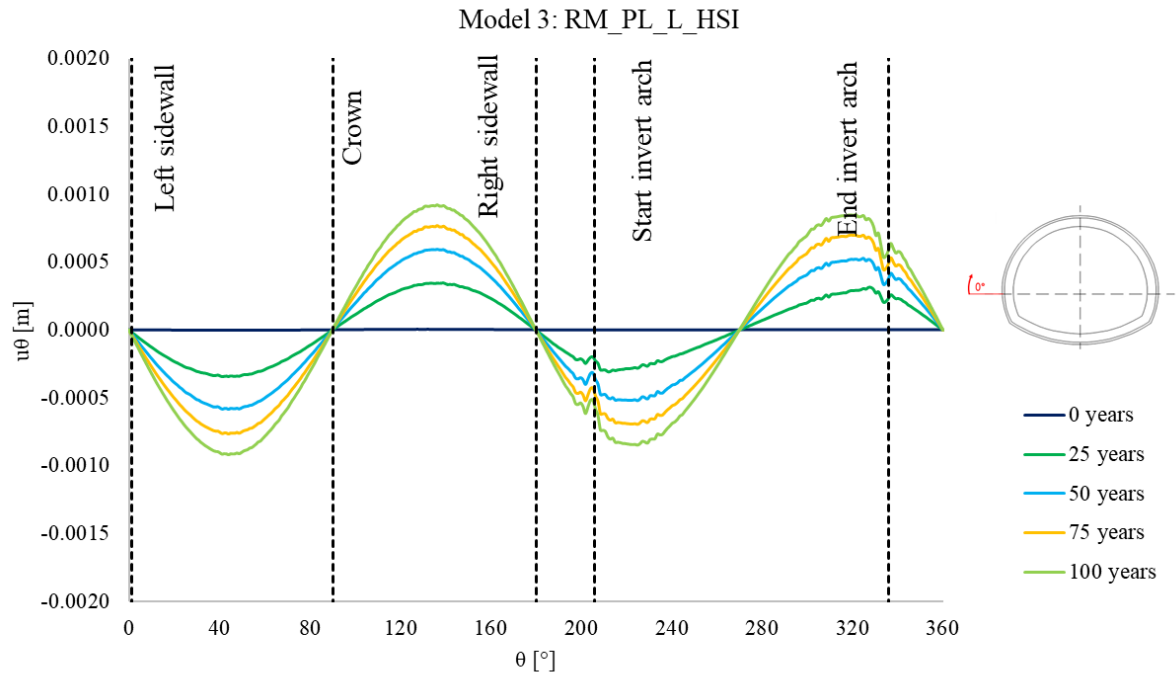


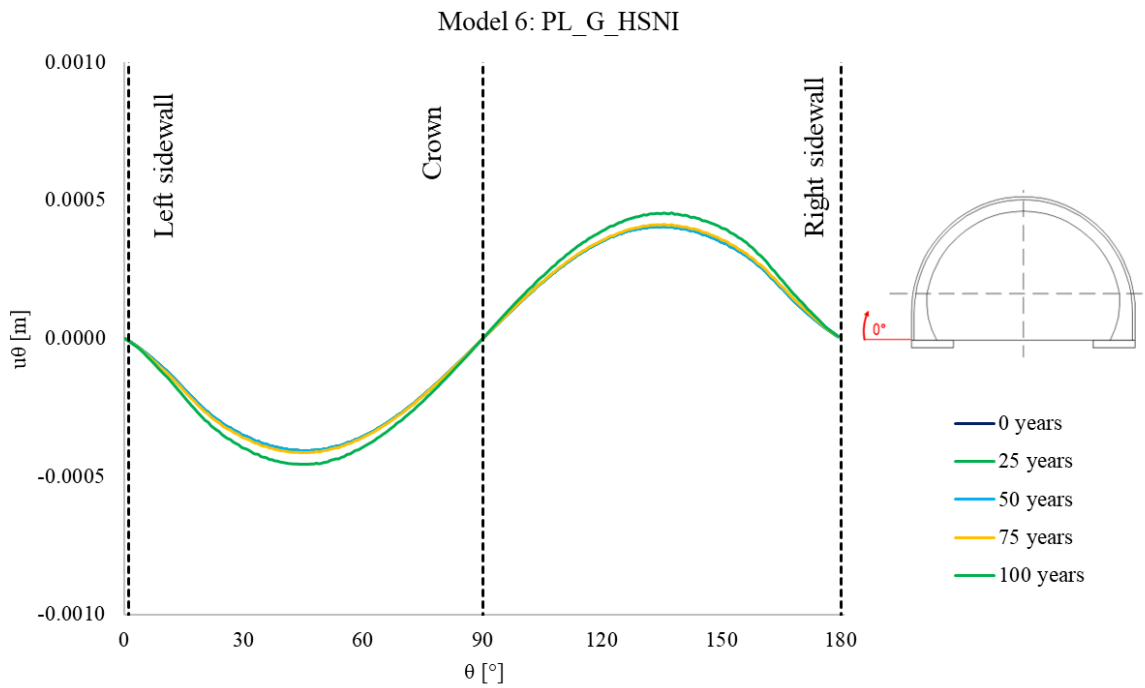
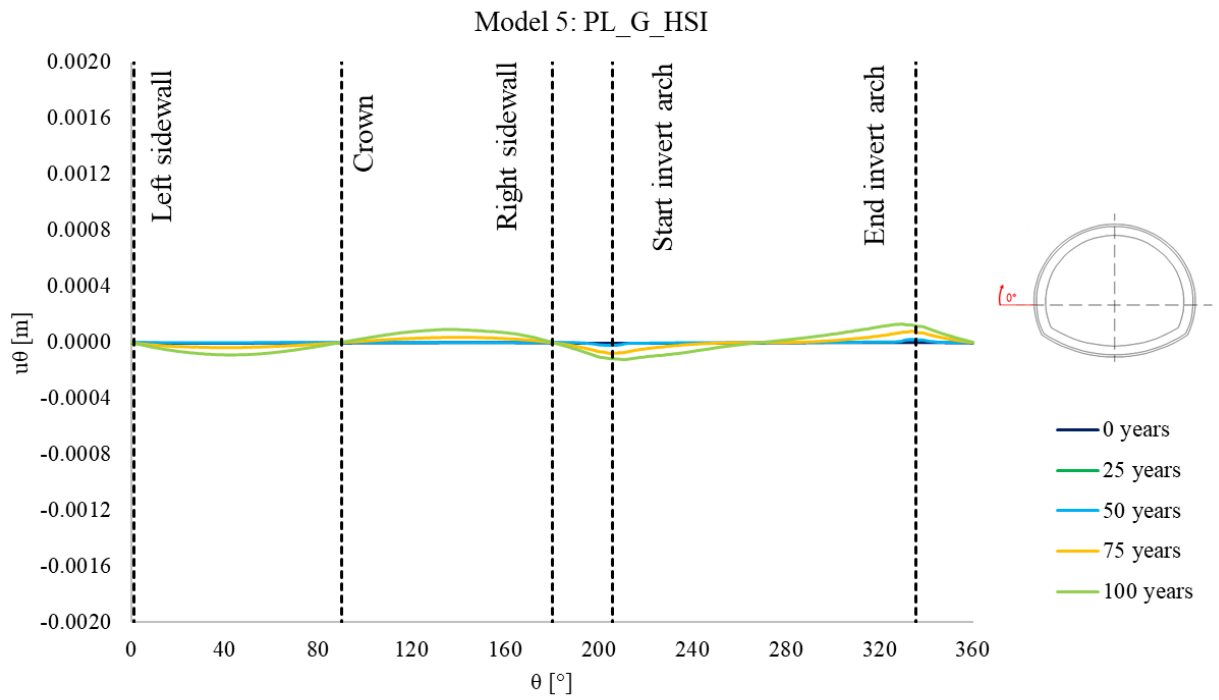


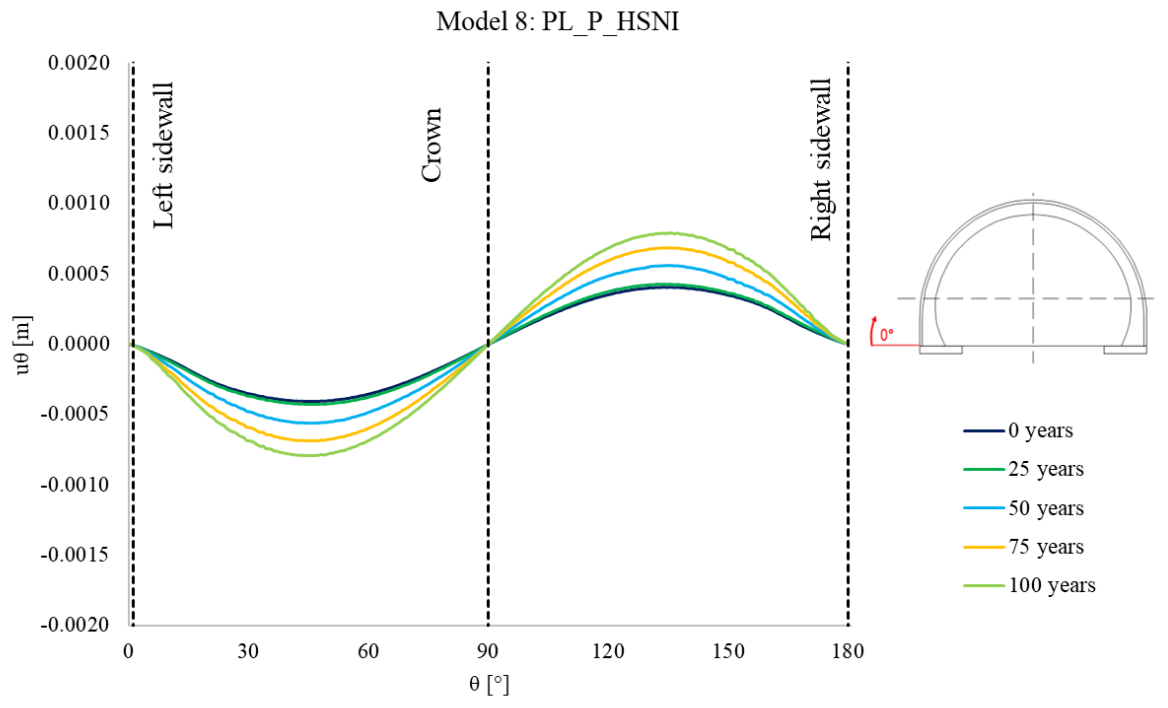
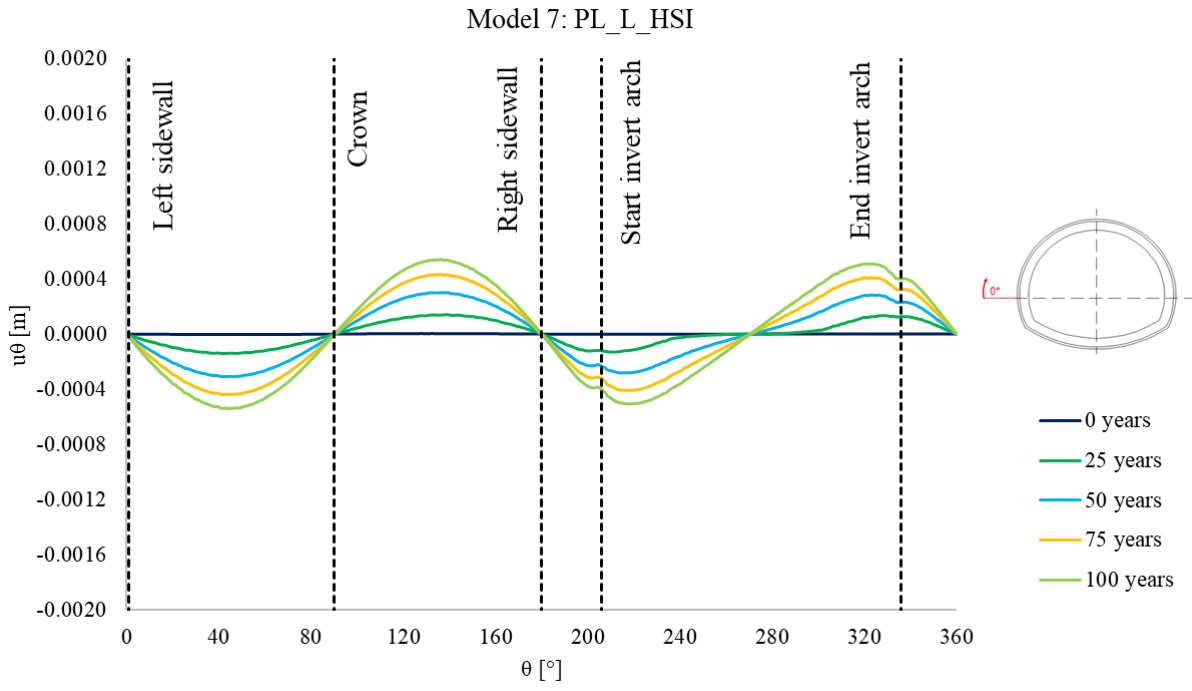


Appendix B.4. Displacements

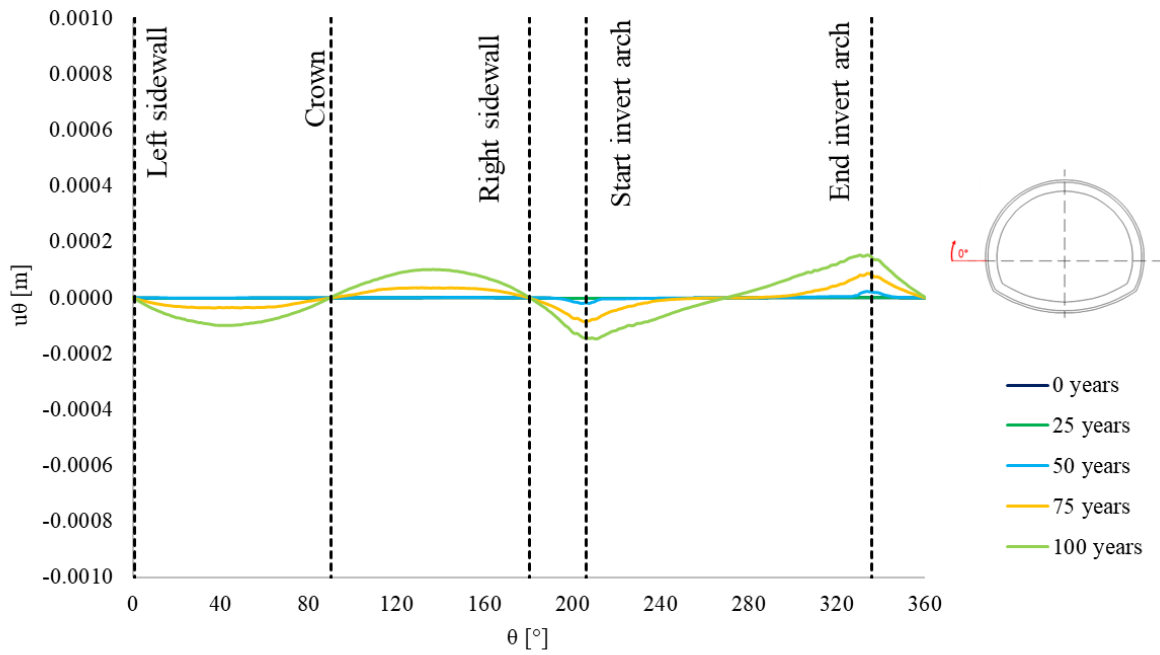




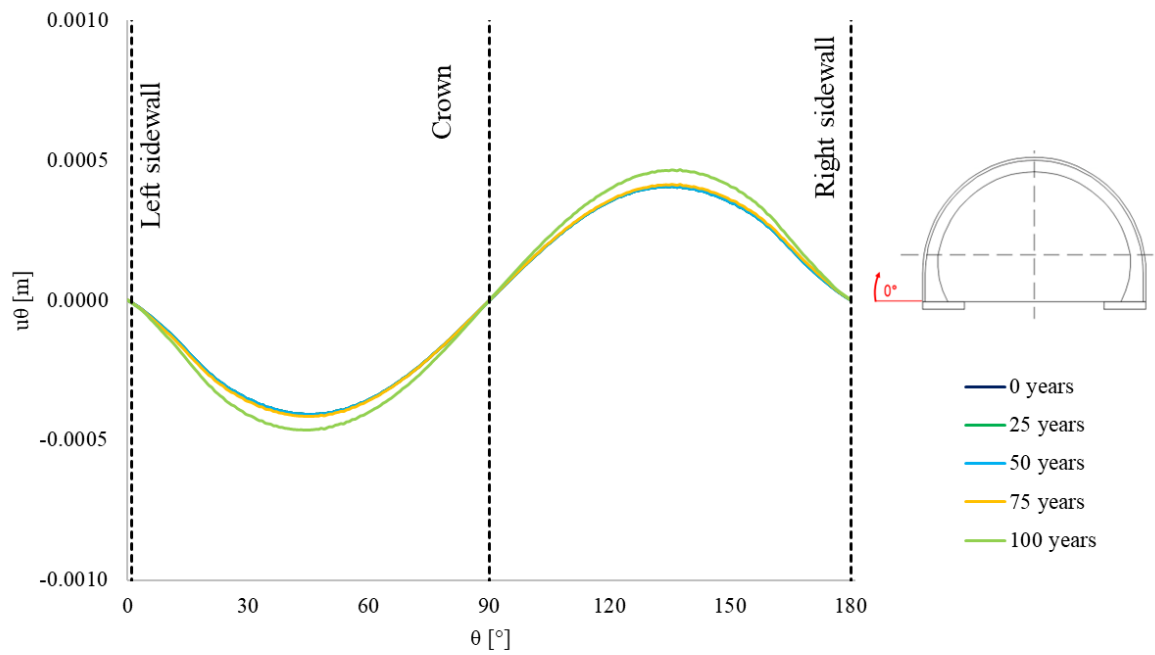




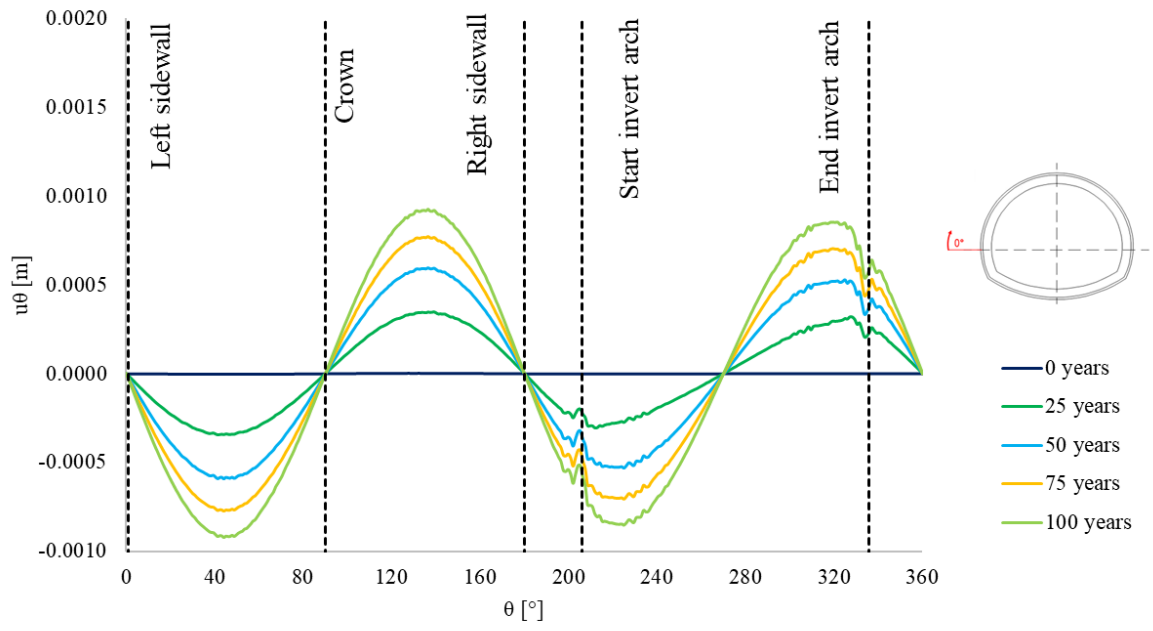
Model 9: RC_RM_PL_G_HSI



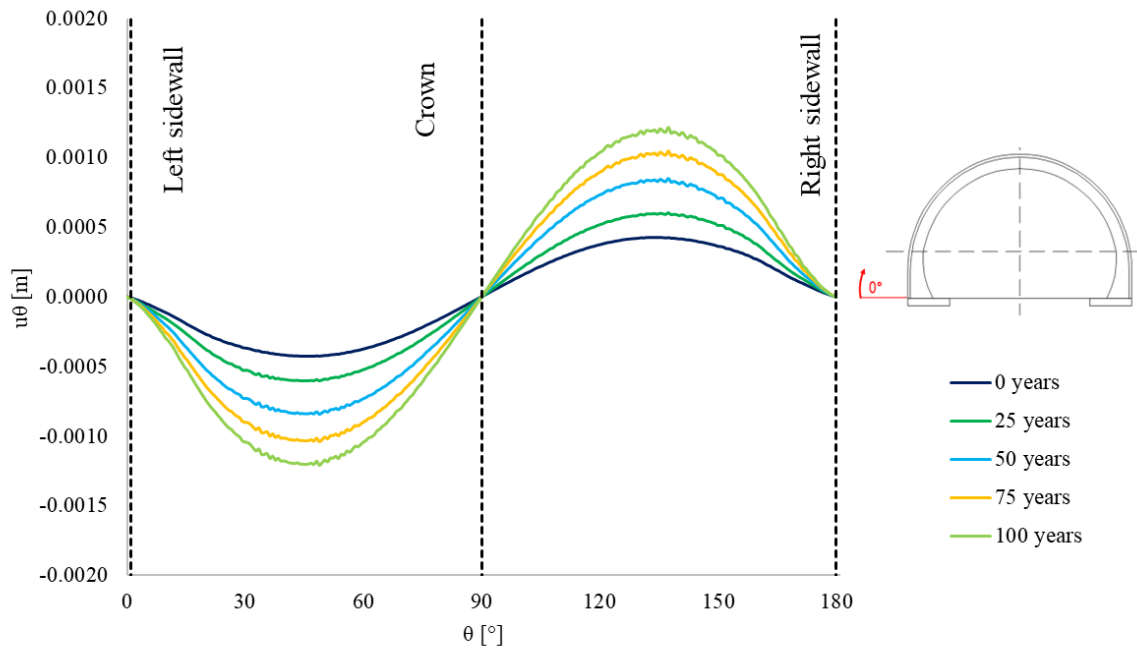
Model 10: RC_RM_PL_G_HSNI



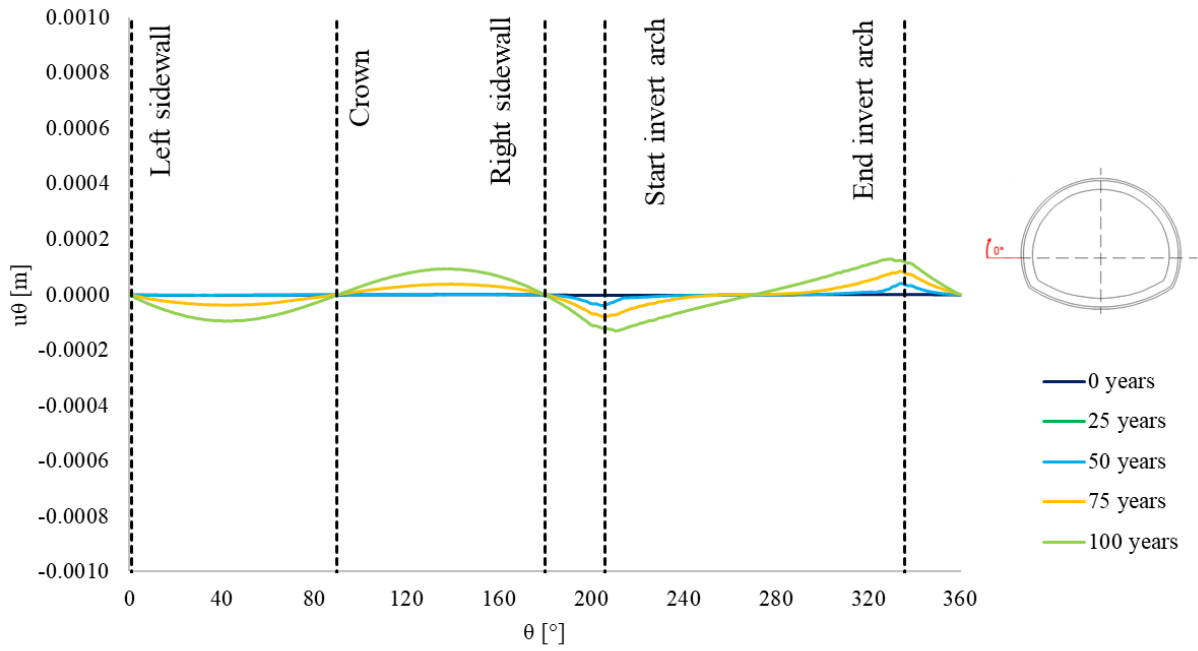
Model 11: RC_RM_PL_L_HSI



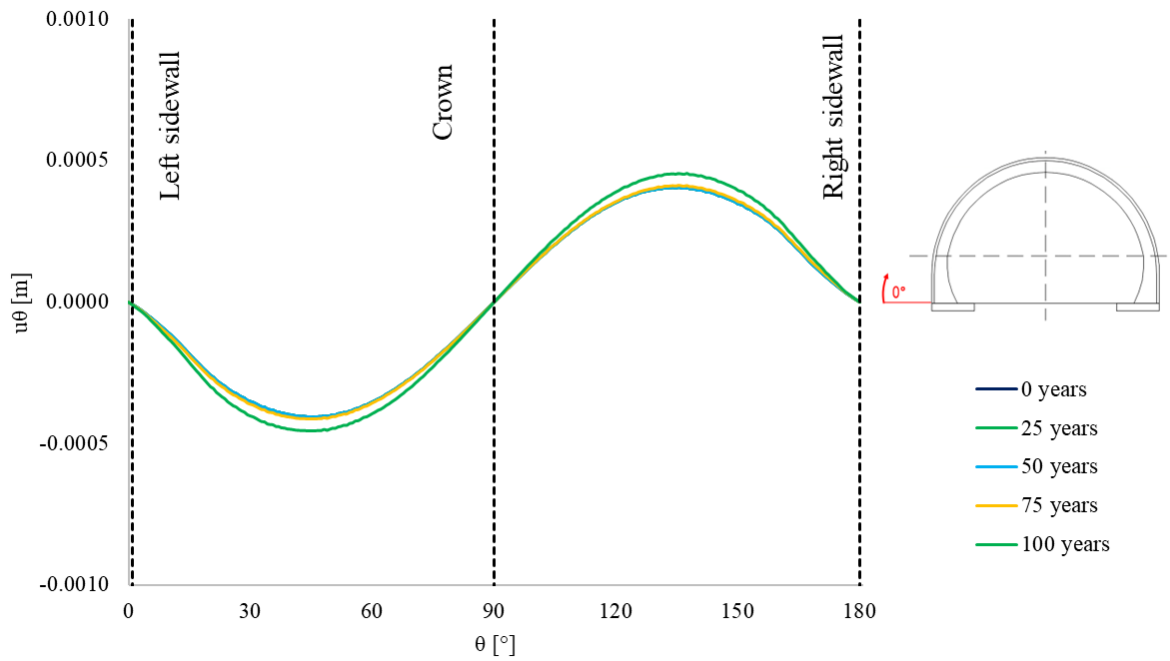
Model 12: RC_RM_PL_P_HSNI



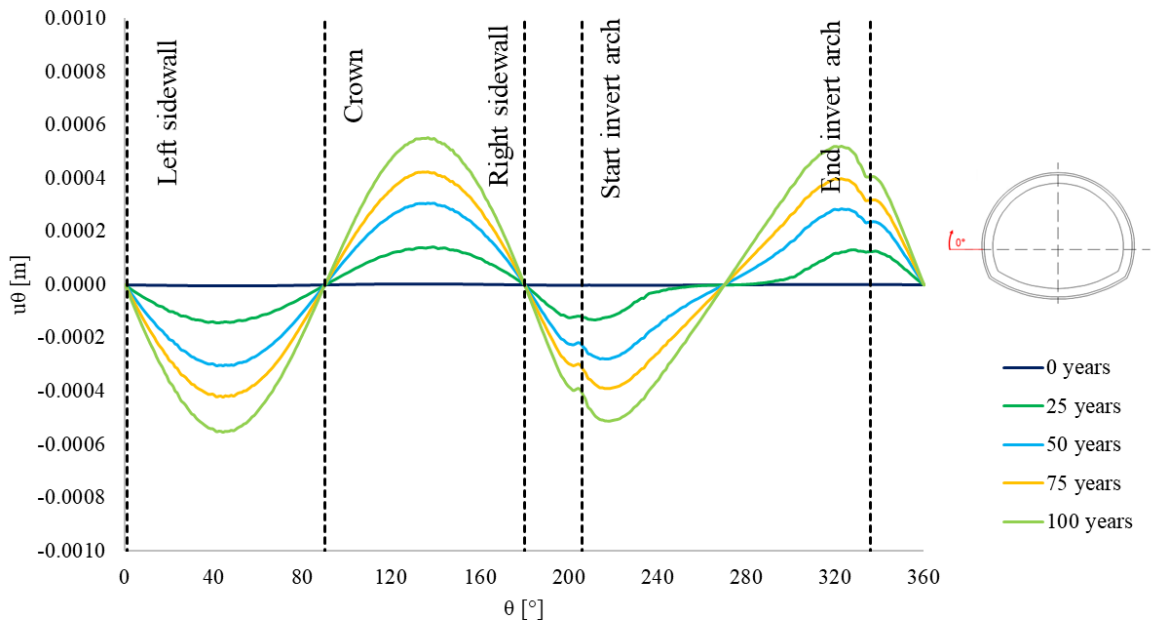
Model 13: RC_PL_G_HSI



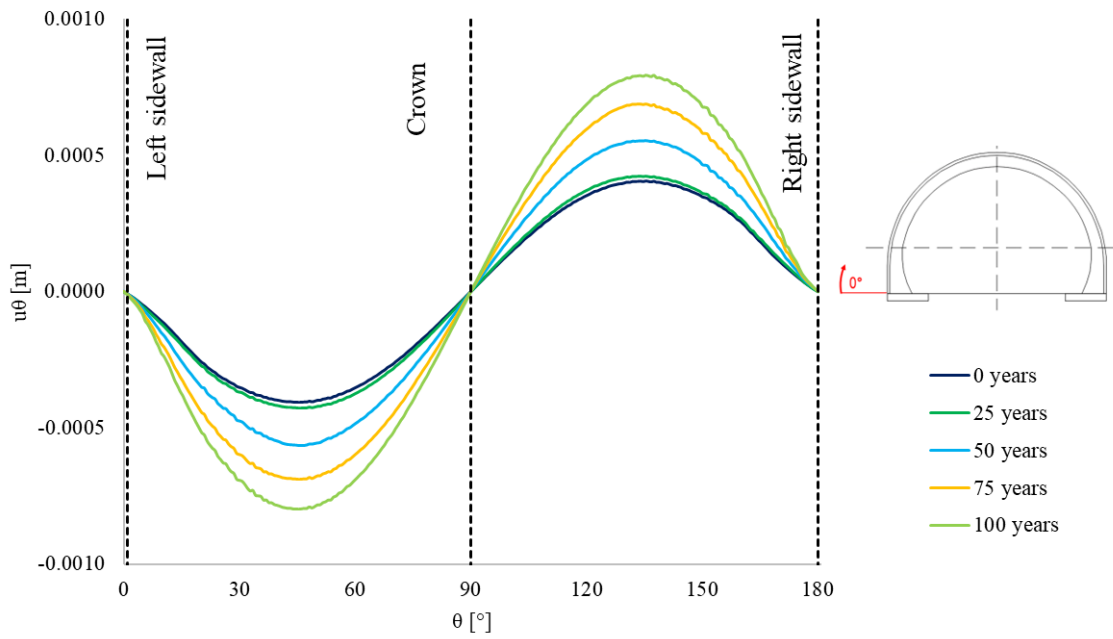
Model 14: RC_PL_G_HSNI



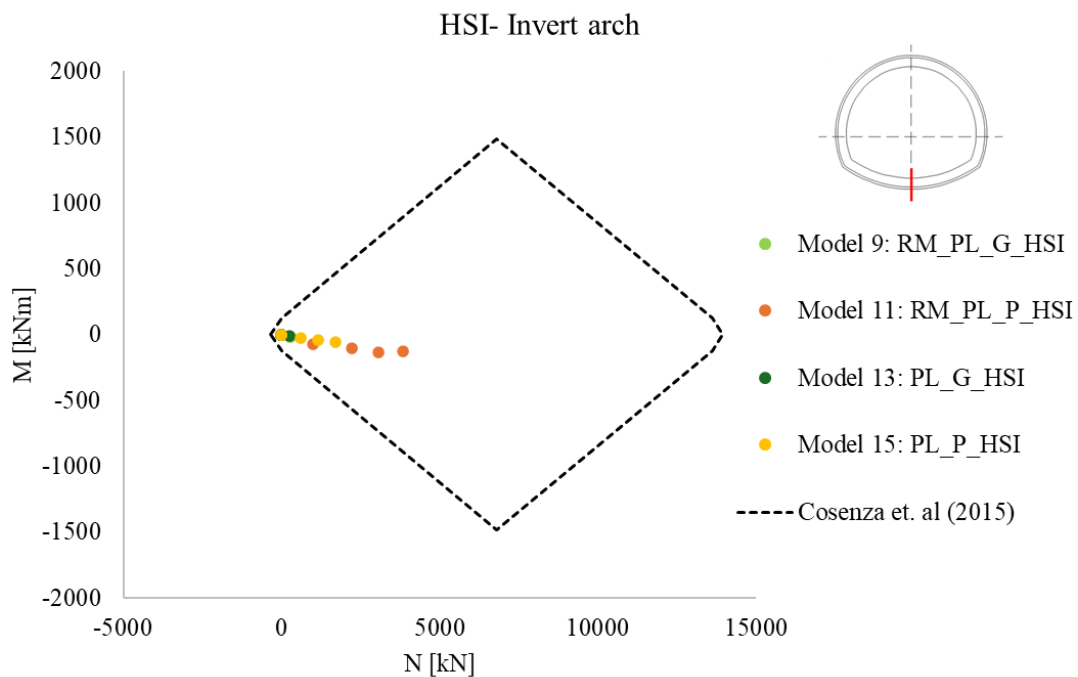
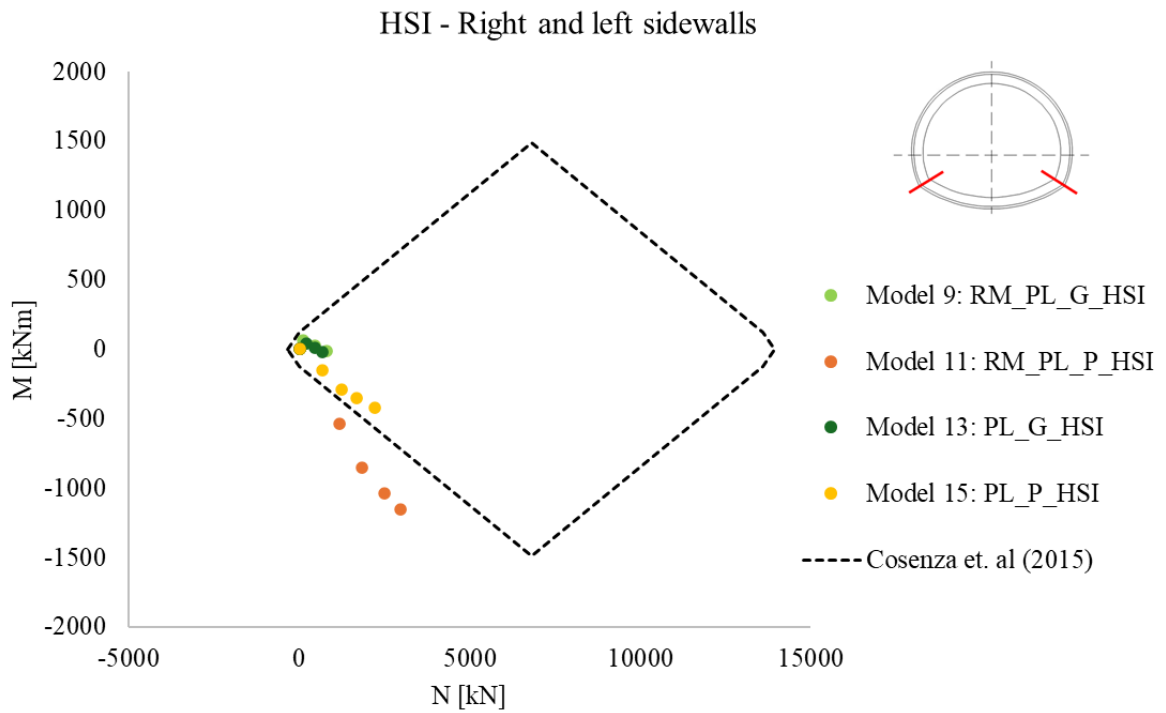
Model 15: RC_PL_L_HSI

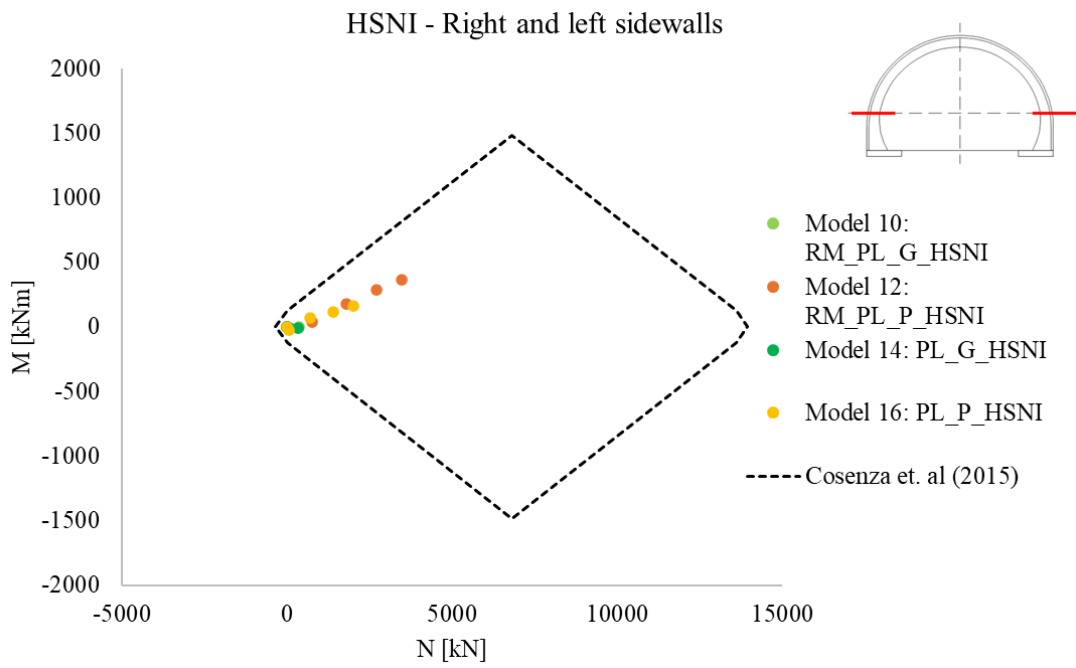
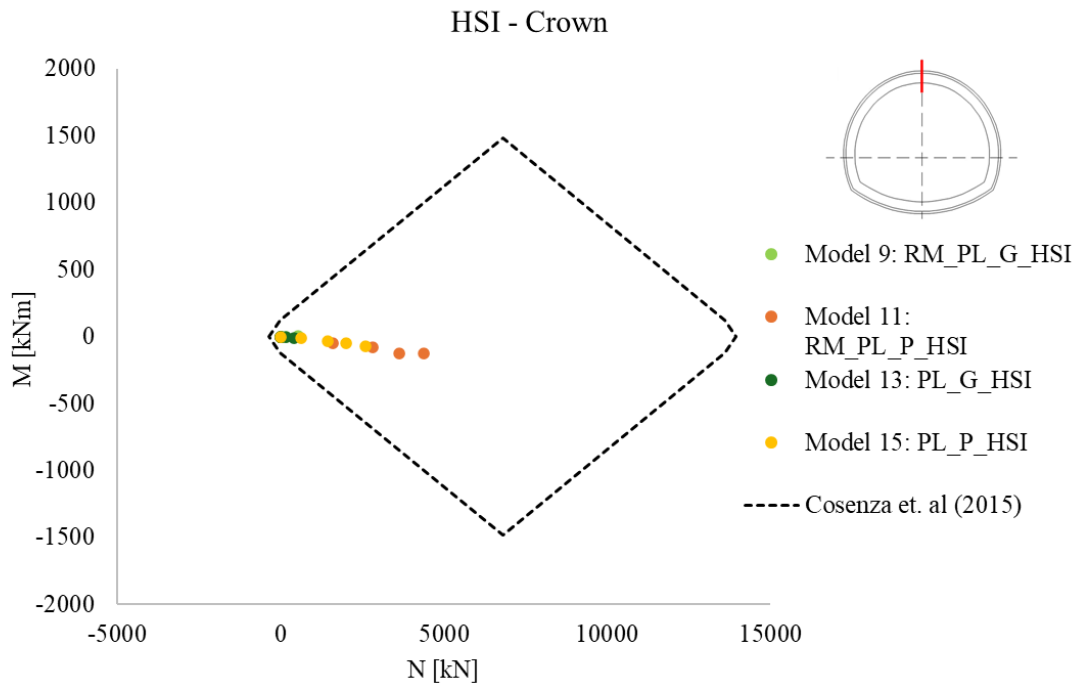


Model 16: RC_PL_P_HSNI



Appendix B.5. Verifications





HSNI - Crown

